Upwelling and Eddy Activity in the Southern Queensland Coastal Marine Zone, Australia

A thesis submitted by

Daniel Esteban Brieva Álvarez

For the award of

Doctor of Philosophy

2016

Abstract

Coastal upwelling systems are characterised by high primary productivity caused by the supply of nutrients into the surface layer of the ocean. These areas are key locations in global fish production despite their smaller size when compared with larger oceans. Another coastal mechanism that enhances primary productivity is eddy activity. It has been shown that eddies have three key features in the formation of the favourable reproductive habitat: enrichment, larval concentration and retention. Additionally, near-coastal eddies enhance primary production upon the neighbouring shelf as well as being mechanisms for the off shore transport. In this thesis, the results from an analysis of upwelling and eddy activity in the Southern Queensland Coastal Marine Zone off eastern Australia are presented. Firstly, the analysis includes the quantification and characterisation of upwelling events using chlorophyll-a data as a proxy. Secondly, a census of near-coastal eddies from a study of sea surface height data, along with the quantification of the potential impact of eddies over the shelf is presented. Finally, the analysis includes an examination of the role of upwelling events and eddies in the general circulation upon the shelf, through the examination of numerical representations.

The analysis of chlorophyll-a data results in the identification of two characteristic patterns. One pattern is associated with upwelling events driven primarily by bottom stress, as well as a less significant wind stress. This pattern is evident during the September to March period each year. From the days related to this particular chlorophyll-a bloom formation, approximately 87% and 60% of these days show upwelling conditions favoured by bottom stress and wind stress, respectively. The periodicity of these events leads to the identification of the Southeast Fraser Island Upwelling System. The second pattern was associated with upwelling events displaying an offshore transport not associated with wind stress, prompting the examination of the eddy activity in this region. It is suggested that the latter pattern is the result of a secondary upwelling system.

It is proposed that this upwelling system is referred to as the Sunshine Coast Upwelling System.

The analysis of the sea surface height data using an eddy detection and tracking tool, results in the identification of three coastal regions. Each region is characterised by its latitudinal distribution of eddies, as well by the main eddy features. The Southern Queensland Coastal Marine Zone is strongly dominated by cyclonic eddies of short (7-24 days) and long (>24 days) life spans, with approximately 31% and 29% of the total number of eddies, respectively. It is shown by quantifying an event in 2012, that near coastal eddies have the potential to extract offshore a high percent of the shelf water. The 2012 eddy extracted approximately 64% of the shelf water, which was replaced by slope water, resulting in a chlorophyll-a bloom. It is suggested, that the eddy activity has a significant role in the generation of chlorophyll-a blooms that are not associated with the Southeast Fraser Island Upwelling System.

Further insight into the ocean circulation of the Southern Queensland Coastal Marine Zone is gained from the analysis of ocean reanalysis data as well as through the implementation and application of a regional ocean model. The examination of ocean reanalysis data describes the role of eddies and upwelling events in the general circulation upon the shelf. The East Australian Current and wind drive most of the coastal circulation. The high variability of bottom stress resulting from the current, enhances the inshore bottom layer transport. The implementation of a numerical model identified high vorticity associated with sub-mesoscale features as contributing to the existence of the Southeast Fraser Island Upwelling System. The numerical results highlight the key role of the Breaksea Spit shallow waters in defining the source of upwelling water off Fraser Island. The Ekman transport by wind stress is significant in the Southeast Fraser Island Upwelling System (Spring and Summer). The northward transport by wind stress (Winter) could be significant in the generation of mesoscale eddies, potentially creating upwelling events by entraining shelf water. Simultaneously, the high concentration of cyclonic near-coastal eddies enhances a northward inner shelf current, supporting the reports of a northward transport of sand, ending at the north of Fraser Island.

In summary, a key finding of this research is the identification of the Southeast Fraser Upwelling System. The examination of the Sunshine Coast Upwelling System leads to the characterisation of the Southern Queensland Coastal Marine

Zone as being strongly dominated by cyclonic eddies. The analysis of numerical representations suggests that sub-mesoscale eddies have a significant influence on marine dynamics along the shelf break. It is suggested that the findings of this research should guide the future design and implementation of oceanographic surveys examining the Southern Queensland Coastal Marine Zone. The first objective of these surveys would be to observe upwelling events driving the Southeast Fraser Island Upwelling System as well as surveying the sub-mesoscale activity in this region. Improved knowledge of this region's physical oceanography would be extremely beneficial in the management of sustainable fishery and would result in clear economic benefits.

Certification of Thesis

This thesis is entirely the work of Daniel Brieva except where otherwise acknowledged. The work is original and has not previously been submitted for any other award, except where acknowledge.

Doctorate Candidate: Daniel Brieva	Date

Endorsement

Supervisor: Associate Professor Dr. Joachim Ribbe	Date
Co-supervisor: Professor Charles Lemckert	Date

Dedication

I thank God for the great support of Marisol and Paz in these years of study.

To you, my lovely wife, this thesis is dedicated.

And to you, my daughter, who arrived in the middle of this
journey and filled our lives with your laughter and play.

Acknowledgements

I would like to extend my many thanks to my supervisor Associate Professor Dr. Joachim Ribbe, who has advised me along this journey with great patience and constant support. His knowledge and experience was a significant contribution to this research project. Besides Dr. Joachim Ribbe , I would like to thank Professor Dr. Charles Lemckert for facilitating this research project.

Additionally, I would like to thank Dr. Andres Sepulveda for his friendly comments and timely advice throughout this study. Dr. Scarla Weeks whose discussion regarding Chlorophyll-a proved to be highly enlightening. Finally, Dr. Moninya Roughan and her team for sharing a new point of view and providing valuable feedback.

I would like to acknowledge IMOS, CSIRO and NOAA for providing data, as well as BecasChile for their sponsorship throughout this research project.

I wish to express my deep thanks to Dr. Francis Gacenga and Jason Bell for giving me vital technical support in the use of the High Performance Computer at Central Queensland University.

I place on record, my sincere gratitude to Nia Hodnett, who without knowing it, played a vital role in the completion of this document. I would like to include Les Barker and Wally Lang for their support in the proofreading of this document.

Johann Gustafson for his technical support and the enjoyable surveying expeditions.

Finally, my thanks goes to the University of Southern Queensland, specifically to the International Centre for Applied Climate Sciences.

My gratitude is given to the church members that supported my family

along this journey.

Supporting Publications

Journal Articles:

Brieva, D, Ribbe, J, and Lemckert, C, Is the East Australian Current causing a marine ecological hot-spot and an important fisheries near Fraser Island, Australia?, Estuarine, Coastal and Shelf Science, 153:121-134, 2015.

Conferences Proceedings:

Brieva, D , Ribbe, J, and Lemckert, C. A Numerical Investigation of the Southeast Fraser Island Upwelling System. In AMOS National Conference, page 109, Brisbane, Australia, 15 July, 2015.

Ribbe, J, Brieva, D, and Lemckert, C. Poster: Evidence of upwelling near Fraser Island, Australia. In EGU General Assembly Conference Abstracts, volume 17, page 110, 2015.

Gacenga, F, Bell, J, Samalca, I, and Brieva, D. Poster: Enabling Research Outcomes Using QCIF HPC Facilities. In eResearch Australasia Conference, Melbourne, Australia, 27-30 Oct., 2014.

Brieva, D , Ribbe, J, and Lemckert, C. Upwelling off shore Fraser Island. In AMOS National Conference, Hobart, Australia, 13 Feb., 2014.

Brieva, D , Ribbe, J, and Lemckert, C. On the physical mechanism of Fraser coast upwelling. In AMSA Conference, Canberra, Australia, 7 Jul., 2014.

Brieva, D, Ribbe, J , and Lemckert, C. Obsevations of High Chlorophyll-a near Fraser Island, Australia. In 4th Australian Chinese Ocean Science & Technology Symposium, Qingdao, China, Sept. 26-29, 2014.

Brieva, D , Ribbe, J, and Lemckert, C. The Coastal Circulation off Southeast

Queensland. In Annual Meeting Asia Oceania Geosciences Society, Brisbane, Australia, 28 Jun., 2013.

Contents

List of Figures

List of Tables

List of Animations

Abbreviations and Acronyms

ACEs: Anti-Cyclonic Eddies
ADCP: Acoustic Doppler Current Profiler
AODN: Australia Ocean Data Network
BODAS: BlueLink Ocean Data Assimilation System
BOM: Bureau of Meteorology
CEs: Cyclonic Eddies
Chla: Chlorophyll-a
CMAR: CSIRO Marine and Atmospheric Research
CQU: Central Queensland University
CSIRO: Commonwealth Scientific and Industrial Research Organisation
CTD: Instrument that measures Conductivity, Temperature and estimates Density
DFT: Discrete Fourier Transform
EA: Eddy Avenue
EAC: East Australian Current
EACM1213: Dataset from moorings deployed off Brisbane, Australia from 2012 to 2013
EDTT: Eddy Detection and Tracking Tool
FTP: File Transfer Protocol
GBRMP: Great Barrier Reef Marine Park
HPC: High Performance Computer
IMOS: Integrated Marine Observation System
ISC: Inner-Shelf Current
JPL: Jet Propulsion Laboratory
KEF: Key Ecological Feature
LACE: Long-lived Anti-cyclonic Eddies
LCE: Long-lived Cyclonic Eddies
MODIS: Moderate Resolution Imaging Spectroradiometer

NASA: National Aeronautics and Space Administration
NCEs: Near Coastal Eddies
NOAA: National Oceanic and Atmospheric Administration
OFAM2: Ocean Forecasting Australian Model version 2
OPeNDAP: Open source Project for a Network Data Access Protocol
P1: First pattern of Chla blooms related to the Sunshine Coast Upwelling System
P2: Second pattern of Chla blooms related to the Fraser Island Upwelling System
PSU: Practical Salinity Unit
ROMS: Regional Ocean Modelling system
SACE: Short-lived Anti-Cyclonic Eddies
SCE: Short-lived Cyclonic Eddies
SCUS: Sunshine Coast Upwelling System
SEC: South Equatorial Current
SFIUS: Southeast Fraser Island Upwelling System
SPO: South Pacific Ocean
SQCMZ: Southern Queensland Coastal Marine Zone
SR: Subtropical Ridge
SSG: Southern Subtropical Gyre
SSHa: Sea Surface Heigh anomaly
SST: Sea Surface Temperature
STS: Synthetic Time Series
Sv: Sverdrup (unit that represent the volume of water transported in a defined period or flux. It is equivalent to 106m3/s)
USQ: University of Southern Queensland

Chapter 1

Introduction

The East Australian Current (EAC) flows poleward along the east coast of Australia and it is the western boundary current of the Southern Pacific Gyre (Tomczak and Godfrey, 2003). The coastal circulation in the central zone of the east coast of Australia is mainly driven by the EAC (Middleton et al., 1994; Ridgway and Dunn, 2003; Rossi et al., 2014; Schaeffer et al., 2013). The presence of the EAC in this area has resulted in upwelling and eddy events, which have been reported by Oke and Middleton (2000), Oke and Middleton (2001), Everett et al. (2012), Pilo et al. (2015) and Everett et al. (2015). The causal physical mechanisms behind these events have been identified and models of their impact have been proposed by the aforementioned studies. However, there is a region excluded from previous descriptions in which the EAC's impact upon the shelf circulation, and the physical dynamics associated with upwelling and eddies have not been addressed.

Reports of a quasi stationary eddy in the Capricorn Channel (figure 1.1) as well as upwelling events and eddies off New South Wales are presented in the literature (Everett et al., 2012, 2015; Pilo et al., 2015; Weeks et al., 2010). However, the Southern Queensland Coastal Marine Zone (SQCMZ), Australia is not included in these aforementioned reports. The SQCMZ is defined for the purpose of this study as the approximated region from 153°E to 155°E and 29°S to 24.5°S (figure 1.1), this region is part of the EAC intensification zone (Ridgway and Dunn, 2003). Two papers (Middleton et al., 1994; Rossi et al., 2014) and one technical report (Dambacher et al., 2012) mention a number of the physical characteristics of the SQCMZ's circulation, however, none have focused specifically on this area. Middleton et al. (1994) suggest a potential zone of

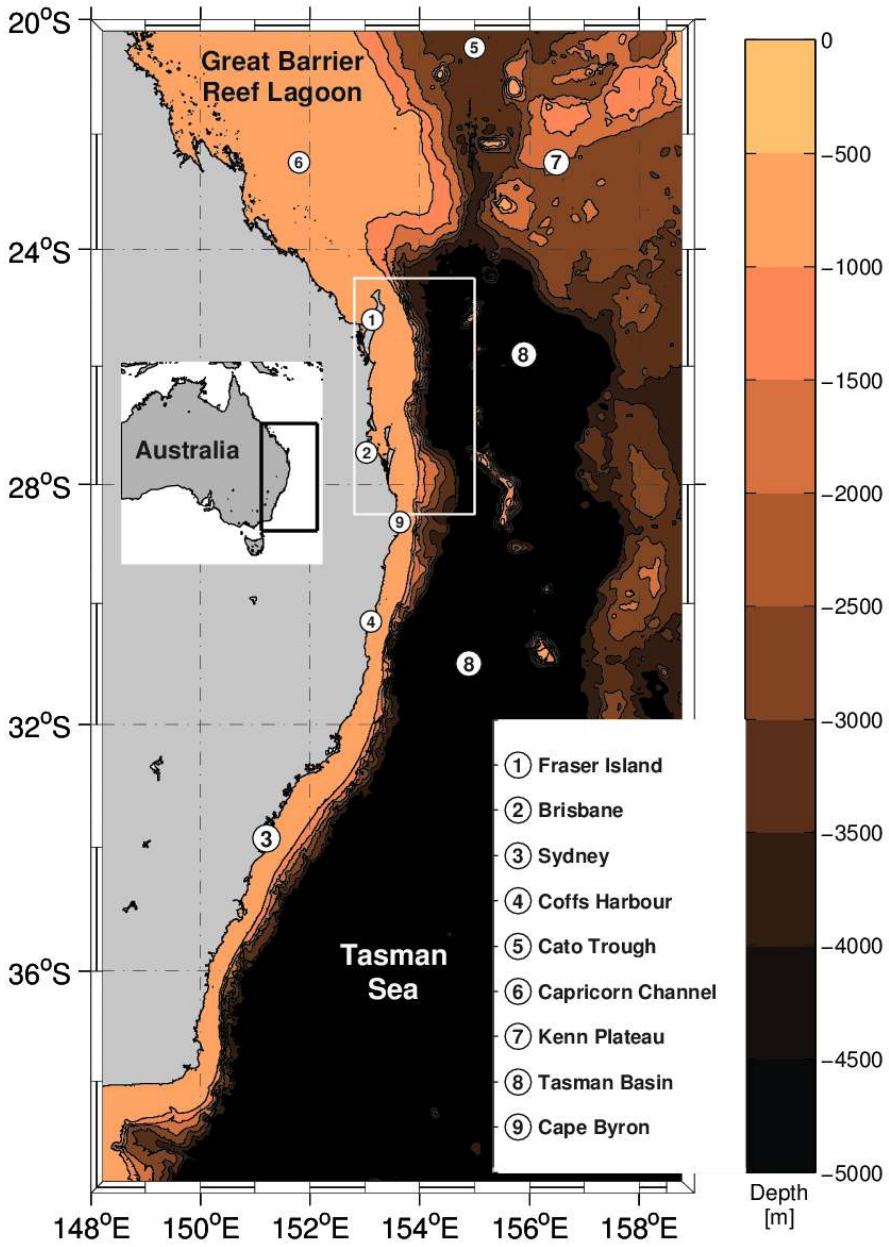

Figure 1.1: East Australian bathymetry (topography) is represented in the main map and scaled according to the colour bar. Small map represents the Australian coastline and the black box highlights the area represented by the main map. White box in the main map represents the study area.

upwelling off Fraser Island based on one transect across the shelf. The following research addressing upwelling in this area is carried out by Rossi et al. (2014), 20 years later. Current-driven and wind-driven conditions are estimated based on remote sensing for a long section of the east Australian coast, where the SQCMZ is the northern edge of the study zone. Dambacher et al. (2012) define the upwelling off Fraser Island as one of the eight Key Ecological Features (KEFs) of the East Coast of Australia and suggest as physical mechanisms, the EAC-shelf interaction and transient eddies. However, only the two aforementioned papers were found to address upwelling in the study area with none addressing near-coastal eddies (NCEs), their characteristics or distribution in the study area.

The review of the current published research studies highlighted many questions regarding marine dynamics and physical features in the SQCMZ. A selection of the identified questions was then used to construct this research project. The selected and answered questions are:

- What are the features of the upwelling events and the variability related to them in the SQCMZ, and which are the physical mechanisms related to these events?
- How is the shelf circulation impacted by NCEs, What is the spatial distribution of the NCEs and how do their features change along the coast? Finally, how do the NCEs and their features vary temporally?
- How the identified features of the SQCMZ are interconnected and which are the physical mechanisms linking them together in the shelf circulation of the SQCMZ?

The lack of physical marine research in the SQCMZ (figure 1.1) provides the motivation for this study. Additional motivation came from the analysis of Chlorophyll-a (Chla) data representing upwelling events and the entrainment of coastal water by NCEs. Additionally, the release of version 3.5 of the Bluelink Reanalysis product (BRAN3.5, Oke et al. 2013), a reanalysis product which claims to achieve a good realistic marine circulation (as it is shown for the study area of this thesis), prompted the start of this project. An implementation of the Regional Ocean Marine System (ROMS, Debreu et al. 2011, Penven et al. 2006) complements the research, by adding extra information about submesoscale features.

This research project can be characterised by the completion of the following research activities. First, the initial analysis and characterisation of upwelling events carried out in the SQCMZ, leading to the identification of two dynamically different upwelling systems (chapters 4 and 5): the Southeast Fraser Island Upwelling System (SFIUS) (Brieva et al., 2015) and the suggested Sunshine Coast Upwelling System (SCUS). Second, the first analysis and characterisation of near-coastal mesoscale eddies (within $100km$ of the shelf break) along the southern section of the East Coast of Australia (chapter 5). Third, the first design of a model of the general shelf circulation in the SQCMZ. The model includes features described in this research project, in previous literature, as well as the physical mechanisms interconnecting these features (chapter 6).

1.1 Purpose and Objectives

The main purpose of this research is to expand the understanding of marine coastal circulation in the SQCMZ. Significant progress has been made in the understanding of the marine circulation in the southern and northern coastal zones of this research's study area (New South Wales and Great Barrier Marine Park). The implementation of the Integrated Marine Observation System (IMOS) has played a vital role in increasing knowledge and understanding. However, physical marine research off Southern Queensland has fallen behind. The main objectives outlined for the completion of this research project, related to the aforementioned questions are:

1. To analyse and characterise the upwelling events in the SQCMZ and propose possible physical mechanisms driving these events (results presented in chapter 4).

2. To quantify, analyse and describe NCEs, including their potential impact upon the shelf circulation (results presented in chapter 5).

3. To analyse and examine the general circulation of the SQCMZ based on BRAN3.5 and the implementation of a numerical model, as well as to design a model showing how the described features are interconnected by physical mechanisms (results presented in chapter 6).

In addition to chapters 4 to 6 where the results are discussed, chapter 1 is a literature review, chapter 3 describes the methodologies, and the final two chapters describe and discuss the completion of this research project as well as potential future work. The analysis and studies are based on observations as well as numerical representations of physical variables in the marine circulation.

1.2 Summary

This physical coastal marine research project has been planned to fit into a knowledge and understanding gap regarding the marine coastal area in the SQCMZ. The SQCMZ gap is highlighted when the current state of knowledge and understanding of the physical marine processes, it is compared against that of its surrounding coastal areas. This research project involves the analysis of observations and numerical representations. Additionally, the project includes the implementation of ROMS to extend the research to submesoscale features, thus completing the model design allowing it to summarise the SQCMZ's circulation. This dissertation is organised into the following chapters:

- Chapter 2 is a review of the current knowledge in published literature regarding the SQCMZ and its surrounding areas. The questions listed previously in this chapter are part of the knowledge gap highlighted in chapter 2.
- Chapter 3 describes the data sets used in this study as well as the tools, technical details and methodologies used to approach the analysis.
- Chapter 4 contains the classification of Chla patterns as a proxy of upwelling events, the analysis and characterisation of two identified patterns related to upwelling events as well as the examination of the physical mechanisms causing them.
- Chapter 5 discusses a single NCE to demonstrate the potential impact of NCEs in the circulation upon the shelf, also quantifying the NCEs along the southern section of the east coast of Australia and characterising variability in their features as well as the spatial and temporal distribution.
- Chapter 6 examines the general circulation upon the shelf in the SQCMZ based on observations and numerical results. A model is then discussed

which describes all the features addressed in this research study as well as the physical mechanisms that interconnect them, which is the final discussion of this thesis.

- Chapter 7 concludes this document highlighting the main findings and contributions of this research project, addressing each objective demonstrating how it was accomplished and proposing future work to expand upon the results of this research project.

Chapter 2

Literature Review

This literature review describes the EAC, upwelling events and eddies in the areas surrounding the SQCMZ, as well as looking at the physical mechanisms associated with them. The description focuses on the SQCMZ, a zone with very limited physical-marine research when compared to the research completed in its surrounding areas. The gap of the SQCMZ identified in the physical marine research leads to the formulation of the questions and objectives listed in chapter 1. The review of literature focusing on the surrounding areas identifies potential physical mechanisms behind the upwelling events in the SQCMZ, which are analysed in chapter 4. Additionally, this literature review highlights the role of eddies in fronts associated with the EAC, leading to the quantification and description of NCEs in chapter 5. Finally, the review briefly describes some marine coastal physical features, these are not analysed in great depth (e.g. inner shelf northward current), however, they support the numerical representations of BRAN3.5. Additionally, in chapter 6 these features are part of the designed model describing the interconnection of the marine characteristics in the SQCMZ.

2.1 Overview

The SQCMZ is a small coastal section of the South Pacific Ocean's (SPO) western boundary. Trade winds (0°S-30°S) and Westerlies (30°S-65°S) are features of the SPO in the low- and mid-latitudes respectively. The SQCMZ is primarily under the influence of Trade Winds, however, the northward displacement of the Subtropical Ridge in winter allows Westerlies to take its place in this zone. The

main SPO marine circulation is anticyclonic, which is an anticlockwise circulation in the southern hemisphere. The name of this marine circulation is the Southern Subtropical Gyre (SSG,Tomczak and Godfrey 2003). Wind stress has been recognised as the main driver of the ocean surface circulation (Stewart, 2009), with the SSG's direction of flow resembling the Trade and Westerly winds. SSG's circulation has as its major currents, the Peru/Chile Current (east side) and the South Equatorial Current (SEC, north side). As part of the western boundary circulation, the EAC flows poleward (Tomczak and Godfrey, 2003).

Western boundary currents have some similar features: They are narrow, fast, extend below the thermocline and their separations from the coast are associated with instabilities (Tomczak and Godfrey, 2003). The EAC is the weakest among the western boundary currents in the southern hemisphere. However, the EAC has a major role in the marine circulation off eastern Australia (Ridgway and Dunn, 2003), particularly in the coastal circulation, as the next section discusses.

2.2 Context of Study Area: Marine Area off Eastern Australia

A large section of the eastern marine coast of Australia is part of the Great Barrier Reef Marine Park (GBRMP). It was listed as a World Heritage Area in 1981 and is well known for its coral reefs. The area has been researched extensively (Coles et al., 2015). The EAC's formation zone is in the southern area of the GBRMP (section 2.2.1.1) with warm oligotrophic waters characterising the EAC formation zone (Everett et al., 2012). Hervey Bay (figure 2.1) is at the south of the GBRMP and has been classified as a laterally inhomogeneous estuary by Ribbe (2006), based on salinity measurements. Extreme climate events can result briefly in different heat and salt distributions in estuaries. Fraser Island is the eastern boundary of Hervey Bay and was listed as a World Heritage Area in 1992 (Mühlhäusler and Peace, 2001). Fraser Island is situated at the end of an equatorward sand transport, named River of Sand (Schröder-Adams et al., 2008), which is the largest sand island in the world (section 2.3.3). A number of marine circulation features between Fraser Island and Moreton Island can be inferred from sand transport as well as the migration and spawning of small fishes (pelagic). However, no study was found to address physical marine mechanisms in this area. Further details about the study area are presented in section 2.3.

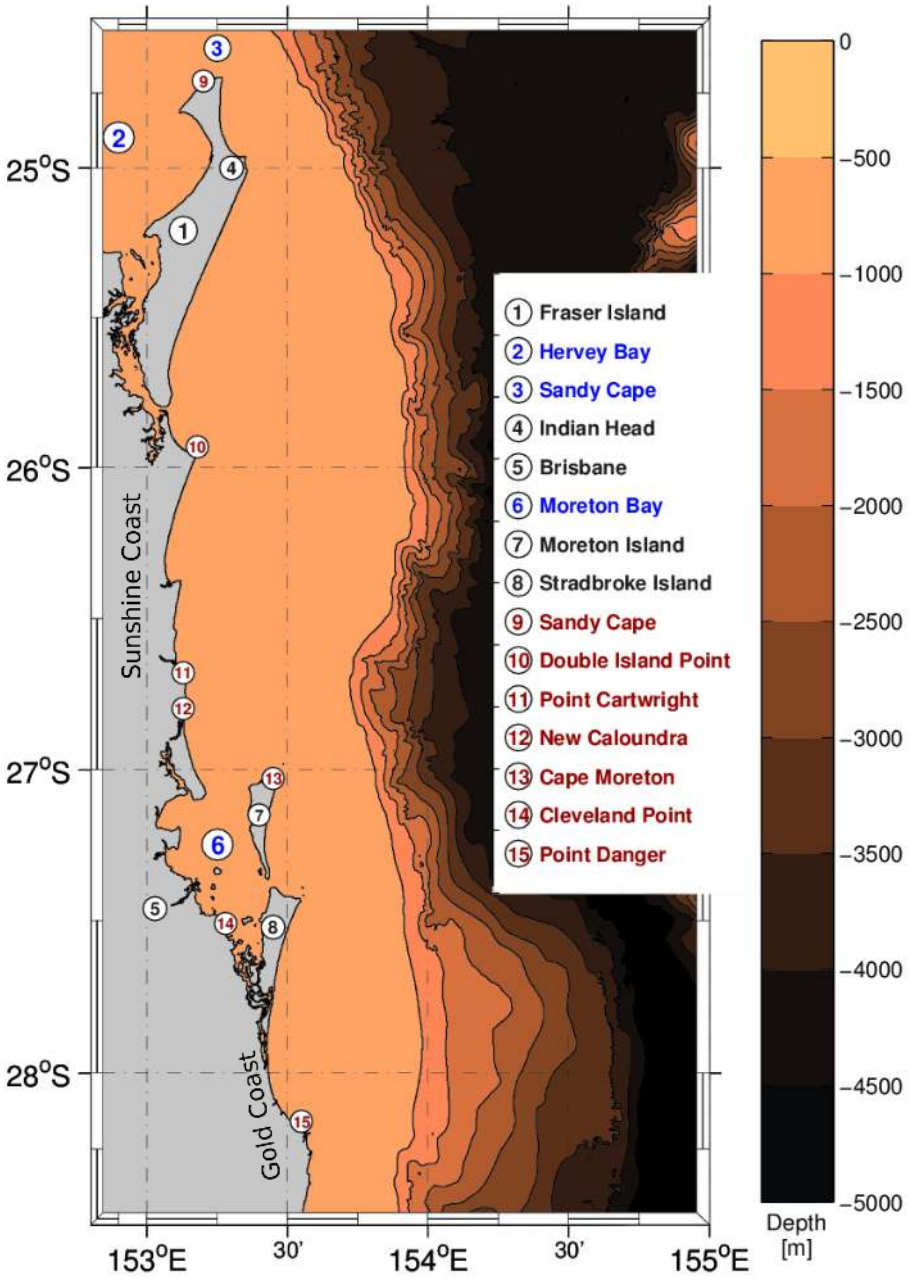

Figure 2.1: The Southern Queensland coastal marine area with places highlighted on the map. Places are classified as land (black), marine (blue) and Lighthouses (red).

At the south of the study area, the separation of the EAC from the coast results in the formation of a mesoscale eddy field (Everett et al., 2012). A recent increase of marine research in this area can be associated with the IMOS (Roughan et al., 2010) and its efforts to make data available from one platform. Research on coastal marine circulation and dynamics in this zone describe the various impacts of the EAC. These impacts affect circulation upon the shelf, eddy distribution and upwelling processes, among others. Sections 2.2.2 and 2.2.3 address some of these impacts.

Condie and Dunn (2006) describe sea surface temperature in the range of 5°C (subantarctic waters) up to 29°C (western equatorial Pacific), in the western Pacific Ocean. The latitudinal temperature gradient is disrupted by the southward transport of heat, resulting from the EAC's poleward transport. This transport of heat results in isotherms parallel to the east coast of Australia, meaning a longitudinal temperature gradient near the coast line. The same temperature features are observed off the western coast of Australia, which is where the Leeuwin Current is located. Temperatures at the surface show the annual fluctuation, with the maximum amplitude in the mid-latitudes (Condie and Dunn, 2006). The distribution of heat is proportionally similar throughout the year. The zone of high annual temperature variability is where the highest values of surface salinity are located (at about 30°S with values over 35.5 psu). These values decrease both southward and equatorward. Isohalines have a similar orientation to the isotherms, including the near coastal longitudinal gradient caused by the EAC. These salinity features are also similar throughout the year.

2.2.1 The East Australian Current

The EAC is part of a set of currents in the eastern coast of Australia which are branches of the SPC. These include the Northern Queensland Current and the Gulf of Papua Current (Ganachaud et al., 2014). The EAC flows along the eastern coast of Australia (Ridgway and Dunn, 2003; Sloyan et al., 2016) and separates from the coast to turn eastward (Cetina-Heredia et al., 2014; Ridgway and Dunn, 2003). The EAC's transport of water has been estimated at over 20 Sv (Mata et al., 2000; Ridgway and Dunn, 2003; Sloyan et al., 2016) and is a path for heat to be transported poleward (Condie and Dunn, 2006; Sloyan et al., 2016). The most commonly reported fluctuation of the EAC is the annual variability of its strength, which has been associated with the simultaneous variability of its

width (Ridgway and Dunn, 2003; Sloyan et al., 2016; Wood et al., 2016). Inter-annual variabilities have been reported in the range of approximately 60 to 180 days (Andrews and Gentien, 1982; Cetina-Heredia et al., 2014; Hamon and Kerr, 1968; Mata et al., 2000; Schaeffer et al., 2014).

Ridgway and Dunn (2003) describe the mean EAC using its behaviour to define four EAC zones: Formation, Intensification, Separation and Decline zones. A double anticyclonic structure, possibly "trapped within the abyssal canyon", defines the eastern boundary of the EAC at the Intensification and Separation zones. The northern cyclonic circulation is weaker than the southern. It is located to the east of the study area which is part of the intensification zone. The following sections examine the literature for these four zones, with a major focus on the intensification of the EAC, as the study area falls within it. The other three zones of the EAC are included in the description to define key features, that will be used to validate the NCEs distribution results along the eastern coast of Australia (chapter 5).

2.2.1.1 Formation Zone (15°S-24°S)

After 1-2 years of travelling across the Pacific Ocean, the waters transported by the SEC arrive at the Coral Sea and become part of the EAC formation zone (Everett et al., 2011). The warm and oligotrophic waters of the Coral Sea characterise this zone (Everett et al., 2012). The EAC is located mainly over the shelf and flows poleward, becoming a well defined current once the shelf narrows from $500km$ to $100km$ (24°S). Approximately $50km$ further south (figure 1.1) the shelf corridor narrows to a few kilometres. The narrowing will result in the current becoming deeper and flowing faster, as the next section discusses.

2.2.1.2 Intensification Zone(24°S-30°S)

Between 23°S and 24°S, the EAC shows a main transition from the shelf to the shelf break (Ridgway and Dunn, 2003), which follows a sharp narrowing of the shelf (from $500km$ to $200km$ wide, figure 1.1). The EAC velocity increases from less than $20cm/s$ to over $90cm/s$ from the Coral Sea to Coffs Harbour at 30°S respectively (in their climatology analysis). The EAC's direction follows the coastline's orientation, including its change at approximately 29°S. In this section, the EAC follows the change in the coastline orientation, flowing south-west.

Around 31.5°S, the EAC detaches from the coastline resulting in the primary separation point, which is part of the EAC separation zone (section 2.2.1.3). The transition from the northern to the southern anticyclonic circulations is located in the intensification zone at approximately 29°S, suggesting a possible secondary separation point (Ridgway and Dunn, 2003).

Fluctuations in the EAC have been reported by a number of different studies. Hamon and Kerr (1968) report a fluctuation in the order of 70-100 days from studies using data from deck navigation logs. Additional studies reporting this EAC fluctuation include: Mata et al. (2000, 90-140 days) and Andrews and Gentien (1982, 90 days). A majority of the estimated speeds are in the range of 0.5 to $1m/s$, with maxima over $2m/s$ and minima under -0.5m/s (negative sign means an equatorward flow in this case). An extended and improved analysis (Hamon et al., 1975) shows that this equatorward current is located near the coast and is not constant throughout the year. Ridgway and Godfrey (1997) describe another temporal fluctuation, a strong seasonal cycle involving the Formation, Intensification, Separation and Decline zones of the EAC. The strongest flow is in Austral summer and estimations of the transport at 28°S are $7Sv$ in winter and $16Sv$ in summer. The current increases its strength from September through to January. The seasonality in the EAC is not related to the seasonal variability of the wind. The amplitude of the seasonal variability seems to be larger than in other western boundary currents and increases northward. Sloyan et al. (2016) quantify the transport of the EAC at approximately 27°S in $22Sv$ and the transport of heat is approximately -1.35PW. Wood et al. (2016) extend the analysis of the annual variability and show that the temperature shows a strong seasonal variability, accounting for approximately 49% of the total temperature variability. In contrast, the velocity shows a weak annual variability representing only 6% of the total. The total variability of velocity is dominated by the inter-seasonal variability.

Harris et al. (1996) study water velocity in the bottom layer to understand the characteristics of sediment transport occurring off Fraser Island. Current meters deployed from November to December, in 1992 and from June to July, in 1993, show a strong daily fluctuation associated with the diurnal tide. This tidal influence is stronger in shallow waters (<60m). However, this tidal signal was not consistently present in the deepest current meter deployed (80m). Velocities of up to 135cm/s were recorded at 1m above the bottom. Middleton et al. (1994) describe the velocity off Sandy Cape based on shipborne Acoustic Doppler Current Profiler (ADCP). The surface current (EAC) is clearly poleward off Fraser Island,

with speeds over $0.5cm/s$ (depth $< 100m$). At the northern tip of Fraser Island, under $100m$ depth, the current heads Northwest. Temperature cross sections at Double Island Point and Sandy Cape, capture in the isotherms the impact of the EAC until 200-250m over the shelf break. Oke and Middleton (2000) describe the physical mechanisms resulting from the EAC-shelf interaction. These lead to the intrusion of uplifted water from a deeper layer over the shelf, at Cape Byron. These different fluctuations of the EAC enhance the bottom layer inshore transport caused by bottom stress (more details in section 2.2.2). One result shown in Chapter 4 confirms that there is a zone of high bottom stress off Fraser Island based on BRAN3.5 (Brieva et al., 2015).

2.2.1.3 Separation zone (30°S-35°S)

Ridgway and Dunn (2003) estimate the position of the EAC detachment point at 31.5°S, in a $150km$ coast range. The detachment point is where the EAC turns back to a poleward current. Upstream from the detachment point, the EAC follows the change in the coastline orientation heading south-west, at approximately 29°S. Further south of the detachment point between 33°S and 35°S, the EAC's main flow turns to an eastward current. Estimations of the area in which the EAC turns eastwards in numerical models, found it in the range of 28°S-38°S and 50% of the time between 30.7°S and 32.4°S (Cetina-Heredia et al., 2014). The candidate attributes this inconsistency to the differences in the methodologies used in the estimation of the turning area. The temporal variability in the turning area is similar to the one observed in the maximum eastward wind speed, thus supporting the idea of wind driving the separation point. This separation zone has been associated with uplifted slope water over the shelf, enhancing the nutrient concentration (Oke and Middleton, 2000; Schaeffer et al., 2014). In this zone (30°S - 32°S), the EAC decelerates by approximately 60%. The southern section of the separation zone shows high eddy activity reported by Everett et al. (2012), the Eddy Avenue.

2.2.1.4 Decline zone (35°S-43°S)

According to Ridgway and Dunn (2003), the decline zone shows a high variability, as a result of the eddies. The remainder of the EAC (southward stream extensions after the separation zone) has a smaller water transport when compared to

the main current, forming eddies (Cresswell, 2001) which propagate southward (Suthers et al., 2011, section 2.2.1.3). Everett et al. (2012) compare eddies in the Tasman Sea with those specifically in the western area of the Tasman Sea, named Eddy Avenue. Eddy Avenue is a corridor $300km$ wide, which includes the marine coastal zone of Southeastern Australia. The results show the differences between the main features of those eddies from the whole and a coastal section of the Tasman Sea. Eddies within Eddy Avenue show a trend of higher amplitudes, larger radii and faster rotational speeds than those in the rest of the Tasman Sea. Eddy Avenue's northern boundary is at 32°S, meaning it does not include the SQCMZ (this research's study area).

2.2.2 Upwelling

Uplifted masses of water rising to the surface, are referred to here as upwelling events (Rochford, 1991; Roughan and Middleton, 2002). Upwelling events enhance primary production due to the transport of nutrients over the shelf. The Eastern Boundary Upwelling Systems are highly productive marine zones (Gruber et al., 2011). One zone of upwelling is located on the east of the SSG, located on the opposite side to the EAC. It is named the Peru/Chile upwelling system. The high upwelling activity is mainly due to the wind, which is favourable to upwelling throughout the year (Rossi et al., 2009). The theory formulated by Ekman (1905) explains, in part, the wind-driven upwelling process.The wind stress results in a normal net transport of water to the wind direction. The normal transport, in the southern hemisphere, is to the left of the wind direction. Under northerly winds (wind flowing to the south) upon Eastern Australia, coastal water is drawn off shore and water from the bottom moves up to takes its place, or more precisely to maintain the conservation of mass. Similarly to the Peru/Chilean Upwelling System, the southerly wind is the most common wind direction along the SQCMZ coast throughout the year (Rossi et al., 2014). Here, this wind is unfavourable to upwelling or favourable to downwelling along the east coast of Australia. The morphology and orientation of the Southern Queensland coastal marine zone's coast line and shelf break could be a factor in Kelvin waves resulting in upwelling events (Kämpf, 2006; Kämpf and Kaempf, 2009). Upwelling events associated to Kelvin waves was suggested by Wolanski and Pickard (1983) in the GBRMP based on the analysis of observations. Other upwelling system have been reported in the Great Bank of Newfoundland (Zhao et al., 2013) and the Malvina Current

(Benthuysen et al., 2015; Matano and Palma, 2008; Valla and Piola, 2015)

Another physical mechanism reported to create upwelling events, in Eastern Australia, is bottom stress caused by the EAC flowing poleward near the shelf. Ekman (1905)'s theory and Prandtl's Boundary Layer theory (Anderson Jr, 2005) are the basis from which to explain the bottom boundary layer, that results in an upwelling mechanism by bottom stress. Oke and Middleton (2000) identify a zone of high bottom stress, off Cape Byron, New South Wales, which leads to upwelling events. Bottom stress could be the main physical mechanism for upwelling on the east marine coast of Australia, as the wind is mostly unfavourable throughout the year. Oke and Middleton (2001) link a bloom of dinoflagellate, in 1997, to a high nutrient concentration caused by an upwelling event. This bloom event is explained by the high bottom stress in the area and later the divergence caused by the separation of the EAC from the coast. Supporting the intrusion of water by bottom stress and as results of this research project, Brieva et al. (2015) show that a correlation exists between high bottom stress and Chla blooms off Fraser Island. Tran et al. (2015) expand on the analysis of Chla blooms, supporting that they are droved by upwelling events. Schaeffer et al. (2014) quantify the impact of bottom stress on the across shelf transport, finding that it is responsible for approximately 64% of it.

Rossi et al. (2014) examine the roles of wind stress and the EAC-shelf interaction (bottom stress) in upwelling events along the southeastern coast of Australia using remote sensing data (estimation of wind and sea surface height). From the quantification of two indices, one for each physical mechanism, bottom stress was found to have a stronger role to play in upwelling processes, along the east marine coast of Australia. Surface temperature changes have different gradients (contrast of the surface signal) due to upwelling events driven by wind or bottom stress. The temperature difference could be related to the fact that the wind pushes the water along the surface. It is the conservation of mass which supports the upwelling event in the vertical transport. At the same time, bottom stress has to do all the work, including "pushing" the water to the surface (vertical transport). The action of "pushing" water from the bottom results in a greater mixing process caused by the vertical transport, when compared to mixing resulting from wind stress which results from "pulling" the water from the surface. This difference will explain why the gradient of Sea Surface Temperature (SST) is higher during upwelling events driven by wind stress than by bottom stress.

Estimation of Chla based on remote sensing is another database used to estimate upwelling events in addition to SST. Claustre and Maritorena (2003) address the issues of using light reflection from the ocean to estimate Chla concentration in the surface. Their study highlights the limitations of assuming a relationship between phytoplankton and the light intensity, in the range of green and blue colours. A number of factors are identified which play a role in modifying the optical properties of the ocean water (reflection and absorption of light). One factor is that not all kinds of phytoplankton reflect and absorb in the same light spectrum range. Additional factors include, the coloured dissolved organic matter affecting the water's optical properties, bottom albedo, bubbles making the ocean water look greener and trapped fine desert dust in the upper layer, causing an overestimation of Chla. However, simultaneously the iron dissolved from the desert dust acts as a fertilizer for phytoplankton, resulting in a realistic increase of Chla concentration. Suthers et al. (2011) list dust as a topic poorly studied in relation to the EAC, despite it being known that eastern Australia is an area in which dust storms have been reported (Aryal et al., 2012; Gabric et al., 2010). Calibration processes aim to minimise the impact of these factors, however, the processes are based on data collected in the Northern Hemisphere. Using data only collected in the Northern Hemisphere may mean the results are not representative of the values in the Southern Hemisphere. In the Southern Hemisphere, the data should be used taking this into account.

Similar surface features resulting from wind-driven coastal upwelling events, are due to the eddies encroaching over the shelf. Both physical mechanisms displace surface water offshore, which is then supplanted by bottom water. Everett et al. (2015) describe one example, based on remote sensing, where the coastal marine water is entrained offshore by the eddy. The entrained water stays at the edge of the eddy and enhances primary production.

2.2.3 Eddies

2.2.3.1 Eddies in the Global Marine Circulation

The earth's major ocean transports have been associated with density gradients (thermohaline) and wind stress at the surface. The magnitude of water transport due to eddy activity is comparable to the large-scale wind and thermohaline-driven circulation (Zhang et al., 2014). The net eddy transport is estimated

between $30Sv$ and $40Sv$. These ocean masses of water, which rotate or spin in a quasi-circular motion (eddies), can trap masses of water, keeping their properties as heat for over a month and transporting them for long distances (Chaigneau et al., 2009). Their horizontal transport and vertical advection have been reported as the main features associated with primary production, in the Eastern Boundary Upwelling Systems (Chenillat et al., 2015). In particular, cyclonic eddies are associated with the uplifting of deep water, which enhances nutrient concentration at the surface. These eddy features have an impact on plankton distribution, eggs, larvae, pelagic species and seabirds (Chaigneau et al., 2009). The large amount of mass transport by eddies, could result in their fluctuation impacting upon the western boundary current (Zhang et al., 2014). This impact is due to the fact that approximately three quarters of eddies moved westward. Eddy formation zones are along the eastern ocean boundaries, and distinct eddy termination areas are located along the western ocean boundaries (Chelton et al., 2011).

In coastal marine areas, eddies are a path between coastal and open ocean waters, creating cross-shore transport. Results achieved by comparing mesoscale eddy resolving and non-resolving numerical models, show that the cross-shore transport reduces net primary production in the east boundary upwelling systems, together with the vertical export of nutrients and phytoplankton biomass. However, analyses of particular events resulted in enhanced primary production (Chenillat et al., 2015). The same conclusion is not applied to western boundary coastal areas, likely due to the lack of research in that area. An example of an eddy causing the entrainment of water in the East Australian coastal waters, is described by Everett et al. (2015). Entrainment of water results in enhanced surface nutrients. However, a climatology analysis of the impact of eddy activity in coastal marine production is absent along the Queensland coast of Australia. For example, from a climatology eddy analysis, eddies suppress production in the eastern boundary upwelling systems according to Gruber et al. (2011). Nevertheless, the east coast of Australia has low production levels and eddies may results in enhancing production. Liu and Levine (2016) propose that mesoscale eddies play a role in the nutrient fluxes, but also submesoscale eddies have a significant contribution. Furthermore, they propose that this is the missed key in the proposed nutrient fluxes, which are based on large-scale circulation, winter convection and mesoscale eddies. The difference of global estimations of nutrients and the proposed nutrient fluxes is associated to the aforementioned missed key, submesoscale eddies. Additionally,Liu and Levine (2016) show that the impact of submesoscale eddies is more significant in winter than in summer. However, their

spatial dimensions limit their analysis and study (Lévy et al., 2014; Mahadevan and Tandon, 2006). Lévy et al. (2012, 2014) suggest that submesoscale eddies are responsible for approximately 20% of the variability in the new production in the oligotrophic subtropics.

2.2.3.2 Eddy Avenue

Everett et al. (2012) describe eddy features in the Eddy Avenue (EA), located from 32°S to 39°S, off South-Eastern Australia. The number of eddies per day is less than in the Tasman Sea (1.6/16.8), however, their density is higher in EA than the Tasman Sea, with ∼74 and ∼62 eddies per $10000km^2$, respectively. EA's eddies show greater sea level anomalies and rotational speed than Tasman Sea eddies in a global average. All these features are based on Chelton et al.'s (2011) global eddy census. The spatial distribution shows higher concentration, in the northern section of EA, it is also there where the eddies with higher amplitudes and larger rotational speeds are located. Anticyclonic eddies in EA tend to present a positive SST anomaly (warm core) and a negative Chla anomaly, however, 33% and 15% are negative SST and positive Chla anomalies, respectively. Comparatively, 71% of cyclonic eddies have a negative SST anomaly, or cold core, and 65% a positive Chla anomaly. These values mean a higher nutrient concentration or primary productivity at the core (Everett et al., 2012). No similar coastal research was found further north than 32°S, along the East coast of Australia.

The formation of eddies can be related to two interactive masses of water with different densities and directions of transport velocity. The interaction of these two masses of water result in an instability between them, due to the shear force (Rayleigh-Taylor and Kelvin-Helmoholtz Instabilities). Eddies resulting from this interaction, are referred to here as Frontal Eddies (Everett et al., 2015). An additional mechanism reported in the formation of eddies is the lee effect. The lee effect results from the interaction of a stream, with a fixed point (e. g. islands or headland). Griffin et al. (1987) postulate that the Capricorn Eddy (Weeks et al., 2010) formation is the result of a lee effect, which is caused by the EAC flowing poleward at the Capricorn shelf-break. Kämpf (2012) describes coastal headlands, resulting in a lee effect. Jia et al. (2011) describe the lee effect in relation to eddy generation in the Hawaiian Islands. Despite no reports being found, the lee effect should be present in both Fraser Island and Moreton island,

when the EAC is in close proximity to them, particularly in the Austral spring-summer when the shelf poleward current intensifies (Wood et al., 2016). The work of Bakun (2006) supports this idea by describing the formation of eddies in the lee effect created from the interaction of major capes and along-coast flows, such as the EAC. As it is described, the shears resulting from this constant flow is particularly strong behind the cape, place where the eddies form.

Cyclonic eddies have a higher Chla concentration in Eddy Avenue than in the Tasman Sea (Everett et al., 2012). Everett et al. (2015) identify and discuss one of the factors creating this concentration difference, the entrainment of shelf water by near-coast eddies, focusing in particular on a cyclonic eddy from October, 2009. Mullaney and Suthers (2013) describe a similar event which took place in October, 2006. It is suggested that frontal eddies entrain and retain nutrients and larval fish, a very successful process for the development of fish larvae, which is therefore greatly beneficial to fisheries. Sub-mesoscale eddies ($<$ $50km$ radius) expected to result from instability, caused by shear flow and horizontal density (Kim et al., 2011), have not been studied, whilst their abundance and potential shelf water entrainment have not been quantified (Everett et al., 2015). Frontal eddies detected by Kim et al. (2011) using high-frequency radar observations show that their diameters range between 10 to $60km$, their speed ranges from 10 to $60cm/s$ and finally 70% of them (from a total of about 2200 eddies) are found within $80km$ of the coast.

There is a coastal area ($\sim$$100km$ width) highly influenced by eddies (Kim et al., 2011) mentioned in studies relating to the California Current System, an Eastern Boundary Current. This zone has been described by Gruber et al. (2011), based on results from the study of horizontal nitrogen transport. This transport has a high level of eddy-induced transport within the near shore $100km$, being particularly concentrated to the near surface ocean. Referencing this same $100km$ coastal zone, Nagai et al. (2015) highlight the important role of upwelling fronts and filaments in off shore transport, and how eddies associated with the filaments' tip are a vehicle to propagate this shelf water farther offshore.

2.3 Study Area: The Southern Queensland Coastal Marine Zone

The SQCMZ, for the purpose of this study, has been defined as the marine area between Fraser Island and the border of Queensland and New South Wales, across latitude. Across longitude, it is defined from the coastline to $100km$ offshore from the $100m$ depth bathymetry line. Sub-tropical and oligotrophic waters are present in this zone, driven by the EAC (Ward and Staunton-Smith, 2002). Section 2.2.1.2 describes the EAC in this zone. The distance covered by the EAC from Fraser Island to North Stradbroke Island is around $320km$, and $420km$ to Coolangatta (figure 2.1). This means that a parcel of EAC water would stay in the SQCMZ ($420km$) for approximately 6 to 8 days, considering an average displacement in the range 0.6-0.8m/s (Ridgway and Dunn, 2003). The following two sections describe the literature found in relation to upwelling events and eddy activity in this research's study area (SQCMZ). As no formal description of the shelf marine circulation was found, section 2.3.3 describes the sand transport aiming to create an idea of the northward transport that exists near the coast. Similarly, section 2.3.4 describes a collection of biological literature, aiming to create an idea of the marine connectivity.

2.3.1 Reported Upwelling Events in the Study Area

First reference to a possible upwelling event, along the SQCMZ, was made by Middleton et al. (1994). Their research focused on the circulation and water properties in the GBRMP as well as to the south of it. As a result, three main mechanisms are suggested for increasing nutrients along the shelf by uplifting waters. The three mechanisms are tidal flow, bottom Ekman layer transport, and coastal trapped waves. Middleton et al. (1994)'s two most southerly sets of measurements were at the North and South of Fraser Island. These measurements are stored in two sections across the shelf. Based on one set of measurements, with strongly sloping isotherms off Double Island Point, they describe a significant bottom Ekman flux, resulting from the enhanced poleward current. Additionally, a particular mass of water over the shelf, captured at station 3, has a similar temperature and salinity to water at 200-300m depth. This supports the thesis of a strong bottom Ekman flux, transporting water from a deeper offshore level over the shelf. Based on these findings, as well as the fact that this last mass of water

over the shelf has high nutrient values, the authors hypothesise that: "Strong EAC currents cause upwelling of low-oxygen, nutrient-rich water from below the salinity maximum to the shelf proper through the bottom Ekman flux." Due to unusual values of oxygen, which are lowest ($136 mmol\ L^{-1}$) under 200 meters in the Great Barrier Reef, they formulated a second hypothesis. The attribute of low oxygen, suggests that mangrove forests, which are common in this area, are the source of the water. The lack of data and literature regarding these possible sources left the question open for further studies in the future.

Dambacher et al. (2012) define eight Key Ecological Features (KEFs), in Australia's East Marine Region. Seven out of the ten initially proposed features passed the qualitative modelling applied. One final feature progressed through the methodology, being included as the last of the 8 KEFs in the marine area, off East Australia. The final feature was named "Upwelling off Fraser Island" (UFI). As Dambacher et al. (2012, pag. 4) states, the requirements to define a KEF are the basis for the model development. They are not a direct justification of the KEF's, "Which can be substantiated on other grounds." In table 4.1 of Dambacher et al. (2012), the UFI's values are productivity and connectivity; its features are: aggregation of marine life, spawning focus for temperate small pelagic fishes, residency hot spot for migrating white sharks, primary productivity via large diatoms and the contribution of the EAC-shelf interaction and transient eddies to upwelling. Rossi et al. (2014) quantify favourable conditions of bottom stress and wind stress for upwelling events. Results show that on average, bottom stress has longer favourable periods than wind stress. Furthermore, wind stress shows extended periods of unfavourable upwelling conditions, which will act to suppress other potential favourable upwelling mechanisms. These calculations were based on satellite products. Upwelling events in this area could be explained using bottom stress as discussed by Oke and Middleton (2000, 2001). The high variability of the bottom speed, described by Harris et al. (1996) in this area, could be a reason the shutdown process is overcome (section 2.2.2) and results in upwelling events. Results from Chapter 4 are part of the analysis examining the upwelling events off FI defining the SFIUS (Brieva et al., 2015).

The threats listed by Dambacher et al. (2012) for the UFI are commercial and recreational fishing, the EAC as well as changes to eddies due to climate change and shipping (oil spill and boat strike). Three anthropogenic pressures are listed: Strength of the EAC, oil spills and biomass removal due to fishing. The increasing strength of the EAC could result in enhanced nutrient concentrations

and increased seabird and turtle numbers. An increase in oil spills will result in enhanced nutrient concentrations and a decrease in seabirds and turtles. Finally, increased biomass removal will have no impact on nutrient concentrations and is ambiguous in its impact on seabirds and turtles.

2.3.2 Studies Related to Eddy Activity in the Study Area

Despite Pilo et al. (2015) being the only eddy research found to include this research study area, other studies point to interesting eddy activity there. For example, ocean stirring is related to mesoscale activity and eddy kinetic energy. Waugh et al. (2006) quantify an index to describe the stirring in the Tasman Sea. High values for this index are related to the high kinetic energy of an eddy. The results show high activity in the western Tasman Sea and low activity in the eastern Tasman Sea. However, the highest index value is located off South Queensland, falling outside the study area of Waugh et al. (2006) and is not discussed by the authors. Nevertheless, significant stirring is captured in the spacial representation of this index. Dambacher et al. (2012) include transient eddies as a physical mechanism behind the UFI (discussed in section 2.3.1). Pilo et al. (2015) describe the eddies in the EAC system and show that the main propagation is westward. Once the eddies encounter the coast, they turn southward following the EAC's direction. Eddy features described at the south of the study area, are listed in Table 2.1.

2.3.3 Vestiges of the Marine Shelf Circulation

The SQCMZ is part of the "river of sand". The river of sand refers to the transport of sand from the Sydney Basin to Fraser Island ($1500km$). The flow has been estimated at approximately $500{,}000m^3$ per year. At the Breacksea Spit, an extension to the north of Fraser Island, the sand is transported downward across the shelf break. It is the presence of quarts clastic sand, 500-700 Ma zircon grain, in a $25km$ long shelf break at the end of the Fraser Island sand extension, which leads to the conclusion about the connection with the Sydney Basin. The specific type of sand originates only in the Sydney Basin, off New South Wales. Sand is not present along the shelf break until the shelf break changes orientation, from north to north-west, intersecting the sand extension off Fraser Island, resulting in the aforementioned $25km$ section (Boyd et al., 2008).

Table 2.1: Summary of eddy features off Eastern Australia found in Pilo et al. (2015) and Everett et al. (2012), in columns 2 and 3 respectively.

Features	Pilo et al. (2015)	Everett et al. (2012)
Number of anticyclonic and cyclonic eddies	• Cyclonic 51% • Anticyclonic 49% • Total 1050	• Cyclonic 50.2% • Anticyclonic 49.7% • Total 2613
Propagation Direction	It is mainly westward, turning southward once they reach the shelf break.	no description
Propagation Speed $[km/day]$	• Cyclonic: 3.2 • Anticyclonic: 3.1	no description
Rotation Speed $[cm/s]$	• Cyclonic: 21.1 • Anticyclonic: 20.1	• Cyclonic: 45 • Anticyclonic: 50
Radii $[km]$	• Cyclonic: 83.4 • Anticyclonic: 82.7	• Cyclonic: 92 • Anticyclonic: 95

It is suggested that the East Australian Longshore Transport System, previously named the "River of Sand", is driven by wave-generated northward currents. At the Breacksea Spit, the tidal ebb flow coming out of Hervey Bay, opposes the sand transport due to wave-generated currents, resulting in the formation of the sand extension off Fraser Island (Breacksea Spit) (Boyd et al., 2008; Schröder-Adams et al., 2008). The shelf section, off Fraser Island, is a transition zone between tropical carbonates, from the Great Barrier Reef, to the cool-water carbonates, at the south. The variations in the type of carbonates supports the thesis of a diversion of the sand transport in this zone (Schröder-Adams et al., 2008).

2.3.4 Evidence of Connectivity from Pelagic Migrations

Ward et al. (2003) found a similar behaviour in some temperate pelagic fishes' migration and spawning, in Southern Queensland, to those described off the east coast of North America. The fish migrate equatorward to spawn, later their eggs and larvae are transported poleward. As mentioned by Ward et al. (2003), some sections of the east coast of Fraser Island are closed to all forms of fishing, or under seasonal fishing restrictions, specifically at Indian Head. These are accepted areas of spawning, however, they lack substantial studies to support this assumption. Their results show a clear increase in the density of eggs, larvae and mean monthly catches from June to November, with maximum values identified around September (Ward and Staunton-Smith, 2002; Ward et al., 2003). A connectivity numerical analysis, completed by Roughan et al. (2011), shows a poleward transport of particles, which is in agreement with the poleward transport of eggs and larvae. However, connectivity matrices and the probability of particle density do not show an inshore equatorward transport, which could support the migration and sand transport (section 2.3.3).

2.4 Summary

The SQCMZ is between the GBRMP, at the north, where the formation of the EAC is found, and New South Wales, at the south, where the separation of the EAC takes place, resulting in the Tasman Front also an area of high eddy formation. Due to the EAC transport, the SQCMZ is under the influence of waters

from the GBRMP and is, therefore, connected to it in a single direction (water transported to the SQCMZ). Similarly, the SQCMZ is connected to marine coastal zones further south, off New South Wales, by the EAC. This latter connection may occur in both directions, given that the River of Sand and migration of pelagic fishes, who migrate to spawn in Fraser Island and Sunshine coast, reveal an inshore equatorward current as reported by Hamon et al. (1975) based on ships' drift. The inshore current carrying sand northward (River of Sand) has not been explored in recent years, and further studies are required to establish a description of the SQCMZ marine connectivity and circulation. This is necessary due to the lack of a description of the cross shelf transport, including bottom layer transport (EAC-shelf interactions) and offshore transport (eddies).

Middleton et al. (1994) point to a potential upwelling mechanism off Fraser Island based on a cross section capturing a mass of water with features consistent with deeper water, the only exception being the oxygen features. Highlighted in their research is the need for further studies as the lack of data resulted in an inconclusive explanation regarding the mechanism(s) behind this particular mass of water. Dambacher et al. (2012) define the "Upwelling off Fraser Island" as one of the eight KEFs, in Australia's East Marine Region. The study mentions Middleton et al. (1994) as the principal description of a physical observation in the study area of a possible upwelling event. Similarly to Middleton et al. (1994) they list the EAC-shelf interaction as one of the physical mechanisms. An additional mechanism listed is transient eddies, however, no reference was found to support this mechanism. Other sources of information include biological research showing a hot spot area for spawning and migration (e.g. description of small pelagic fish and shark migrations). These features point to high levels of nutrients, which agrees with the idea of upwelling events. More expansive research has been carried out on this topic for the New South Wales coastal marine zone, when compared with Southern Queensland. These studies enhance the thesis of the EAC-shelf interaction as a physical mechanism behind the upwelling. Rossi et al. (2014) shows the current driven upwelling conditions are present for a longer period than wind-driven conditions. The study area is mostly subject to southerly winds, throughout the year, which is favourable to downwelling, suppressing upwelling events. Bottom stress (the EAC-shelf interaction) has not been addressed off Fraser Island to identify a relationship with upwelling events, as has already been done off New South Wales.

Descriptions of eddies have been carried out off New South Wales, showing

their important role in the across shelf transport. These are usually studies focusing on individual events. Two studies describing the eddies off the east coast of Australia include: Everett et al. (2012) and Pilo et al. (2015), with only the latter including the SQCMZ. It has been reported that eddies within $100km$ offshore of the shelf break have an important role in the across-shore transport and primary production (Nagai et al., 2015). It is expected that the formation of eddies would be seen in areas of high instability such as the EAC intensification zone (that could be an important instability for eddy formation), however, the role of near coast eddies and their impact in the SQCMZ is unknown due to a lack of research addressing this topic.

To expand the current knowledge regarding the SQCMZ marine circulation, further study is required about the EAC behaviour (in its intensification zone), the inshore equatorward current, potential physical mechanisms involved in upwelling events (particularly off Fraser Island), NCEs and their impact on the shelf marine circulation. This research project aims to increase knowledge regarding the aforementioned topics. Satellite products are used to contribute new information and understanding of the Upwelling off Fraser Island, as well as to create an initial description of eddies within the study area. A survey which deployed 5 moorings off Brisbane will provide new information regarding EAC behaviour in the intensification zone. Finally, analysis of results from numerical models will expand understanding of the near shore equatorward current. All previous research outcomes contributed to an increased understanding of the marine circulation and connectivity off the SQCMZ.

Chapter 3

Data and Methodology

The research project and its description have been organised into two phases. In the first phase, the description of phenomena is based on observations (e.g. estimations founded on remote sensing, marine moorings and weather stations). In the second phase, the description is constructed using numerical modelling products (BRAN3.5 and the implementation of ROMS for the study area). Chapters 4 and 5 are part of the first phase, where the frequency and characteristics of upwelling events and NCEs are quantified for the first time in the SQCMZ. Sections 3.2.2 and 3.2.3 summarise the methodologies used in phase 1, whilst Section 3.2.4 summarises the methodologies used for the numerical descriptions in phase 2. Following the second phase, chapter 6 describes features in the circulation over the shelf identified in the examination of the numerical representations. These features are the links required to design a model of marine dynamics in the SQCMZ, including the findings described in chapters 4 and 5. With the purpose of simplifying the description of methodologies in phases 1 and 2 (see sections 3.2.2, 3.2.3 and 3.2.4), databases and tools are initially described in sections 3.1 and 3.2.1, respectively, later being referenced in the description of methodologies of chapters 4 to 6, in sections 3.2.2, 3.2.3 and 3.2.4 respectively. The questions relating to chapters 4 to 6 are listed as three points in chapter 1 (page 3) .

3.1 Data

The main source of data in this research project is the IMOS - an initiative of the Australian Government being conducted as part of the National Collaborative

Research Infrastructure Strategy and the Super Science Initiative.

3.1.1 Estimations based on Remote Sensing

Five variables estimated using remote sensing were obtained for this research project. Four of these variables were used extensively: surface concentration of Chla, SST, Sea Surface Height anomaly (SSHa) and wind velocity. The fifth variable, K-490 was used for a single analysis to estimate mean optical depth (Mueller and Lange, 1989; Trees et al., 2000) and to define a minimum depth (maximum optical depth) to be used in Chla estimations. By using the Chla estimations in water deeper than the maximum optical depth, the bottom albedo is negligible in the analysis. Table 3.1 lists the main features of these four products. IMOS provides Chla, SST and K490 as a single product, all of which are sensitive to cloud cover. Wind velocity (SeaWind) is provided by NOAA through one of its FTP servers. The wind velocity data is analysed and used in chapter 4 to examine and characterise wind in relation to upwelling events. SSHa is provided by IMOS through an OpenDAP server of AODN, whilst a second SST is obtained from NASA (Jet Propulsion Laboratory (JPL)), who interpolate the values where there is cloud cover. Chapter 5 utilises SSHa for detecting eddies and quantifies the approximated gradients of Chla and SST (JPL) between the core and the edge of the eddies. The purpose of shifting from IMOS to JPL in the SST was to increase the number of temperature gradients, as the latter product fills in gaps resulting from cloud cover.

Brown and Minnett (1999) describe the algorithms for SST and O'Reilly and coauthors (2000) describe the algorithms used to estimate Chla concentration based on remote sensing, including the OC3. The data used in this research project is Chla estimated using the OC3 algorithms from the MODerate resolution Imaging Spectroradiometer (MODIS). The issues of using estimated Chla from remote sensing (over- or underestimations) are discussed by Claustre and Maritorena (2003). The impact of coloured sediment and bottom albedo in coastal water is known and efforts have been made to develop algorithms that better estimate Chla in coastal water, for example Cannizzaro and Carder (2006). Increasing iron experiments in the water results in Chla blooms (Abraham et al., 2000). Iron is present in dust, particularly in Australia, the impact of dust on the estimation of Chla has been related to increased Chla concentrations (Gabric et al., 2010). For example, the Australian dust storm in 2009

Table 3.1: Summary of the characteristics of the remote sensing data used in this research project's analysis. Period described in first row refers to the period used in this study analysis, however, all the databases are up to date with few days lag. The name of each data source has associated the link to the formal network address.

Features	Chla/SST/K-490	SST	SSH	Wind
Institution	IMOS	JPL / NASA	IMOS	NOAA
Period analysed	From 2002 to 2015	Middle 2012 to 2015	From 1993 to 2015	1990/01/01-2014/01/31
Total duration (Years)	∼13.5	∼ 13.5	23	26
Spatial Data Density (data per distance)	$1.2km$	0.011 degrees (longitude and latitude)	1/5 degree (longitude and latitude)	1/4 degree (longitude and latitude)
Temporal resolution	daily	daily	Every two days 1993-2010 daily 2011-2015	6 hrs
Source	CSIRO OpenDAP server	NASA OpeNDAP server	AODN OpenDAP server	NOAA ftp server
Reference Link	CSIRO server	NASA, Jet Propulsion Laboratory		NOAA/NCDC Blended 6-hourly 0.25-degree Sea Surface Winds
Citation	(IMOS, 2014a, 2015b)	(Brown and Minnett, 1999)	(IMOS, 2015a)	
Units	mg/m^3 $^\circ C$ $1/m$	$^\circ C$	m	m/s

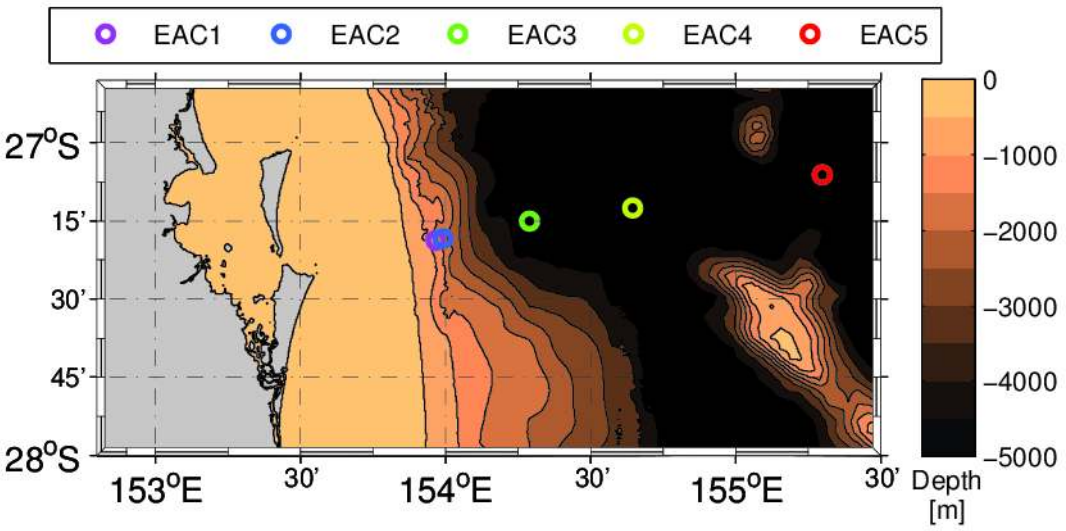

Figure 3.1: Circles represent the location of the moorings deployed by CSIRO from April 2012 to August 2013.

(Aryal et al., 2012) impacted Chla values, resulting in a sudden increase in concentrations along the east coast of Australia. The second SST data set was obtained from `ftp://mariana.jpl.nasa.gov/mur_sst/`, funded by NASA's Making Earth System data Records for Use in Research Environments (MEaSUREs) Program in Science Mission Directorate. The advantage of using this product over the IMOS product is its ability to estimate data in areas where the IMOS does not (Chin et al., 2013).

3.1.2 Mooring Data

Five moorings were deployed off Brisbane (27°S) across the shelf break to the abyssal waters, from April 2012 to August 2013 (∼17 months). Variables measured by the moorings were velocity profiles (ADCP), velocity at one point (current meters), temperature (CTD and transistors) and salinity (CTD). The data set is distributed by IMOS through a FTP server of French Research Institute for Exploitation of the Sea (IMOS, 2014b). CSIRO Marine and Atmospheric Research (CMAR) deployed and retrieved the moorings. Ridgway and Sloyan (2012, 2013) describe both the process of deploying and retrieving the moorings, as well as the array for each one. Figure 3.1 illustrates the position of the moorings. This research project refers to this database as the Eastern Australian Current moorings 2012-2013 (EACM1213).

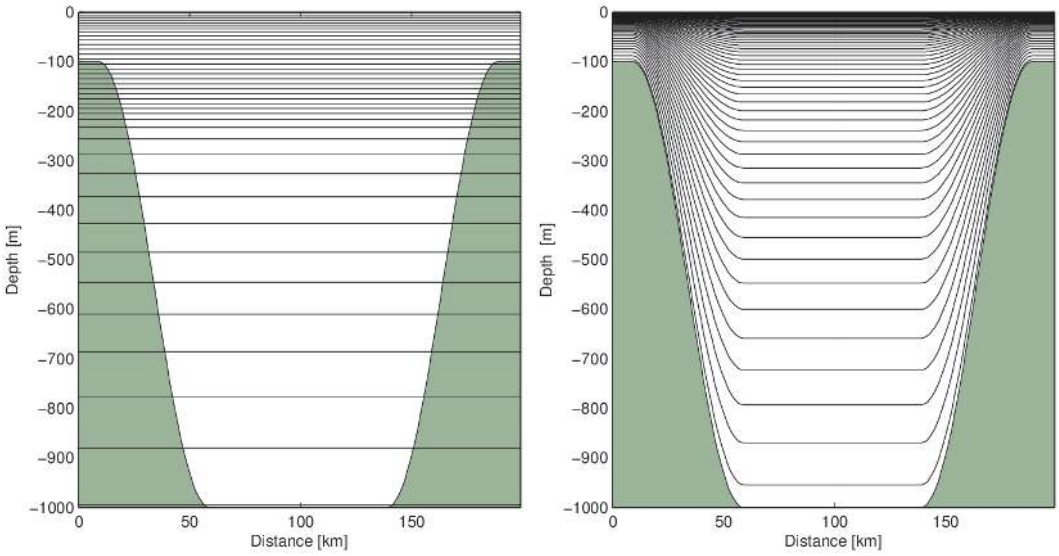

Figure 3.2: Illustration of vertical coordinates of BRAN3.5 (left) and ROMS (right) in a hypothetical bathymetry. BRAN3.5 last coordinate is approximately at $4500m$.

3.1.3 Wind from the Australian Bureau of Meteorology's stations

Wind records were provided by the Australian Bureau of Meteorology (BOM) from a set of land stations in Southern Queensland. From the set of land stations, a group of 11 stations near the coast were selected for the analysis. Table 3.2 lists the 11 stations, their coordinates and periods of wind recordings. The shortest time series used was 10 years, from station 040478 (Fraser Island Eurogen) and the longest were 56 years from three stations: 039085 (Sandy Cape Lighthouse), 040068 (Double Island Point LightHouse) and 040043 (Cape Moreton Lighthouse). The measuring frequency is inconsistent, varying between every 3hrs or 6hrs, wind velocity magnitude is measured in m/s. All data was provided in ASCII files which were read in Matlab.

3.1.4 BLUElink Reanalysis version 3.5

BLUElink ReANalysis version 3.5 (BRAN3.5) is based on the Ocean Forecasting Australian Model version 2 (OFAM2), using the Bluelink Ocean Data Assimilation System (BODAS). BRAN3.5 has undergone an extensive improvement process to achieve more accurate results (Andreu-Burillo et al., 2010; Brassington

Table 3.2: List of BOM stations used in the wind analysis along the southern coast of Queensland, Australia.

Station ID	Station Name	Coordinates (long , lati)	Period (year/month/day)
039085	SANDY CAPE LIGHTHOUSE	153.2083, -24.7297	1957/01/01-2013/12/04
040478	FRASER ISLAND EURONG	153.1292, -25.5047	1989/03/02-1999/04/30
040068	DOUBLE ISLAND POINT LIGHTHOUSE	153.1906, -25.9319	1957/01/01-2013/12/11
040861	SUNSHINE COAST AIRPORT	153.0903, -26.6006	1994/07/05-2013/12/11
040040	CALOUNDRA SIGNAL STATION	153.15, -26.8017	1970/09/07-1992/12/02
040043	CAPE MORETON LIGHTHOUSE	153.4661, -27.0314	1957/01/01-2013/12/11
040209	POINT LOOKOUT	153.5456, -27.4361	1997/02/05-2013/12/10
040764	GOLD COAST SEAWAY	153.4283, -27.939	1989/11/17-2013/12/11
040190	SOUTHPORT RIDGEWAY AVE	153.4056, -27.9829	1957/01/01-1992/01/10
040717	COOLANGATTA	153.5053, -28.1681	1987/10/01-2013/12/11
040052	COOLANGATTA BOWLS COMP	153.5383, -28.1783	1972/12/01-1981/10/31

et al., 2007; Oke et al., 2008, 2005). Oke et al. (2013) describe the configuration and set up of BRAN and table 3.3 summarises some of its features. The period simulated by BRAN3.5 is from 01/01/1993 to 31/07/2012. The vertical resolution is higher near to the surface and decreases with depth, meaning there are 14 points of data in the first 100m (over the shelf). The deepest point in the BRAN3.5 grid is located at approximately 4500m, with the closest point to the surface being at 2.5m (figure 3.2). The physical variables available are the velocity field (u, v and w), salinity, temperature and surface heigh.

Data was accessed through the CSIRO OpenDAP server using a bash script under a Unix operative system (Ubuntu), allowing individual sections of the data to be downloaded, minimising the issue of storage space. The downloaded data is delimited by 148.8°E to 172.1°E and 20.5°S to 38.2°S. The data contains all the aforementioned physical variables for each day of the whole period simulated by BRAN3.5 (1993-2012). The final database is comprised of monthly NetCDF files which also contain daily data for the aforementioned area.

3.1.5 Bathymetry

Bathymetry was obtained from the Geoscience Australia (Whiteway, 2009). The database is divided into two, the Western and Eastern sections of Australia. This study uses the second section delimited by 132°E to 172°E and 8°S to 60°S. The database describes bathymetry (under water) and topography (land). The resolution is 0.0025 degrees latitudinally and longitudinally ($\sim 260m$ near the study area). The data is stored in an ASCII file and a head file, the latter describes the number of elements and how they are stored in the ASCII file. Using a script written in Matlab, the data was transformed into a NetCDF file. The transformation of the file format results in a 15999×20804 matrix stored in the NetCDF file. The Geoscience Australia's webpage was the source of the equation used in the estimation of distance between two points throughout the research project (Spheroidal model for the Earth1).

Table 3.3: List of main features of BlueLINK Reanalysis (BRAN3.5) and the implementation of ROMS_AGRIF.

Features	BRAN3.5	ROMS AGRIF
Name of numerical code used for calculations	OFAM2 based on Modular Ocean Model version 4.1(MOM4p1) (Griffies et al., 2005)	ROMS AGRIF
Type of Grid	Structured Grid	Rotated Structured Grid
Vertical coordinates	Regular with variable resolution	Sigma layers
Period represented	01/01/1993 - 31/07/2012	Climatology: loop of 10 years Year 2010: loop of 5 year
Horizontal Spacial resolution	1/10 degrees around Australia	Variable resolution in the range of 2km to 3km
Topography	Smith and Sandwell (1997)	Geosciences data base
Temporal recording frequency	Daily	Daily

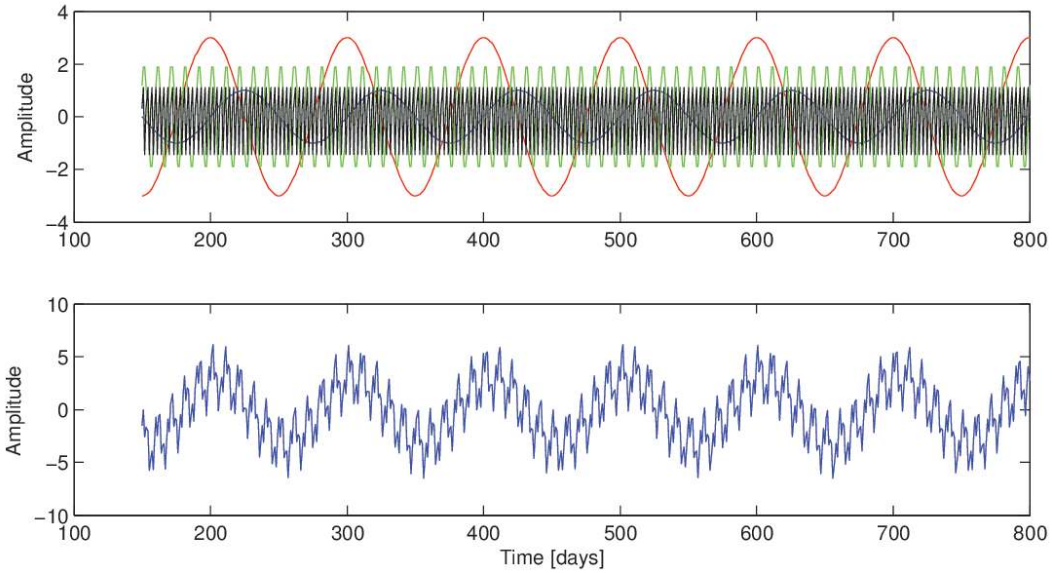

Figure 3.3: Synthetic time series used to validate the scripts with the Fourier and Wavelet Analysis. The top graph shows the four synthetic time series separately. The bottom graph shows the time series resulting after the addition of the three synthetic time series.

3.2 Methodology

A set of tools were implemented in this research project, these are described below. The following described tools are implemented by the candidate and the team behind their creation and development are referenced. Analysis scripts written by the candidate are described in sections 3.2.2 to 3.2.4, discussing the methodology as well as the approach to the study and data analysis.

3.2.1 Tools

The first two tools described in sections 3.2.1.1 and 3.2.1.2 are part of the analysis carried out in chapter 4, which is the examination of upwelling events. The frequency analysis is applied to physical mechanisms discussed in chapter 2 which drive upwelling events along the coast (bottom and wind stresses). The results from an implemented eddy detection and tracking tool (section 3.2.1.4) are the basis for the study of NCEs in chapter 5. The last tool is a numerical model (ROMS) implemented to examine submesoscale features that BRAN3.5 was unable to resolve.

3.2.1.1 Fourier and Wavelet Frequency Analyses

The Fourier Analysis was implemented according to Matlab help[1] based on the Discrete Fourier Transform (DFT). The script was tested using a synthetic time series created by the candidate. The use of a synthetic time series allows the results of the Fourier analysis to be known, validating its implementation in the research project. Figure 3.3 illustrates the synthetic time series (STS). The period, phase and amplitudes are listed below indicating the colour of the line representing each STS in figure 3.3, top graph.

- STS 1: Period 100 Phase 0 Amplitude 1 (blue line)
- STS 2: Period 100 Phase 25 Amplitude 3 (red line)
- STS 3: Period 10 Phase 1 Amplitude 2 (green line)
- STS 4: Period 3 Phase 0.1 Amplitude 1.5 (black line)

A similar process was completed for the Wavelet analysis based on the Matlab script distributed by Torrence and Compo (1998)[2]. Daubechies (1990) addresses the theory behind the Wavelet analysis, therefore, it is not included in this document. In the research project this frequency analysis method is used to analyse the marine time series. The wavelet base function used is Morlet (Morlet et al., 1982), similarly to other studies (Combes et al., 2015; Corredor-Acosta et al., 2015; Everett et al., 2014). Figure 3.4 illustrates the results from both, Fourier and Wavelet analyses. The frequencies identified by both analyses correspond to the periods listed for the 5 STS, this result demonstrates that the scripts written are correctly implemented and accurate.

3.2.1.2 Maximum-cross correlation

The method of maximum-cross correlation is predominantly used for tracking purposes, e.g Abraham and Bowen (2002), Bowen et al. (2002) and Bowen et al. (2005). By comparing two images it is possible to obtain the two dimensional lag (usually x and y) for the maximum correlation. For tracking purposes, the lag is transformed into velocity, describing the displacement from one image to

[1] http://au.mathworks.com/help/matlab/ref/fft.html
[2] http://atoc.Colorado.edu/research/wavelets/

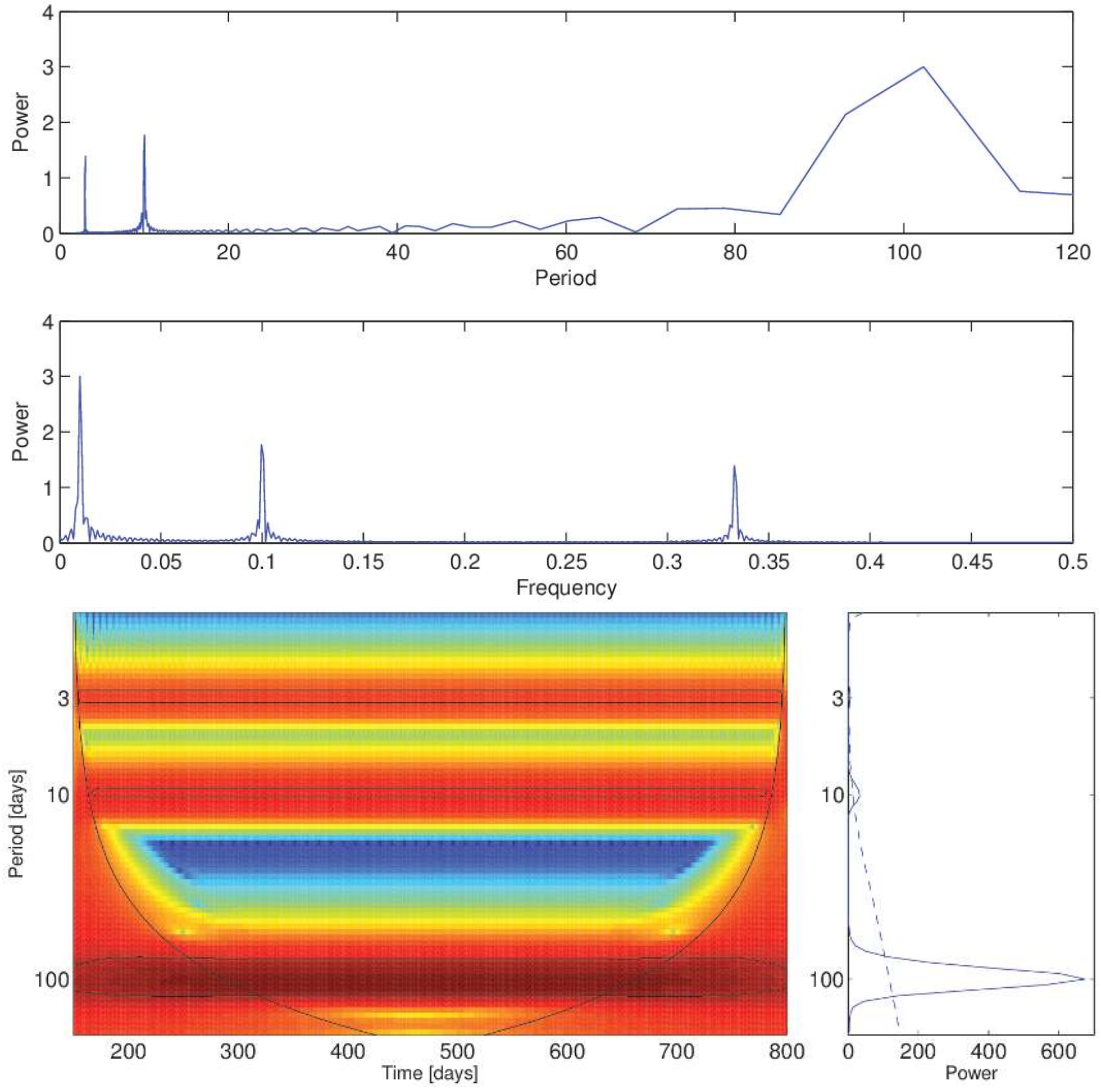

Figure 3.4: Main periods detected by the Fourier (top two graphs) and Wavelet (bottom two graphs) analysis.

the next. In the case of this research, the method was implemented to obtain an approximate distance of water displacement between the climatology figure of bottom stress and the composition figure of Chla off Fraser Island.

3.2.1.3 Eddy detection and tracking tool

Geometrical and dynamical methods are the most utilised in eddy detection (Chaigneau et al., 2009; Chelton et al., 2011; Halo et al., 2014b; Mason et al., 2014; Nencioli et al., 2010). The chosen eddy detection and tracking tool (EDTT) is described by Halo et al. (2014a). It was selected as it uses both detection systems (geometric and dynamical). There are 4 parameters required to implement the detection: distance between the isolines of SSHa, maximum radius (to avoid, for example, the detection of gyres), maximum value for the Okubo-Weiss parameter (Okubo, 1970; Weiss, 1991) and the number of times a Hanning filter needs to be applied to make the Okubo-Weiss parameter less noisy. The scripts are written for Matlab and the complete tool is distributed through http://www.simocean.org.za/tooleddy.php. The code was modified to read the SSHa data from IMOS (section 3.1.1) for the whole recorded period. The input parameter for the maximum value of the Okubo-Weiss parameter was set to 0 and later in the selection process this parameter could be altered to the desired value by filtering for another value.

The geometrical detection looks for closed loops in the SSHa contour graph. The distance between each contour line is defined by one of the input parameters. Following the detection of a closed loop, the next step is to quantify the Okubo-Weiss parameter. Henson and Thomas (2008) summarise the purpose of this parameter as being to separate the vorticity from the strain, based on the velocity field. The EDTT looks for areas within the closed loop where the vorticity dominates as a result of the eddies rotation. The minimum possible radius is defined, in the code, as the radius of a circumference with an area equivalent to the area of 4 pixels of the SSHa data. The EDTT does not consider an event to be an eddy if the closed loop contains less than four pixels of data (the restriction is in `get_one_eddy.m` line 168). The resolution of the SSHa data is 0.2 ($\sim 20km$), therefore, the minimum radius is described by equation 3.1, meaning the EDTT should not detect eddies with a radius less than $\sim 22.6km$. The Chelton et al.'s (2011) census used a minimum of 8 pixels, resulting in a minimum radius of approximately $39.9km$ for a database of 0.25 degrees of resolution.

$$r = \sqrt{(20km \cdot 20km \cdot 4)/\pi} \approx 22.6km \tag{3.1}$$

Once the eddies have been detected and tracked they are stored in a database. Two terms are used to reference the eddies detected by the eddy detection and tracking tool, these are "detected eddies" and "eddy events". An eddy event is a set of detected eddies which the code has tracked and considered to be a single event throughout time.

3.2.1.4 Regional Ocean Modelling System

ROMS_AGRIF (Debreu et al., 2011; Penven et al., 2006) is based on ROMS with the property of scaling a selected area by nesting a grid with higher resolution (AGRIF). IRD and INRIA are the main institutions supporting its development. ROMS_AGRIF is currently evolving into the Coastal and Regional Ocean Community model (CROCO), a non-hydrostatic numerical model. ROMS_AGRIF has a set of Matlab tools to complete or support post- and pre-processing (Penven et al., 2007, ROMSTOOL). The numerical model considers the Boussinesq and hydrostatic approximations.

The first implementation of ROMS_AGRIF was at a local work station where the upwelling example was completed and successfully simulated. Following the model implementation, a climatology configuration for the SQCMZ was run over a few days (refer to section 3.2.4 for details). In the next step, configuration files (initial conditions and forcing files) for the created scenario of the SQCMZ were moved to the University of Southern Queensland (USQ)'s High Performance Computer (HPC). A relocation of the model took place after approximately 10 months of technical issues in the implementation of the numerical model's source code at USQ's HPC. Dr. Francis Gacenga facilitated a solution, looking for an external HPC to implement the model and solve the SQCMZ scenario (these two activities are referred to in this study as "run the model"). Finally, the model was implemented and run at Central Queensland University (CQU)'s HPC. With the support of Jason Bell the model was running in less than a week.

Following the configuration of the numerical model in solving the marine circulation of the SQCMZ and before the models calculations were initiated, a key step had to be undertaken to identify the optimal configuration for the parallel mode based on MPI. The main idea is to find the number of subsections resulting

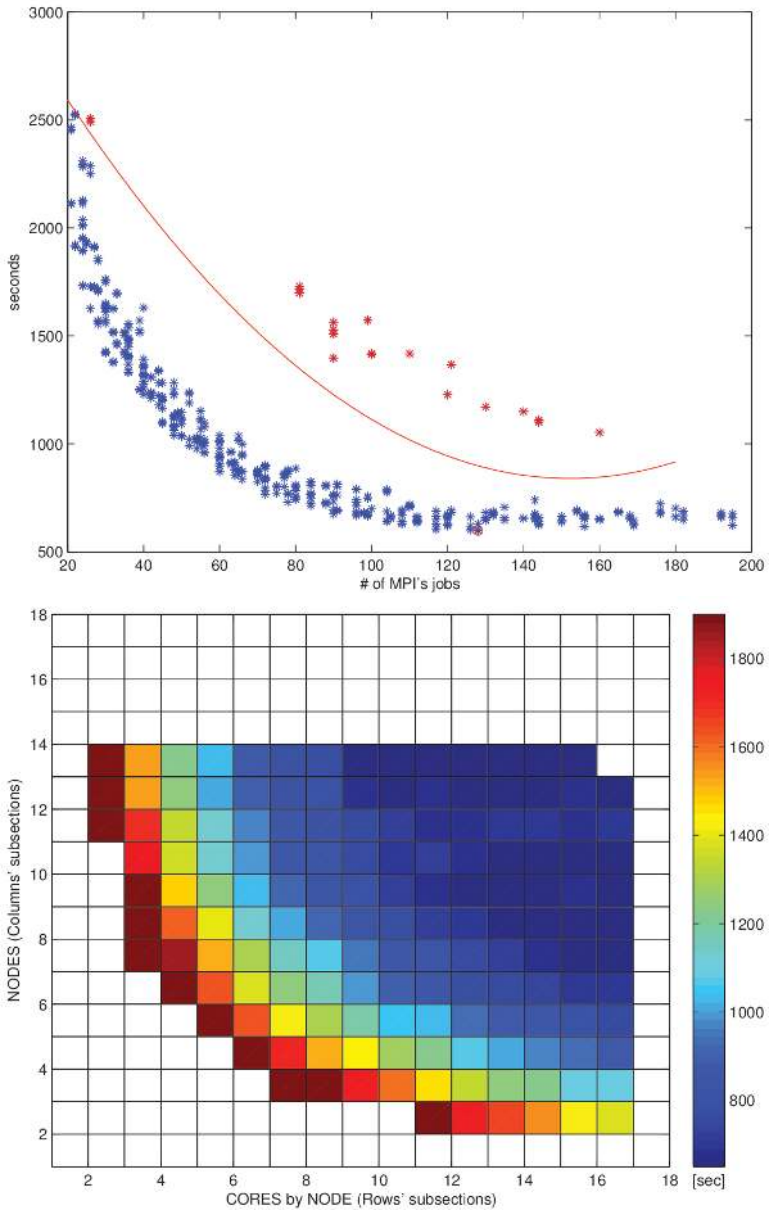

Figure 3.5: Performance of ROMS implementation in CQU cluster. Top graph illustrates the time required to run a short simulation versus the number of divisions of the grid that result in the number of MPI subjobs. Values over the red line are potentially calculations that took longer to initiate for some unexplored reasons, possibly related to technical details related to the data reading and loading. The bottom graph extends the top information by showing the time required in relation to the number of nodes and cores per node used.

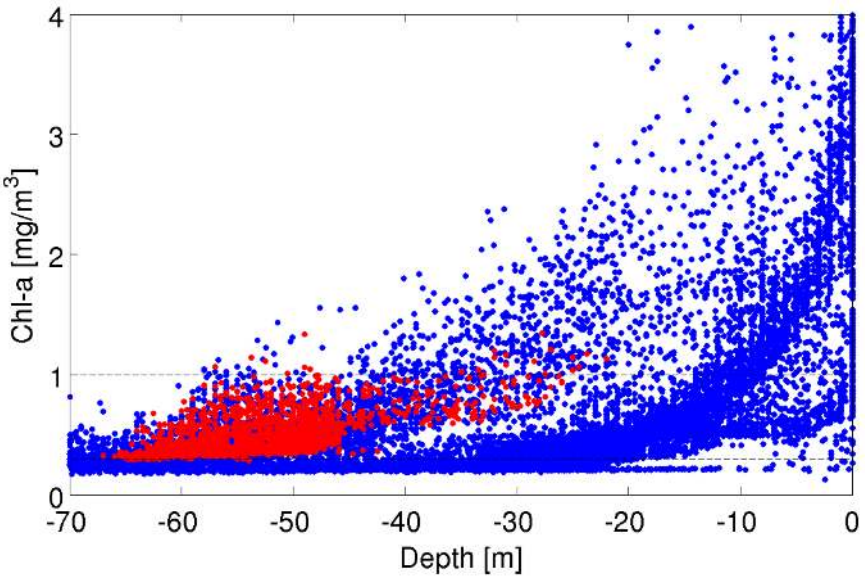

Figure 3.6: Average of Chla versus bathymetry showing the exponential increase of Chla estimations as the water becomes shallower. The area evaluated is from 152°E to 154.0°E and from 24°S to 26.5°S. Red dots illustrated just the section off Fraser Island.

in the best performance (least time to solve the same number of steps). The results are illustrated in figure 3.5 with the top graph showing a clear improvement (less time in the y-axis) by increasing the number of subsections (x-axis). The bottom graph shows the average time required to solve it according to the number of nodes and cores. The last graph leads to the conclusion, as mentioned in the parallel simulations, that the best performance was observed when using the maximum number of cores per node (blue colours at the right side). However, the number of nodes for which the maximum performance is observed was not identified, as the performance continues to improve (blue colour in top) up to 12 nodes. Finally, the model was implemented using the maximum number of cores allowed which was 192 (12 nodes times 16 cores).

3.2.2 Examination of Upwelling Events

The observation of Chla evolution throughout time led to the identification of a set of common Chla bloom patterns (animations B.1 and B.2). The analysis and characterisation of these patterns led to the definition of two upwelling systems in the SQCMZ. The role of bottom and wind stress in these Chla blooms are explored in chapter 4.

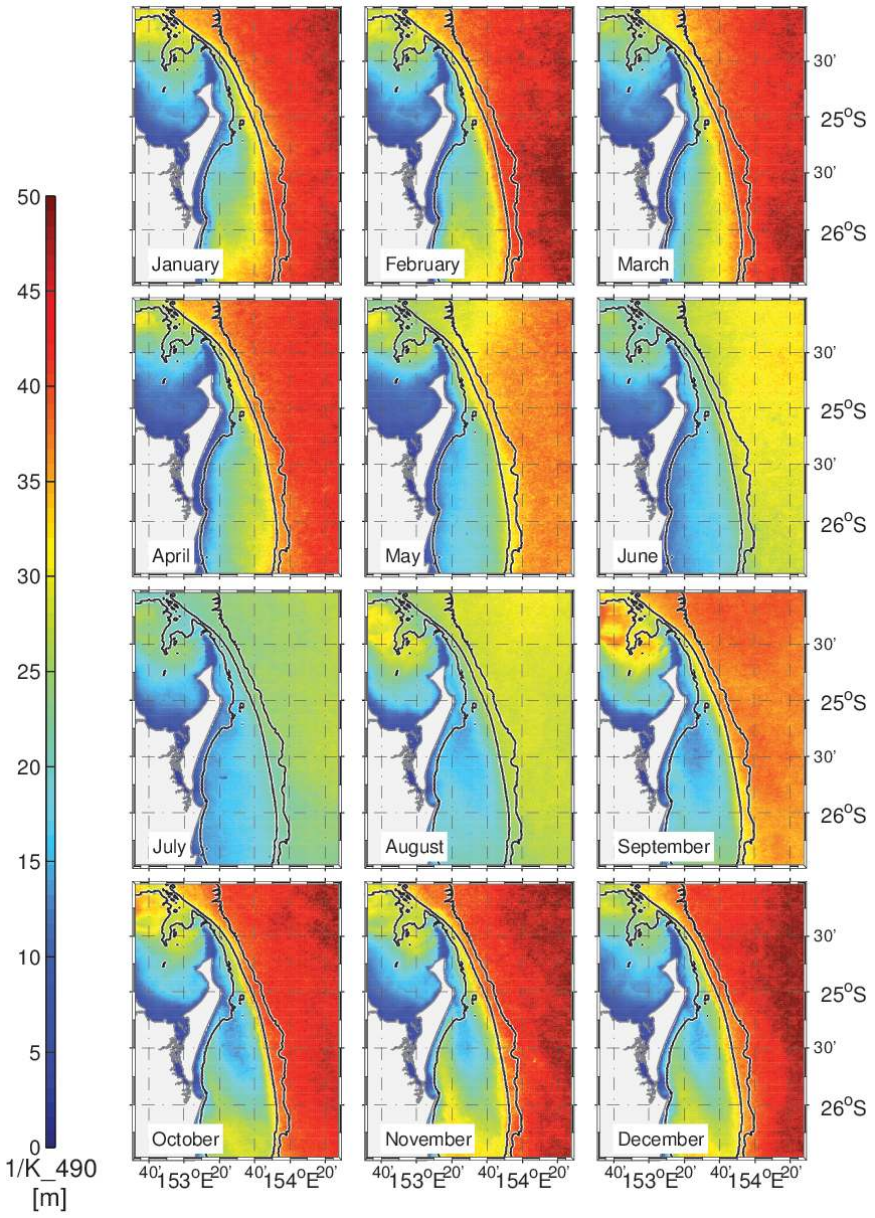

Figure 3.7: Monthly averages of 1/K490, which can be used as a proxy of the optical depth (Mueller and Lange, 1989; Trees et al., 2000).

3.2.2.1 Chlorophyll-a Pattern Classification

As previously mentioned in section 3.1.1, estimation of Chla surface concentration in shallow waters is sensitive to many factors, such as the bottom albedo. The sensitivity to bottom albedo as well as high concentrations of sediment in the water can result in an overestimation of Chla concentrations. Figure 3.6 shows Chla values versus their depth according to the bathymetry database (section 3.1.5). The increase in Chla concentration, occurring as the depth decreases, resembles an exponential increase. The relationship between Chla and shallow water could be a "realistic" incrementation of Chla as well as an overestimation. This study does not solve the question "Is the estimation of Chla an accurate value in shallow waters or not?". However, this study restricted the analysis of Chla to water deeper than $40m$ to avoid that question, due to the lack of Chla measurements in shallower waters in the SQCMZ. The selection of $40m$ as the minimum depth is based on figure 3.6 where the exponential increase begins between $30m$ and $40m$. Waters deeper than $40m$ do not show an exponential relationship with depth, the increments observed are blooms of Chla. A second method used in the estimation of average maximum optical depth in this zone was employing the inverse of K-490 (Mueller and Lange, 1989; Trees et al., 2000). Using the inverse of the K-490, makes it possible to obtain an approximate optical depth. Figure 3.7 illustrates 1/K-490 in monthly climatology averages. For the open ocean, the optical depth reaches its deepest values around $40m$, supporting the aforementioned estimation.

Considering known factors that may result in upwelling events (see section 2.2.2), as well as an initial visual inspection of Chla surface concentrations, two potential patterns of Chla values could be defined. Spatial climatological description is based on the average of a set of events classified as one of the main patterns observed, which was one that had sufficient (>70%) remote sensing data available. A rectangular area over the pattern was selected to quantify the cloud cover. The area is defined by the longitudinal range 153.25°E to 154.0°E and the latitudinal range 26.5°S to 25°S.

3.2.2.2 Wind Analysis

The format in which wind data is stored by the Australian BOM is not vectorial, which is the system used in this study. Figure 3.8 illustrates the difference between

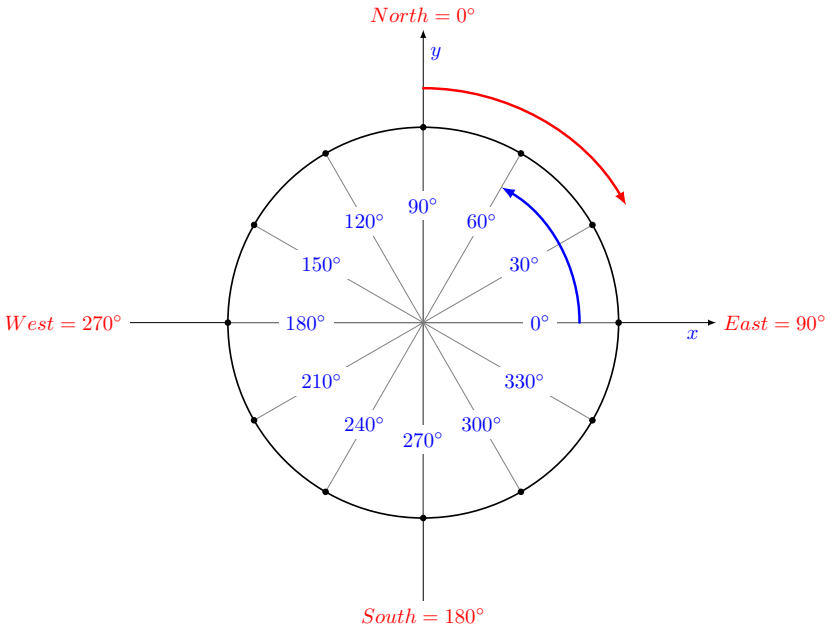

Figure 3.8: Wind direction format of Australian BOM data is described by red (clockwise rotation) indicating where it is coming from. Blue describes the system used in this study (anticlockwise rotation) which allows for the use of sine and cosine to decompose a vector and point to where the wind is heading.

both systems. Through personal communication with the Australian BOM, see below how the system is described.

- North (N): 0° = 360°
- East (E): 90°
- South (S):180°
- West (W); 270°

To maintain the vectorial system, the Australian BOM wind data was transformed. Equations 3.2 and 3.3 describe the transformations required for this, including the transformation of wind direction (from where it comes to where it is heading). The wind analysis was completed using the west-east and south-north components of the wind, due to the orientation of the study area's coast line is almost parallel to the latitude coordinates.

$$W_u = -\left|\vec{W}\right| \sin\theta_W \tag{3.2}$$

Table 3.4: Definition of wind drag coefficient (C_D) according to the wind conditions (w) following Smith (1980).

Wind Conditions	C_D
$w < 6m/s$	1.1×10^{-3}
$6m/s < w < 22m/s$	$(0.61 + 0.63u)/10^3$

$$W_v = -\left|\vec{W}\right| \cos\theta_W \tag{3.3}$$

The estimation of wind stress (τ^W) is described by Kowalik and Murty (1993, page 27), including the equation 3.4. The variables of the equation are wind drag coefficient (C_{10}), air density and wind (W) at $10m$ above sea level. The value described for the average air density is $1.2{\times}10^{-3} g/cm^3 d$ and the wind drag coefficient has a maximum of $2.7{\times}10^{-3}$.

$$\tau^W_{x,y} = C_{10}\rho_a \left|\vec{W}\right| W_{x,y} \tag{3.4}$$

The wind is recorded by land-stations, meaning it requires pre-processing to obtain a wind estimation over the ocean at a height of $10m$. Wood et al. (2012) found a superior representation of wind at ocean moorings from a lineal transformation applied to land-station wind recorded off Sydney, rather than wind based on remote sensing. Equation 3.5 describes the linear transformation. The next step is to adjust the altitude to the agreed $10m$. The adjustment is made following the description provided by Gill (1982) is represented in equation 3.6.

$$W^{sea}_{x,y} = 1.80 + 0.96 \cdot W^{land}_{x,y} \tag{3.5}$$

$$W^{10m} = W^h \left(\frac{10}{h}\right)^{1/7} \tag{3.6}$$

At this point it is possible to estimate the wind stress from equation 3.4. The wind drag coefficient is used following the description by Smith (1980) who define it according to the wind conditions. Table 3.4 summarises the drag coefficient values according to the wind conditions. To implement the aforementioned transformations as well as the estimation of wind stress, a Matlab code was written. Eleven time series (table 3.2) of estimated wind stress along the coast of the SQCMZ are based on the Australian BOM wind database. This is the wind database analysed for Australian BOM wind and referred to in this study as "BOM wind" or "BOM wind stress". The eleven time series of Australian BOM wind stress data were averaged to create daily climatology years. Periods vary in their duration, however, it is assumed that the climatology year per station will not show a substantial change in behaviours when comparing the different periods. The last assumption is supported by the shortest time period being 10 years, with average wind having a similar behaviour throughout the years. After the climatology year was calculated for each station, a linear interpolation, from north to south, resulted in equally distant points along the coast. The eleven daily climatology years were linearly interpolated latitudinally to create a Hovmeller graph of the wind stress conditions. Interpolation results in the description of usual coastal wind stress conditions for both components (south-north and west-east) along the SQCMZ's coast throughout a year. Additionally, the time series created using wind recorded in Sandy Cape (table 3.2) was analysed, to identifying the main frequencies using Fourier and Wavelet methods, as described in section 3.2.1.1.

3.2.2.3 Bottom Stress

The estimation of bottom stress uses a similar equation to equation 3.4. In this case the assumption is that the bottom is moving with the same velocity as the water at the bottom, however, it is moving in the opposite direction. The assumption of the "bottom moving" results in bottom stress and a similar equation can be stated. However, this time the drag coefficient will be different and the averaged density will not be used, as it just scales the data. The values of bottom stress are comparable with those of Oke and Middleton (2000). Bottom stress is calculated following the theory described by Oke and Middleton (2000). This theory has been applied previously by Everett et al. (2014) as well as by Schaeffer et al. (2014). Equation 3.7 is a quadratic bottom friction law, where C_D is the drag coefficient with a value of 0.003 (Kowalik and Murty, 1993), whilst

u and v are the west-east and south-north velocity components at the bottom respectively.

$$\tau_{x,y}^{bottom} = C_D v \sqrt{u^2 + v^2} \tag{3.7}$$

The velocity field is obtained from BRAN3.5 (section 3.1.4). A Matlab script examines each vertical profile looking for the deepest valid data. Following the identification of the deepest valid data, it is assumed that this value represents the bottom velocity at that point. The last valid data point is defined as grid cell nearest to the bottom. BRAN3.5 does not go down to the deepest points of the ocean, meaning the bottom stress estimation using this method is restricted to marine areas no deeper than $4500m$. The restriction does not apply for the study area because it is shallower than $4500m$. The assumptions that the last valid data is at $10m$ above the bottom and the drag coefficient is a constant value in BRAN3.5 is required to use equation 3.7. Results are validated by comparing with Oke and Middleton (2000).

Daily estimations of bottom stress from 1993 to 2012, along the East Coast of Australia, are constructed on a monthly basis. These estimations provide information leading to the identification of areas exposed to high bottom stress. A time series of bottom stress was constructed by averaging the zone delimited by 153.25°E to 154.0°E and 26.5°S to 24.5°S. The time series is the source of the bottom stress values associated with the classified Chla blooms (section 3.2.2.1). The Fourier and Wavelet analysis identified the main frequencies of the bottom stress, these are compared against the described frequencies of the EAC. Finally, a daily climatology year was constructed using the time series, allowing it to be compared with the wind and for the identification of the periods of maximum and minimum bottom stress throughout the year.

A maximum cross-correlation method was used to estimate spatial displacement and create velocity fields based on sea surface temperature and Chla, filling any gaps with SSH geostrophic currents (Abraham and Bowen, 2002). In this research, the displacement calculated was between a composited Chla pattern and a climatology pattern of bottom stress.

3.2.3 Examination of Near-Coastal Eddies

The study of NCEs is completed in two stages. The first stage focuses on the description of a single NCE which took place in June-July 2012. Similar studies have been done off New South Wales (table 3.5), however, none have been carried out off Southern Queensland, Australia. The second stage is the completion of an eddy census used in the characterisation of NCEs.

3.2.3.1 Characterisation of a Single Near-Coastal Eddy Case and its impact upon the shelf

The eddy recorded in June-July 2012 (2012 eddy) off southern Queensland is described based on Chla (section 3.1.1), SST (section 3.1.1), EACM1213 (section 3.1.2), BRAN3.5 (section 3.1.4) and SSHa (section 3.1.1). The eddy detection and tracking tool described in section 3.2.1.3 is implemented to describe features such as radius, displacement velocity and vorticity, among others. The steps in the process of studying the 2012 eddy were:

1. To describe the Chla and SST conditions for the period of the eddy, June-July 2012.
2. To describe the EACM1213 data. This step is a vertical description of the eddy, this is the component which can not be described based on remote sensing products.
3. To describe BRAN3.5 for the period of the 2012 eddy. The impact of the eddy over the shelf, by the entrainment of coastal water is observed in the Chla and SST, however, it can be quantified using a 3-dimensional representation of the 2012 eddy, done using BRAN3.5. Additionally, the description of this data based on the 2012 eddy aids in understanding the genesis and dissipation of the eddy.
4. To describe the physical features based on SSHa. The implemented eddy detection and tracking tool estimates a set of eddy physical features (section 3.2.1.3) which characterise the 2012 eddy.
5.

3.2.3.2 Near-Coastal Eddies in a Climatology View

The eddy climatology description is based on an EDTT (section 3.2.1.3). This analysis is organised in three stages. The first stage is the implementation of EDTT, the second is the validation of the results and the third is the description of the NCEs. The following paragraphs describe these stages. The EDTT is implemented with SSHa. The zone selected is 140°E to 171°E and 9°S to 50°S. The detection of eddies was completed for the whole time period of SSHa estimations (1993-2015). The detection was completed using the following values as the input parameters:

- Minimum radius: $0.0km$
- Maximum radius: $200km$
- Minimum Okubo number: $2\text{x}10^{-11}$

The next step in the EDTT is the selection of eddies, the last step in the EDTT is the tracking of eddies. The result of this analysis is a database with a census of eddies in the aforementioned zone.

A majority of the validation is based on the definition of a corridor being approximately $600km$ wide. The west border of the corridor is the coastline. The east border of the corridor is defined at $600km$ eastward of the $200m$ bathymetry isoline. All eddies within this corridor are considered in the analysis. The width of the corridor is defined in an attempt to capture the majority of the eddies from both the Coral Sea and Tasman Sea. Considering these two seas it is possible to compare the results with Pilo et al. (2015) and Everett et al. (2012). Additionally, the region in which the Capricorn Eddy is located is included in the analysis, allowing it to be seen if the model represents this coastal feature (Weeks et al., 2010). As a final simple test, the eddy database is checked to identify if it contains those eddies listed in table 3.5. Eddies in table 3.5 are reported by the literature in the area contained within the $600km$ corridor.

Tranter et al. (1986) associated the intrusion of slope water over the shelf with eddies and meanders within $90km$ of the shelf break. Gruber et al. (2011) described the maximum impact of the mesoscale features on net primary production within the nearshore $100km$ zone. A single eddy description carried out by Mullaney and Suthers (2013) located the eddy $100km$ off the coast in October

Table 3.5: List of reported and described eddies in the southern section of the east coast of Australia.

Eddy Reference	Period	Approx Coordinates
Oke et al. (2013)	13-15 October 2009	153.25°E , 33.5°S
Mullaney and Suthers (2013)	1-14 October 2006	152.7°E , 33.2°S
Everett et al. (2011)	14-16 October 2008	152°E , 34.25°S

2006. Another individual event described using a similar approach to this research project was carried out by Everett et al. (2015), who located the eddy up to 102km from the shelf. Nagai et al. (2015) described the zone within 100km-200km off shore as being highly influenced by filaments usually attached to eddies, this is based on numerical simulations of the California Current System. Using the aforementioned studies, a 100km distance was selected from which to collect all the NCEs along the southern section of the east coast of Australia. In the third stage, a narrow corridor was defined following the same methodology as in the 600km corridor. The west border is the coast line. The east border is at 100km east of the 200m bathymetry isoline. The purpose of this corridor is to capture the NCEs which could result in an entrainment of shelf waters, as seen in the 2012 eddy. Both corridors are from 20°oS to 38°S, however, the discussion of the analysis focuses on the area from 25°S to 38°S.

As part of the third stage, three zones are defined according to the results in the 100km corridor. Features of the latitudinal distribution of the number of eddies are used to define Zone 1, the zone containing this project's study area. The definition of Zone 2 is based on the quasi-normal distribution of the number of near-coastal eddies per latitude, which agrees with the separation zone of the EAC. Zone 3 is characterised by a quasi-linear increase of the number of near-coastal anticyclonic and cyclonic eddies. These three zones are characterised by the features of the eddies occurring within them.

A simple method was implemented to estimate anomalies of Chla and SST. For the eddy analysis, the anomalies were estimated using Chla from IMOS and SST from JPL (section 3.1.1). The source of the SST data was changed, this decision came from the fact the JPL product, using implemented methodologies, was able to fill in the missing data observable in the IMOS product. By using the JPL product an estimation of SST anomaly can be produced for almost every eddy. The method works in three steps. The first step is the quantification of the Chla (if there is no interference, e.g. cloud cover) and calculation of the SST average within a $20km$ radius. The circular radius is centred at the averaged coordinates estimated by the EDTT. The second step repeats the first step, however, altering the size of the circle to a $40km$ radius. The second step excludes the original data from the inner circle which has a $20km$ radius. These two steps result in two averaged values of Chla and SST for the core of the eddy ($20km$ radius) and a ring in the edge of the eddy ($40km$ radius). The third step subtracts the average values of the ring from the values of the core (core-ring gradient). Negative gradient values indicate the external ring has higher values than the core, in contrast positive gradient values indicate the external ring has values lower than the core. chapter 5 describes and discusses the results from the methods introduced in this section (3.2.3). To validate the results achieved from the $100km$ corridor in Zone 1, the detected eddies are graphed for Chla using the time and averaged coordinates from the EDTT. Following a visual check, it would be expected to see an entrainment of Chla or enhanced values for the detected events. This validation aims to take into account the fact that SSH is interpolated for waters shallower than $200m$.

3.2.4 General circulation and connectivity

Following the exploration and characterisation of upwelling events and NCEs, the examination of the simulation results from BRAN3.5 led to the description of key features (supported by the literature) in the SQCMZ circulation. The information collected and generated by this research project led to the design of a model of the SQCMZ circulation, considering the previously described features as well as the physical mechanisms linking them together.

3.2.4.1 Analysis of BRAN3.5

By validating the general circulation represented by BRAN3.5, the examination of its physical variables can be used to identify the final connections and features required to design a model of the circulation of the SQCMZ.

3.2.4.1.1 Monthly Analysis of BRAN3.5

The temperature, salinity and velocity represented by BRAN3.5 are monthly averages for the surface and cross sections from 25°S to 28°S every 0.5 degrees. These results produce a more cohesive view of the circulation over the shelf, creating a base from which to identify the areas requiring improvement in the implementation of ROMS simulations (section 3.2.4.2). Results from the monthly averages, particularly the cross section at 27°S, are compared with the main features observed in the moorings located in the same area (see section 3.1.2).

3.2.4.1.2 Characterisation of the EAC transport in BRAN3.5

The EAC's transport in the cross sections is estimated by multiplying each velocity point with the corresponding area in the grid. The area associated with a velocity point is defined as the box delimited by half of the distance to an adjacent velocity point (below, left, above and right). Once the transport is calculated in each area of the cross section, the total (equation 3.8) and average transport are estimated. Equation 3.9 describes the method used to estimate the average transport in the defined cross sections, a weight relative to the size of each cell in the cross section where the flux was estimated is used.

$$Flux = \sum_{i=1}^{n} (v_i \cdot area_i) \tag{3.8}$$

$$\overline{Flux} = \sum_{i=1}^{n} (v_i \cdot area_i) \cdot \frac{area_i}{TotalArea} = \frac{\sum_{i=1}^{n} (v_i \cdot area_i^2)}{\sum_{j=1}^{n} area_j} \tag{3.9}$$

3.2.4.1.3 Surface Deformation and Vorticity in BRAN3.5

The Okubo-Weiss parameter (Okubo, 1970; Weiss, 1991) measures the deformation and vorticity of the water and compares them to determine which is dominant (Reynolds et al., 2007). The definition of this parameter is describe in equation 3.10 according to Isern-Fontanet et al. (2006) and each term is described in

table 3.6.

$$W = S_n^2 + S_s^2 + \omega^2 \tag{3.10}$$

Deformation terms can be modified to explore which dimension (x or y) the deformation is stronger in. The modifications to the terms are listed in table 3.7. From the index of dominant dimension in the shear component of the deformation it is expected to see a positive value in the edge of EAC. The edges of the EAC are areas where the shear is great resulting in zones of instability. These are the formation zones for frontal eddies (e.g. Marchesiello and Middleton, 2000).

3.2.4.2 ROMS scenarios

The implementation of ROMS_AGRIF to describe marine circulation off Southern Queensland aims to test different scenarios, which is not possible with BRAN3.5. Simple scenarios will aid in understanding features of the SQCMZ circulation described using observations. The implementation of the code, as well as the technical details are summarised in section 3.2.1.4. Initial and forcing conditions are described in the following sections, 3.2.4.2.1 and 3.2.4.2.2. A regular rotated grid was created and used in both implemented scenarios. Figure 3.9 illustrates the point of the grid where the scalar variables are solved (e.g. temperature and salinity).

The grid is rotated to reduce the number of elements representing land and to optimise the calculations. The horizontal resolution of the grid is in the approximate range of 2 to $3km$. The higher horizontal resolution is over the shelf and decreases moving eastward. The change in horizontal resolution is observable in 3.9, where the density of points decreases. The resulting grid is a 200x400 matrix. The vertical coordinates are 64 sigma layers, their distribution results in a higher resolution near to the surface. Figure 3.2 illustrates the distribution of the 64 sigma layers with a hypothetical bathymetry. The grid's bathymetry was interpolated using the topography and bathymetry data base from Geosciences Australia (section 3.1.5), the minimum depth interpolated was $10m$. Minimum depth means that all areas shallower than $10m$ will be given a depth of $10m$. This minimum restriction allows for the use of a larger time step than an interpolation extending to shallower waters. The restriction does, however, create changes in the bottom morphology, e.g. the channel between Fraser Island and the coast

Table 3.6: Description of the terms of the Okubo-Weiss parameter described in equation 3.10

Name of the term	Term in equation 3.10	Extended term
Deformation Term: Normal Component of Strain	S_n	$\frac{\partial u}{\partial x} - \frac{\partial v}{\partial y}$
Deformation Term: Shear component of Strain	S_s	$\frac{\partial v}{\partial x} + \frac{\partial u}{\partial y}$
Vorticity Term: Vertical vorticity	ω	$\frac{\partial v}{\partial x} - \frac{\partial u}{\partial y}$

Table 3.7: Definition of indices to quantify the dimension where the normal and shear components of the deformation are dominant.

Index name	Definition	Dimension where the deformation is dominant
Index of dominant dimension in the Normal component of the deformation	$D_n = \left\lvert\frac{\partial u}{\partial x}\right\rvert - \left\lvert\frac{\partial v}{\partial y}\right\rvert$	• $D_n > 0$ x-dimension • $D_n < 0$ y-dimension
Index of dominant dimension in the Shear component of the deformation	$D_s = \left\lvert\frac{\partial v}{\partial x}\right\rvert - \left\lvert\frac{\partial u}{\partial y}\right\rvert$	• $D_s > 0$ x-dimension • $D_s < 0$ y-dimension

line, originally a few meters in depth it becomes a $10m$ deep channel, similar to the Breaksea Spit, north of Fraser Island.

The results of both scenarios are described based on their monthly average behaviour for the surface and cross sections. The transport through the cross section is estimated, allowing for comparisons between it and the BRAN3.5 results. The transport estimation for ROMS simulations considers the oscillation of the surface. The average transport is weighted by the corresponding area of each flux evaluated in the average, as described in equations presented in 9.

3.2.4.2.1 Climatology scenario

Initially climatology boundary conditions were created using BRAN3.5. The first step was to create a database with a climatology year based on the BRAN3.5 daily averages (section 3.1.4) for its whole period. The result is a year of 366 days for velocity, temperature and salinity. The boundary conditions were interpolated from the aforementioned climatology year database. The surface forcing conditions are constructed following the databases available with ROMS (section 3.2.1.4). The simulation was completed in approximately 4-5 months for 12 years, this was achieved using ROMS. As discussed in chapter 6, the calculation for this scenario did not represent the EAC as a current throughout the year, this is the reason for the setting of the second scenario. However, the results from the presence and non-presence of the EAC over the shelf are discussed as they contribute to a better understanding of the shelf circulation.

3.2.4.2.2 The 2010 scenario

The model was run using the climatology simulation as the initial condition. The boundary conditions were interpolated from BRAN3.5 for 2010. This year shows high values for the v-velocity component related to the EAC. 2010 was selected to represent a current along the shelf break for the whole year. This current will emulate, to some degree, the effects of the EAC over the shelf circulation. The simulation was an annual cycle for 5 years, with the interpolated boundary conditions always based on the results of BRAN3.5 for 2010. The jump from the end of the year to the beginning will create a signal (when the year restarts, 31st December to 1st January) as the change in the boundary conditions is not smooth. The issue of a generated signal due to the set-up of the boundary condition is not addressed in this study, however, it could be addressed by adding an extra week of simulation at the end of the year. The addition of a

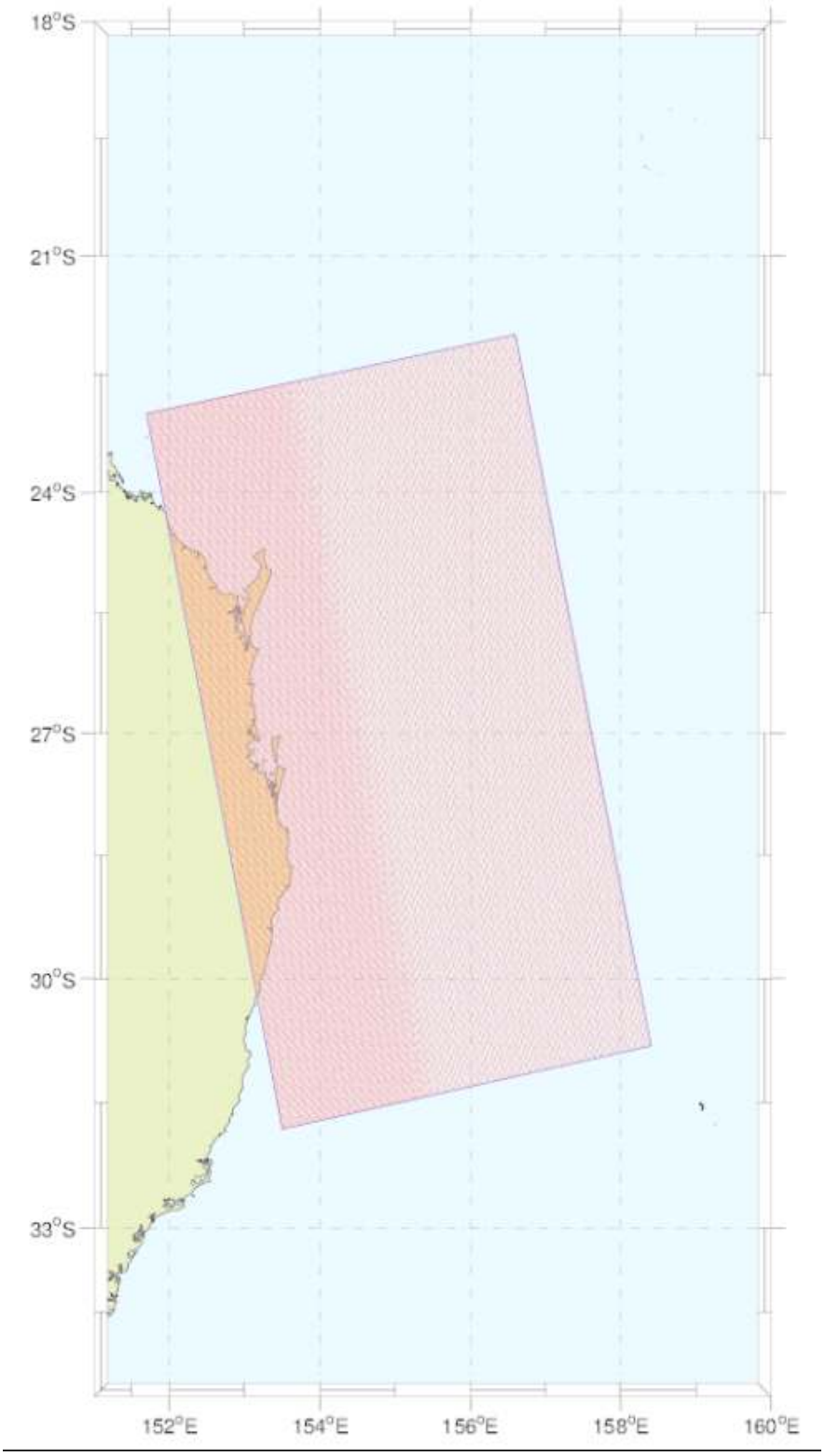

Figure 3.9: Structured grid created for ROMS calculations. Red dot represents the place where ROMS solve scalar variables (e.g. temperature). The resolution changes offshore, with the highest resolution over the shelf and shelf break.

week will create a smooth transition. Improvements to the model configuration are discussed in this study, however, they are not implemented, pointing to the objective to implement a downscaling model in the future.

3.3 Summary

The research project described here was organised to study three distinct dynamical features of the SQCMZ marine circulation: upwelling events, near-coastal eddies and the linking of the identified features by physical mechanisms. For section 3.2.2, chapter 4 describes the evidence of upwelling events in the SQCMZ, describing the quantification of their main features as well as the possible physical mechanisms behind these events. For section 3.2.3, chapter 5 reports the impact of a NCE over the shelf circulation, describing climatology physical features of the NCEs and their distribution in space and time. For section 3.2.4, chapter 6 contains a description of the main circulation over the shelf, discussing the design of a model with the marine circulation features previously described, as well as the physical mechanisms that interconnect them. The basis for the analysis of chapter 6 is BRAN3.5, however, the ROMS implementation contributes two key features.

Chapter 4

The Southeast Fraser Island Upwelling System

The first examination and quantification of upwelling events in the SQCMZ is discussed in this chapter, using Chla blooms as proxy. The main result is the definition and characterisation of the SFIUS (Brieva et al., 2015). Middleton et al. (1994) describe the first vertical profiles that show a possible uplifting of deep water off Fraser Island, suggesting as one of the possible causes, the bottom layer transport. Dambacher et al. (2012) define the upwelling off Fraser Island as a Key Ecological Feature of the East Australian marine zone. The definition of this Key Ecological Feature is mainly based on biological features reported in this area. Two possible mechanisms are suggested: EAC-shelf interaction and transient eddies. These two suggestions are based on studies and reports in coastal areas farther south, off New South Wales. Rossi et al. (2014) extend the description by showing that current-driven upwelling conditions are more frequent than the wind-driven upwelling condition in the SQCMZ. In this chapter the physical approach of the analysis results in the characterisation of the SFIUS' periodicity and the physical mechanisms associated with it. As a secondary result, the existence of a weaker upwelling system off the Sunshine Coast is suggested, evidence for which comes from its features, periodicity and potential physical mechanism(s) differing from the SFIUS.

4.1 Examination of Chla daily estimations

Animations B.2 and B.1 illustrate daily estimations of Chla provided by IMOS. In their representations the impact of the cloud cover is observable, resulting in blank spaces. Animation B.2 illustrates the Chla in the whole study area, whilst animation B.1 illustrates specifically the southern section of the study area. Animation B.1 is included as similar patterns to the ones observed in Fraser Island were observed in Moreton island, only on a smaller scale. The highly dynamic Chla behaviour is concentrated in the western edge of the EAC, this is a zone of instability resulting from the interaction of EAC waters and shelf waters. A careful examination of animation B.2 leads to the identification of two main Chla bloom patterns.

The first pattern, Pattern 1 (P1), involves a large section of the coast, if not the whole coast, between 25°S and 27°S. The blooms of Chla are connected to the shore and their transport is eastward (offshore), across the shelf and at $40m$ depth reaching the shelf break. The $40m$ depth is represented by the black line (of the three represented in the animations $40m$, $200m$ and $1000m$) on the left side (western line). The $40m$ depth is defined in chapter 3 as the minimum depth where the Chla product is used in this research, based on the optical depth and the relationship of Chla with the bathymetry. The second pattern, Pattern 2 (P2), is a bloom of Chla observed at the northeastern section of Fraser Island. It involves the north section of the eastern coast of Fraser Island. Its formation occurs near the shore and propagates along the shelf break. The high Chla values are located in what could be the area of instability resulting from the interaction of the EAC waters and shelf waters. The intensity of the blooms associated with P2 is larger than those associated with P1. A pattern similar to the P2 identified off Fraser Island is also observed in blooms of Chla off Moreton Island, however, the latter is on a smaller scale and magnitude.

4.2 Chlorophyll-a analysis and pattern examination

Figure 4.1 illustrates monthly averages of Chla from late 2002 to 2012. The results highlight areas where Chla patterns do not agree with the orientation of

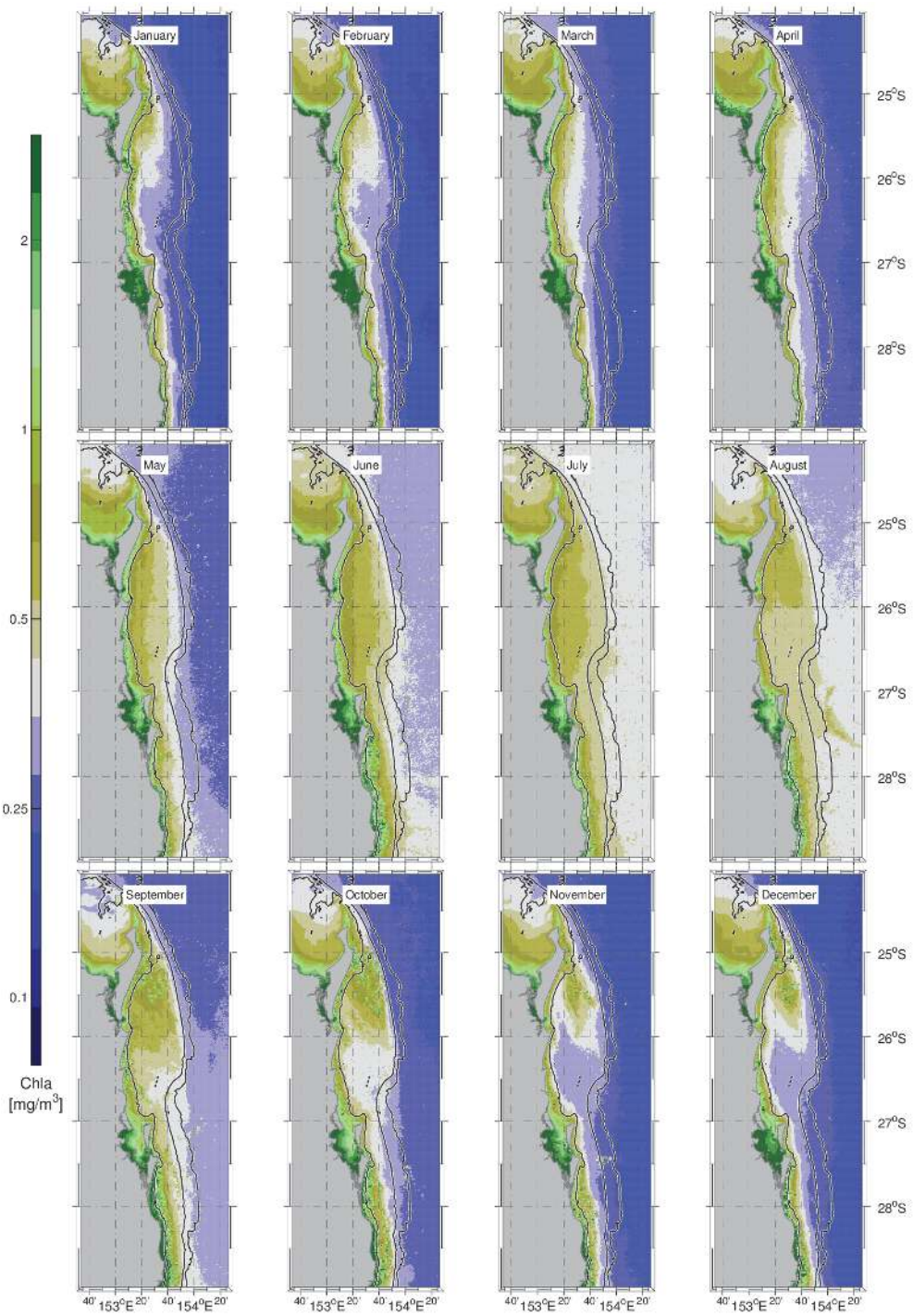

Figure 4.1: Chla monthly averages from IMOS Chla oc3 product. This figure should be used with caution as there is a high impact of cloud coverage (see page 61 for further details). Black lines represent the depths of $40m$, $200m$ and $1000m$, in an off shore sequence respectively.

the bathymetry isolines. One area in disagreement with the bathymetry isolines is located off Fraser Island. From August to February, the area displays a distinctive pattern, with maximum values over $2mg/m^3$ in the average. The pattern is weaker and has a smaller area in January and February, with maximum average values over $0.5mg/m^3$. The contrast in Chla values is strongest from October to December as the background values decrease throughout this period. An additional feature observed is the coastal zone of high Chla advancing off shore over the shelf in autumn-winter (May to August). The annual variability of Chla shows the greatest amplitude over the shelf when compared to the open ocean. The difference in the amplitude could be explained by more nutrient rich water, usually deep water, being found nearer to the surface over the shelf.

An additional section located between 27.5°S and 28°S has a coast line morphology (area in animation B.1) resembling the one between 25°S and 27°S (area in animation B.2), however, on a smaller scale ($\sim$1/4 smaller). Both sections have an island as their northern boundary and a land mark at the south. Each section could be referred to as an "open bay". The smaller section, in waters deeper than $40m$, shows similar behaviour in the seasonal advance and retreat of the coastal zone of high Chla, offshore and inshore respectively. Rather than a particular pattern formation in spring-summer, which is not observed in the smallest section at Moreton Island, a filament appears in the monthly averages at approximately 27.5°S in August. Animations B.2 and B.1 show daily frames of the Chla surface concentration. Particularly high Chla events are observed off Moreton Island. These resemble those seen off Fraser Island. However, the monthly averages do not show an impact due to the Chla blooms off Moreton Island, as it is seen off Fraser Island, probably due to the smaller magnitude of their Chla values. The physical mechanisms behind the aforementioned events in these two locations could be the same, with events merely having a weaker impact at 27.5°S.

The Chla surface concentration product used in this study is based on remote sensing and is sensitive to cloud cover. In the occurrence of cloud cover, it is not possible to estimate Chla concentration as the light reflected is unable to reach the satellite. The sensitivity to cloud cover is the explanation for the absence of 38.4% of the data from 08/08/2002 to 31/12/2014. Specifically for 4643 composited days, 32.2% of them have an estimation of Chla with >60% of the total number of pixels representing the marine area having a valid estimation (no cloud cover). Over the study period, August to October, is when the cloud

cover has its lowest impact, whilst January to March it has its highest impact. On average, the percentage of pixels (points of observation) covered by cloud in the period from 08/08/2002 to 31/12/2014 is 60.7%. The cloud cover leaves a considerable set of data excluded from the analysis. This may impact upon the yearly distribution of the aforementioned patterns. The aforementioned results are restricted to the rectangular zone delimited by 153.25°E-154.0°E and 26.5°S-25.0°S.

The classification of high Chla concentration events off Fraser Island focuses on two main patterns. Examples of P1 and P2 are presented in figures 4.2 and 4.4 (shown by Brieva et al. (2015)). For the purpose of the classification analysis both patterns were defined based on two features: their spatial distribution and the length of the coastline connected to the pattern. P1 events involve high Chla values connected to the coastline by a long section ($>50km$) as shown in figure 4.2. In comparison, P2 events are connected to the coastline by a short section ($<50km$), originating off the northeastern section of Fraser Island and extending over the shelf break (examples in figure 4.4). P2 is observable in the monthly climatology figures from October to December. In the remaining months this pattern is not present or not clearly identifiable.

Tables 4.1 and 4.2 summarise the results of the pattern classification analysis. The difference between both tables is the magnitude and size of the event summarised. Table 4.1 summarises the larger events, with maximum values over $0.8mg/m^3$ and covering a large portion of the shelf in the case of P1 or the shelf break in the case of P2. Table 4.2 summarises all the events classified. By comparing the highlighted cells (that indicate different values in both tables), it is possible to observe that P2 events show greater variability in their intensity and size. Additionally, the P2 days show a greater number of events and days involved in these events. The number of P1 events tends to be around 6 with the exception of 2005, 2008 and 2011, where the number of events was approximately double that of the remaining years. 2012 is a year that differs from the norm with just one P2 event being observed, which is out of the usual range (7 to 13 event per year). The average number of P2 events is reduced considerably due to the 2012 anomaly, excluding 2012, the average increases to 7.5 and 8.3 for tables 4.1 and 4.2, respectively.

Examples of both patterns are in agreement with the Chla monthly averages seen in figure 4.1 in terms of the months in which they occur. Figure

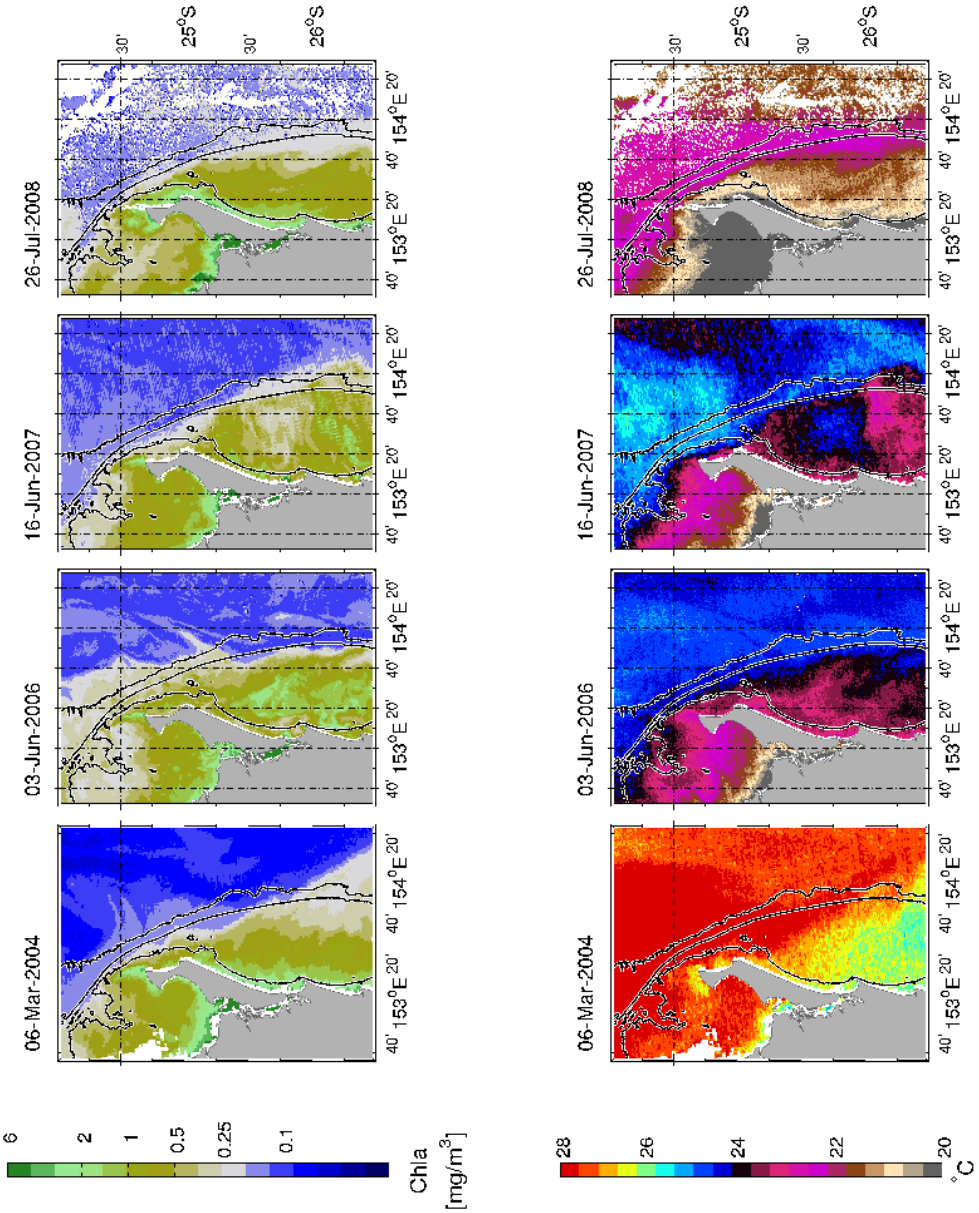

Figure 4.2: Examples of Chla blooms classified as P1 (a further four examples in figure 4.3). Chla concentration as well as SST is illustrated by the graphs. Black lines represent constant depth at $40m$, $200m$ and $1000m$ from left to right respectively. This figure was published by Brieva et al. (2015)

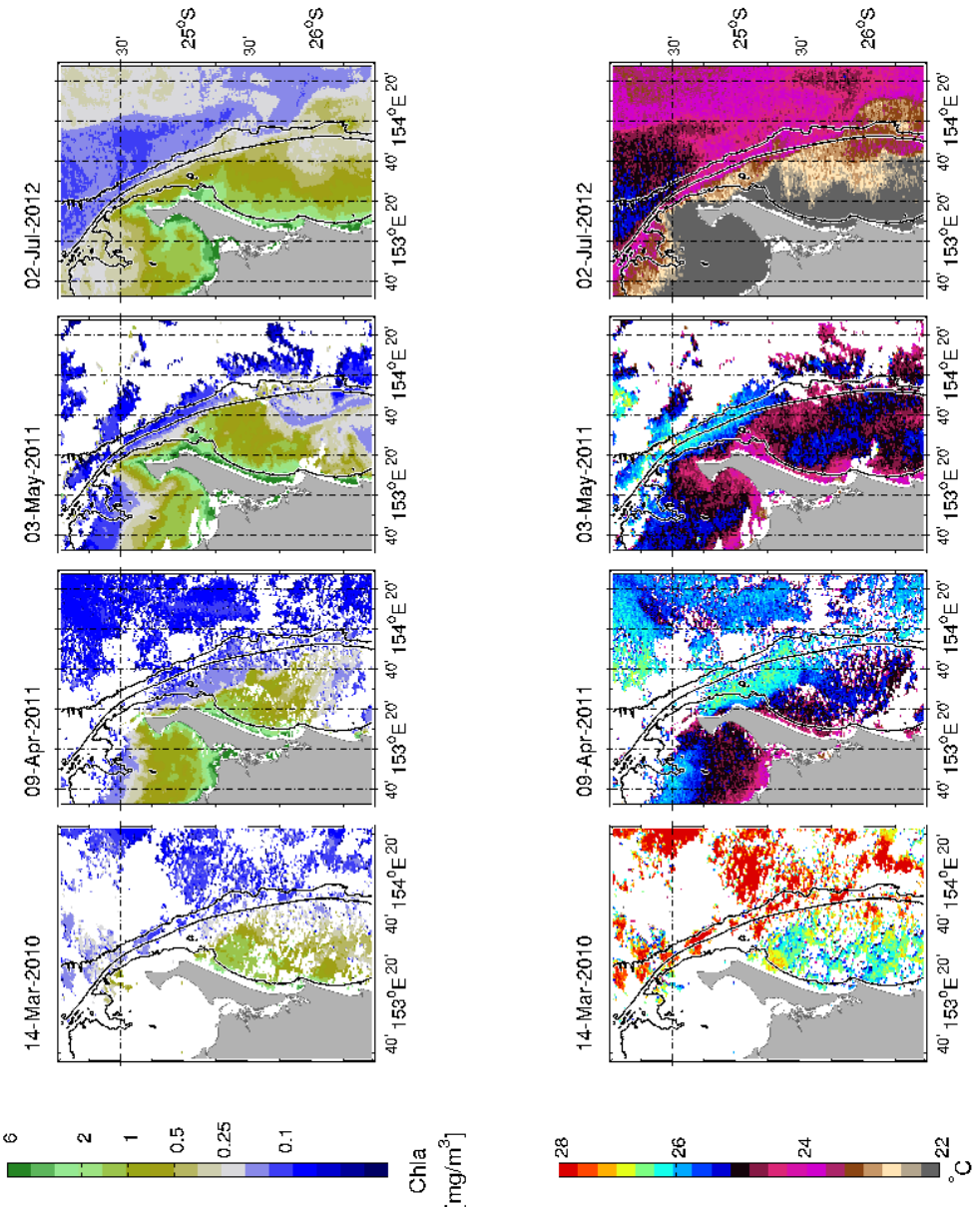

Figure 4.3: Example in addition to figure 4.2.

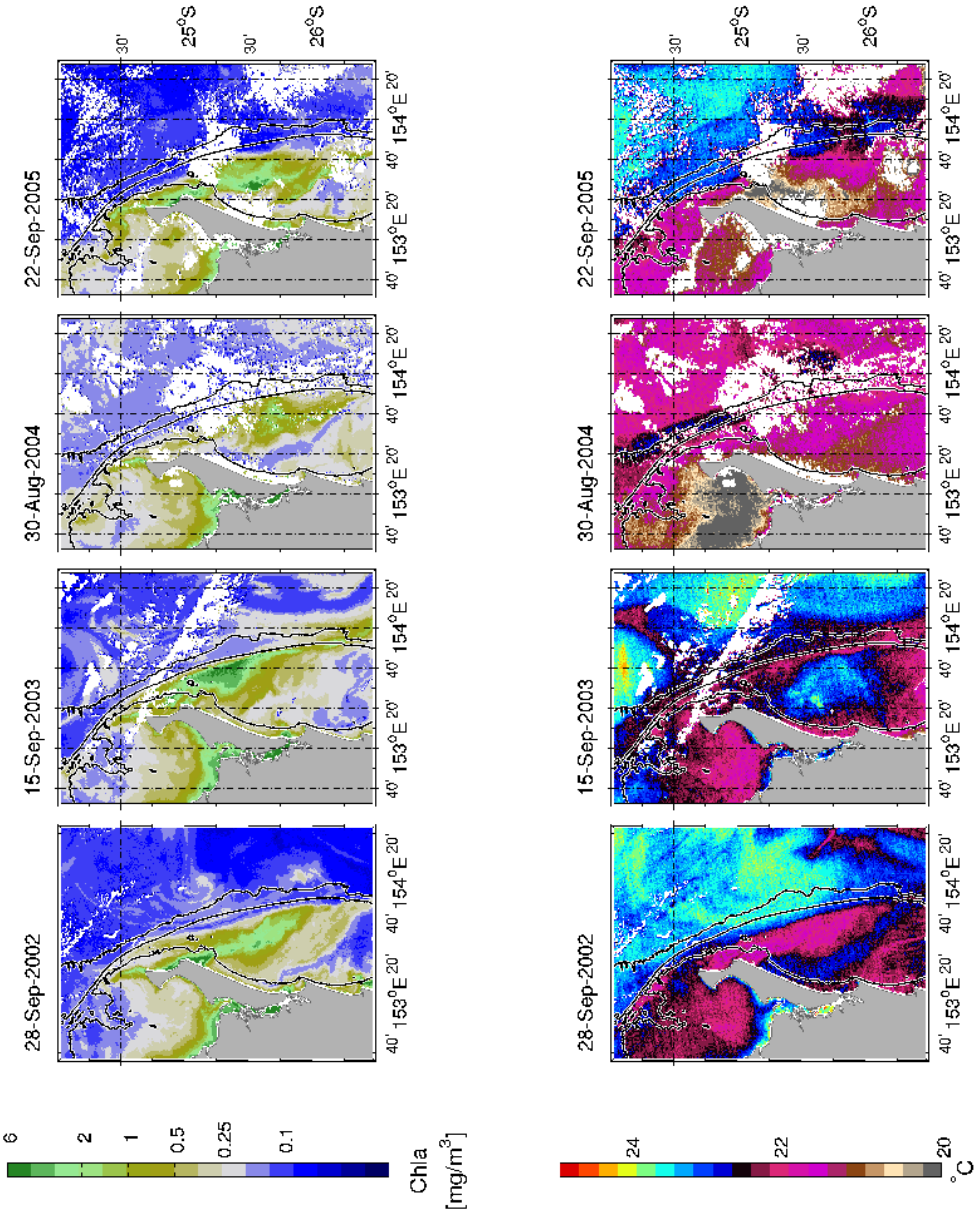

Figure 4.4: Examples of Chla blooms classified as P2 (a further four examples in figure 4.5). Chla concentration as well as SST is illustrated by the graphs. Black lines represent constant depth at $40m$, $200m$ and $1000m$ from left to right respectively. This figure was published by Brieva et al. (2015)

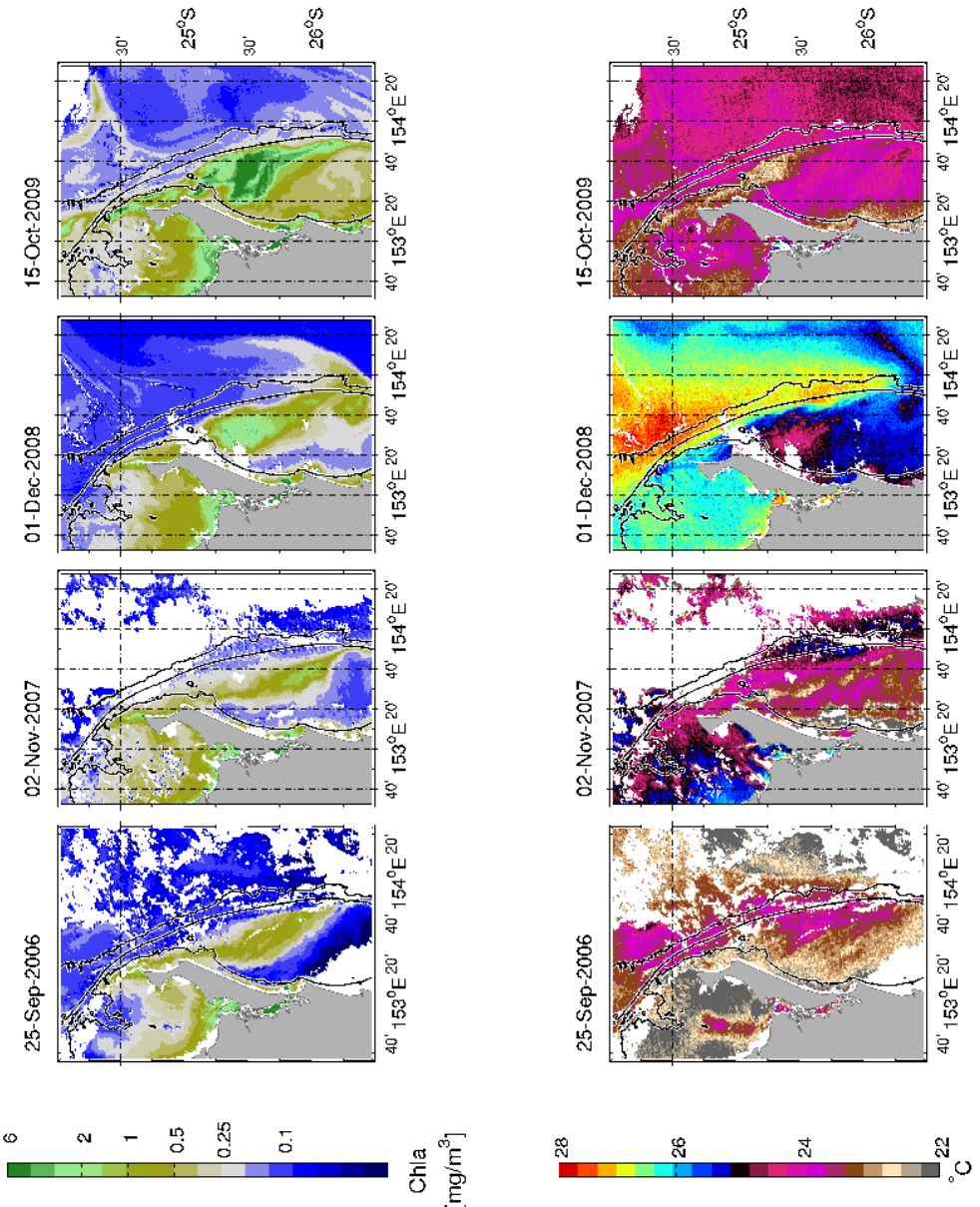

Figure 4.5: Example in addition to figure 4.4.

Table 4.1: Results of the classification of Chla blooms per year considering events that were observed with Chla values over 0.8 mg/m^3 and covering a large section of the shelf.

Year	Total Days		Number of Events		Aprox. Averaged Wind Stress (10^{-2})		Aprox. Averaged Bottom Stress (10^{-5})		Approx. Chla (mg/m^3)	
	P1	P2	P1	P2	P1	P2	P1	P2	P1	P2
2002	11	57	3	5	0.38	-1.5	-4.7	-7.6	1.3	4.1
2003	25	50	6	10	2.9	-0.4	-0.17	-5.1	2.2	4.0
2004	33	59	5	10	1.0	-0.06	-5.8	-4.8	1.8	2.6
2005	51	57	11	6	2.1	-1.1	-2.2	-9.1	1.3	2.9
2006	29	57	5	7	2.9	0.12	-2.5	-5.8	2.3	1.8
2007	64	85	5	6	0.66	-0.38	-2.3	-4.3	2.6	2.5
2008	59	42	10	7	1.9	0.34	-3.6	-5.1	2.2	2.5
2009	30	86	6	12	1.3	-0.52	-5.0	-5.16	3.0	3.3
2010	15	26	5	6	2.4	1.6	-6.0	-10.2	1.7	2.9
2011	70	57	10	6	1.8	0.37	-3.6	-7.1	3.1	1.9
2012	49	9	5	1	2.6	1.61	-0.51	1.1	2.9	4.0
Mean	39.6	53.2	6.5	6.9	1.8	-0.0036	-3.3	-5.7	2.2	3.0
Addition	436	585	71	76	–	–	–	–	–	–

Table 4.2: Results of the classification of Chla blooms per year considering all events classified as P1 and P2. A filter for the maximum observed value of Chla is not applied as it is done in table 4.1

Year	Total Days		Number of Events		Aprox. Averaged Wind Stress (10^{-2})		Aprox. Averaged Bottom Stress (10^{-5})		Approx. Chla (mg/m^3)	
	P1	P2	P1	P2	P1	P2	P1	P2	P1	P2
2002	11	57	3	5	0.38	-1.5	-4.7	-7.6	1.3	4.1
2003	29	52	7	11	2.8	-0.32	-0.44	-4.9	2.0	3.7
2004	33	60	5	11	1.0	-0.14	-5.8	-4.9	1.8	2.4
2005	51	65	11	8	2.1	-0.98	-2.2	-8.6	1.3	2.3
2006	29	57	5	7	2.9	0.12	-2.5	-5.8	2.3	1.8
2007	64	89	5	7	0.66	-0.42	-2.3	-4.1	2.6	2.3
2008	62	42	11	7	1.9	0.342	-3.7	-5.1	2.0	2.5
2009	30	93	6	13	1.3	-0.4	-5.0	-5.6	3.0	3.5
2010	15	28	5	7	2.4	1.44	-6.0	-9.7	1.7	2.6
2011	70	61	10	7	1.8	0.27	-3.6	-7.4	3.1	1.7
2012	49	9	5	1	2.6	1.6	-0.51	1.14	2.9	4.0
Mean	40.3	55.7	6.6	7.6	1.8	-0.0076	-3.3	-5.74	2.2	2.8
Addition	443	613	73	84	–	–	–	–	–	–

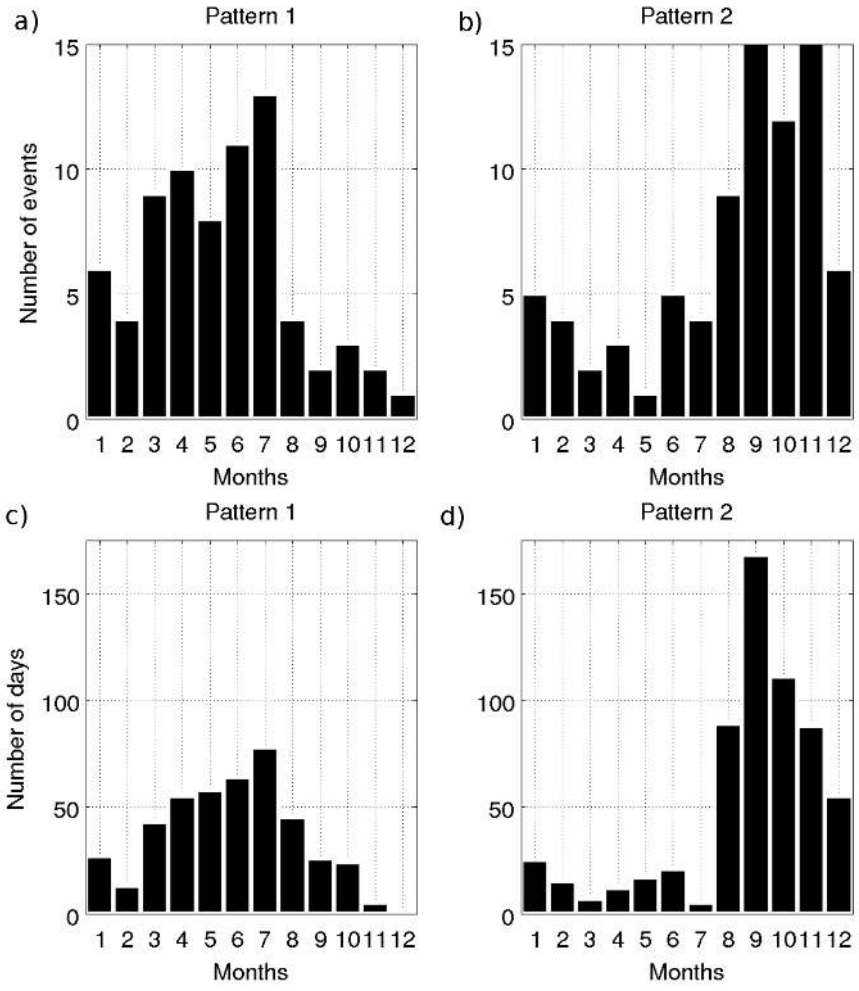

Figure 4.6: On the top panel the monthly distribution of Events classified as P1 and P2 through the year are found. At the bottom panel, the monthly distribution of days under the influence of events type P1 and P2 are illustrated at the left and right, respectively.

4.6 illustrates the monthly distribution of all classified P1 and P2 events. Each pattern is present throughout the year, however, their periods of maximum concentration differ. There appears to be a lag of 6 months between P1 and P2 maxima annual concentrations, this lag is observed when comparing the months of maximum concentration in figure 4.6 graphs a and c with graphs b and d. P1 events are predominantly found in autumn-winter, whereas P2 events typically occur in spring-summer. The number of events was greater for P2 during the analysed period, P2 events have a larger average number of days per event (approx. 7 days compared to 6 days for P1) and also have higher Chla concentration values than P1 events ($\sim 2.8 mg/m^3$ compared to $\sim 2.2 mg/m^3$ in P1 from tables 4.1 and 4.2). The aforementioned P1 and P2 maximum periods of concentration are in agreement with the Chla monthly averages (figure 4.1). The period where the high Chla coastal zone advances (March-July) agrees with the period of maximum annual concentration of P1 events. The months containing the maxima annual concentration of P2 events (August-December) agree with the months showing a distinctive pattern in the Chla monthly averages (figure 4.1), off Fraser Island.

September is the month containing the highest number of P2 events, as well as the largest number of days under the influence of P2 events (figure 4.4 b and d). In the monthly climatology illustration (figure 4.1), October is the month where the P2 pattern has its maximum values, these values are in a formation that evolves from August to February. From November onwards the Chla pattern decreases in size and concentration. The maximum Chla values in October are in the range of approximately 2-3mg/m^3. It should be clarified that the evolution of the high Chla concentration in the monthly averages is not a single event, it is instead the average of many events taking place in different periods. Single events illustrated in figure 4.4 show values over $5 mg/m^3$. All these values are well over the maximum average values of Chla in the open ocean, $0.2 mg/m^3$, which is similar to the values describe by Condie and Dunn (2006). The histograms in figure 4.6 describing the monthly distribution of P2 events shows the greatest concentration of events between September and November.

The monthly climatology average of Chla from March to July resembles a P1 event. The event reaches its point farthest east in July. This is when the average values of Chla in the open ocean are in the range of 0.4-0.5mg/m^3. The distribution of events has its greatest concentration from March to July, with July being the month of greatest monthly concentration. The greatest number of days involved in P1 events are concentrated in July (figure 4.6). This congruence

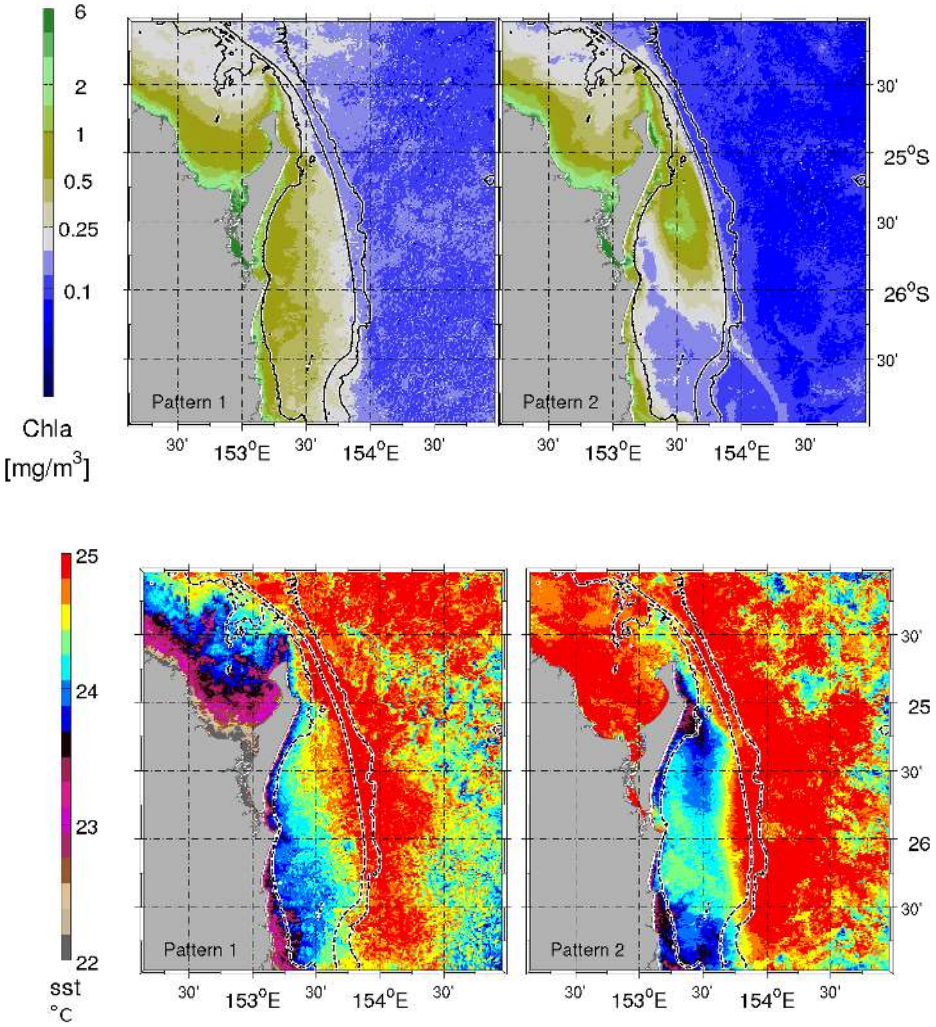

Figure 4.7: Compositions of a set of events for P1 and P2, on the left and right panels respectively. The top panels shows Chla compositions whilst the bottom panels show the SST compositions.

between the results of Chla bloom classification and monthly Chla averages supports the validity of the classification results. Additionally, the intensity of the values observed in the monthly averages of Chla, showing higher values in the P2 formation, agrees with the information in table 4.1 and 4.1 displayed in the last two columns. The average values of Chla for P1 and P2 at the bottom of both columns show that P2 Chla blooms have a greater intensity than the P1 blooms.

A selection of P1 and P2 events with more than 80% of the marine area available in the Chla product have been averaged to create a composition of P1 and P2 events (figure 4.7). Examples of P1 and P2 events as well as compositions of these two patterns, demonstrate that P1 events involve the whole or

the majority of the east coast of Fraser Island and the Sunshine Coast. The examples also demonstrate that the isolines of Chla have a similar orientation to the bathymetry lines, whilst the evolution of P1 events points to a main eastward transport. Comparatively, P2 composition involves the northern section of eastern Fraser Island, extending close and parallel to the shelf break. The evolution of P2 events points to a southward transport over the shelf and near the shelf break, similar to the transport of the EAC. The low nutrient mass of water between the coastline and P2 events could be the result of an inshore northward transport. Alternatively it may just be shelf water, that has been encroached by waters with high Chla levels.

Chla surface concentration is used as a proxy for identifying surface water from potential upwelling events. The identification of upwelling events is supported by the estimation of SST, which shows cold masses of water associated to the P1 and P2 events. The inverse relationship between Chla and SST is observed in the examples illustrated in figures 4.2 and 4.4, where high values of Chla are associated with low values of SST, particularly in P2 events. The lifted deep water has a lower heat content and higher concentration of nutrients in comparison to the water in the surface and created the blooms of Chla classified as P1 and P2.

The following two sections will explore whether there is any link to conclude that wind or bottom stress have a role to play in the formation of these two types of high Chla concentration surface formations. The wind description is addressed as the shape of P1 events resemble wind-driven upwelling events, which transport water offshore. Wind behaviour is described in section 4.3 based on land station observations and remote sensing. Due to the location of the P2 pattern near to Fraser Island, the physical mechanisms for the SFIUS (Brieva et al., 2015; Dambacher et al., 2012) described in the literature are investigated. These physical mechanisms are the EAC-shelf interaction resulting in bottom stress (section 4.4) and transient eddies discussed in chapter 5.

4.3 Wind along the study area and its impact on upwelling

Figure 4.8 illustrates a climatology year along the coast, based on the Australian BOM's data (Chapter 3, section 3.2.2.2). A similar analysis by Rossi et al. (2014),

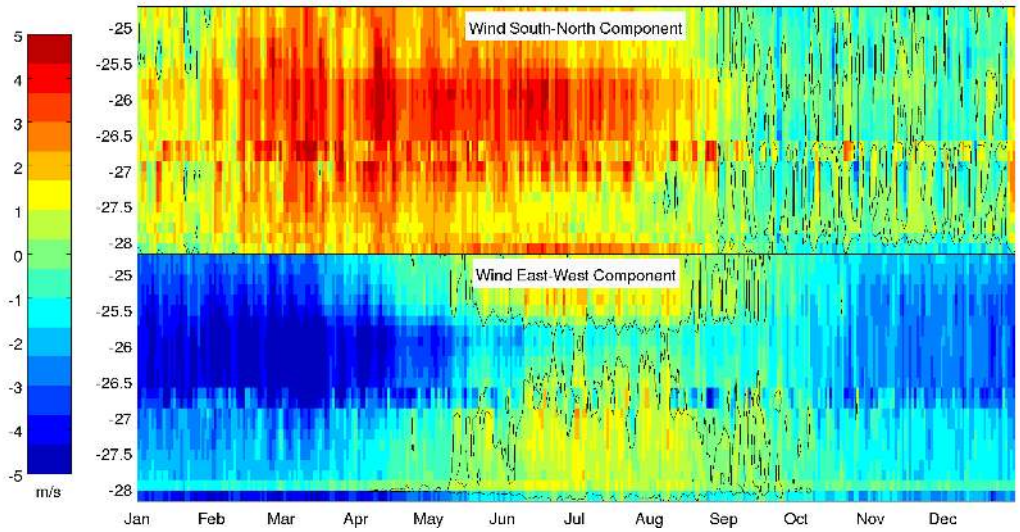

Figure 4.8: Climatology wind year, with daily calculations, based on Australian Bureau of Meteorology (BOM) wind data, from selected land stations. X-axis is time in days, with labels indicating the starting of each month. Y-axis is latitude along Southern Queensland. Top panel represents V wind component or South-North wind flow. Positive values represent wind blowing or heading north, following vectorial representation of wind. Bottom panel represents the U wind component or the East-West wind flow. Positive values represent wind heading West.

based on remote sensing, indicates periods of wind driven upwelling (wind flowing south) and downwelling (wind flowing north). These periods agree with the information displayed, in the top panel, of figure 4.8. Wind blows westward (Easterly wind) for the majority of the year and for a large proportion of the year these Easterly winds have a northern velocity component. Annual climatology wind can be separated into three main periods: January to April, May to September and October to December. January, May and September are the transition months. For these periods the wind is heading North-west, North-east-north and West-south-west, respectively. It can be stated that wind along the coast of Southern Queensland usually (climatology) follows a cyclonic rotation throughout the year.

SeaWinds data shows the same three wind periods for a climatology year (as the one display in figure 4.8). By examining the monthly average of the data, these wind periods can be observed. From June to August, the wind features in the study zone are related to the northward displacement of the Subtropical Ridge (SR) in Austral Winter, reaching its mostly northerly point. Following this shift, the poleward movement of the SR, in Australian spring, agrees with the October to December wind period. In this last annual period, the south-north wind component tends to flow to the south, with a magnitude approximately 3 times smaller than the west-east component, which tends to flow to the east in this same period. It is during the October-December period when the wind tends to favour upwelling events, this is also the period with the highest concentration of P2 Chla events (figure 4.6).

Estimations of wind stress, using the method described in section 3.2.2.2, at Sandy Cape Lighthouse station, are represented for a climatology year in figure 4.8. The wind represented in figure 4.9 is equivalent to the top section of the south-north wind component seen in figure 4.8. As equation 3.4 describes, wind stress is based on wind velocity at $10m$ altitude. Using the method described by Wood et al. (2012), estimations of wind stress from near shore land stations, such as Sandy Cape Lighthouse station, are made. The method described by Wood et al. (2012) scales the magnitude of the wind, however, it does not change the direction of wind (wind and wind stress have the same direction), therefore, the three wind periods still apply to wind stress. Tables 4.1 and 4.2 show per year the average magnitude of the wind in the South-North component, for the days where P1 or P2 events are observed. Wind-driven upwelling conditions are associated with P2 events (negative values of wind stress), whilst wind-driven downwelling

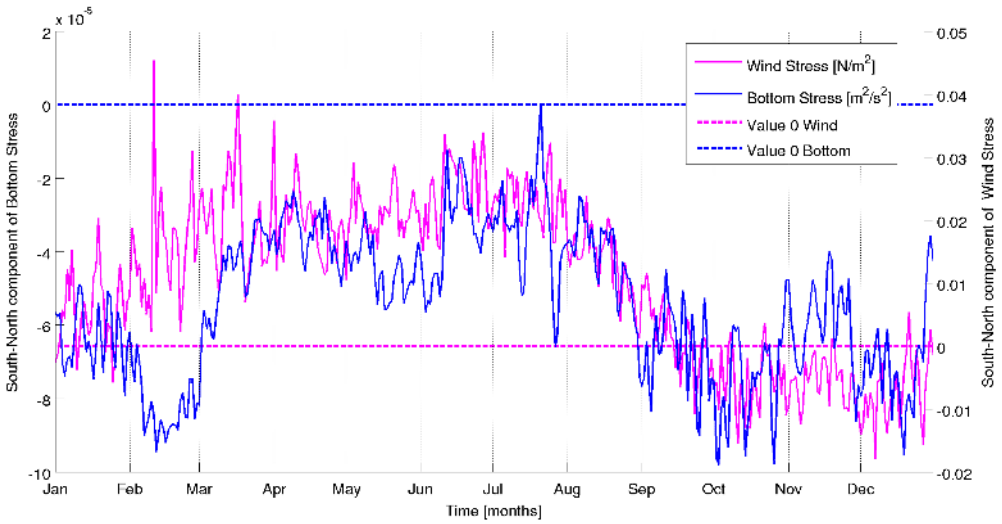

Figure 4.9: Climatology description for bottom stress and wind stress south-north component. Bottoms stress scale is on the left axis and wind stress on the right axis. The colours are as legend describes. Check the period considered for the average. This figure was published by Brieva et al. (2015)

Table 4.3: Distribution of all days involved in the blooms of Chla classified as P1 or P2 according to the wind and bottom stress conditions. The table separates both quantified scenarios that are described in table 4.1 (Scenario 1) and table 4.2 (Scenario 2).

Bottom and Wind Stress	Scenario 1 [%]		Scenario 2 [%]	
Possible Conditions	P1	P2	P1	P2
$\tau_{yb} < 0$ and $\tau_{yw} < 0$	**19.95**	**59.15**	**19.87**	**59.22**
$\tau_{yb} < 0$ and $\tau_{yw} > 0$	**48.17**	**28.38**	**48.53**	**28.39**
$\tau_{yb} > 0$ and $\tau_{yw} < 0$	1.37	1.37	1.35	1.47
$\tau_{yb} > 0$ and $\tau_{yw} > 0$	**21.33**	7.00	**21.22**	7.02
Days without wind data	7.8	4.1	7.65	3.92
Days out of BRAN3.5 period	1.35	0.0	1.35	0.0

conditions are associated with P1. Table 4.3 extends this information by showing the percentage of days where P1 or P2 events were observed and the wind was favourable (<0) or unfavourable (>0) to upwelling events. For example, for large events (scenario 1, table 4.1) 69.5% of the days where P1 event was observed, the wind was unfavourable to upwelling. On the other hand, 60.5% of the days when a P2 event was observed were favourable to upwelling events. However, when considering all of the classified events (scenario 2, table 4.2), these two aforementioned percentages change to 69.75% and 60.69%, respectively. These are not significant changes.

4.4 Fraser Island high bottom stress zone

Monthly averages of bottom stress are represented in figure 4.10. The strongest period of bottom stress in the monthly climatology year is from August to February, whilst the weakest is from March to July. The period with the strongest bottom stress overlaps with the period where P2 events have their greatest monthly concentration (figure 4.6). A more in-depth examination highlights that in January bottom stress is weaker than in December. It is February when bottom stress temporally recovers, meaning January is a local minimum point. Following the short intensification of bottom stress in February, the bottom stress commences its weakest annual period, beginning in March. The increased magnitude of bottom stress observed in February can be seen in the monthly climatology of Chla (figure 4.1). In February, the P2 is both weaker and smaller than in November and December. However, it is still larger than in January, which is a local minimum in the P2 Chla distribution. The behaviour observed in February is evident in the climatology year time series of bottom stress (figure 4.9). The climatology time series is calculated from the area in the range of 153.0°E to 153.75°E longitude and 26.5°S to 24.5°S latitude. The area used to calculate the time series includes the zone of high bottom stress off Fraser Island. Similar behaviour to that observed in February can be identified in the middle of May-June (local minimum) and in November as a local maximum. A feature also highlighted in the analysis was the seasonality of the west-east component. The bottom stress for this research purpose has the same direction as the current at the deepest layer of BRAN3.5, meaning the west-east component of bottom stress (bottom transport) has a climatology inshore direction from September to February and offshore direction from March to August.

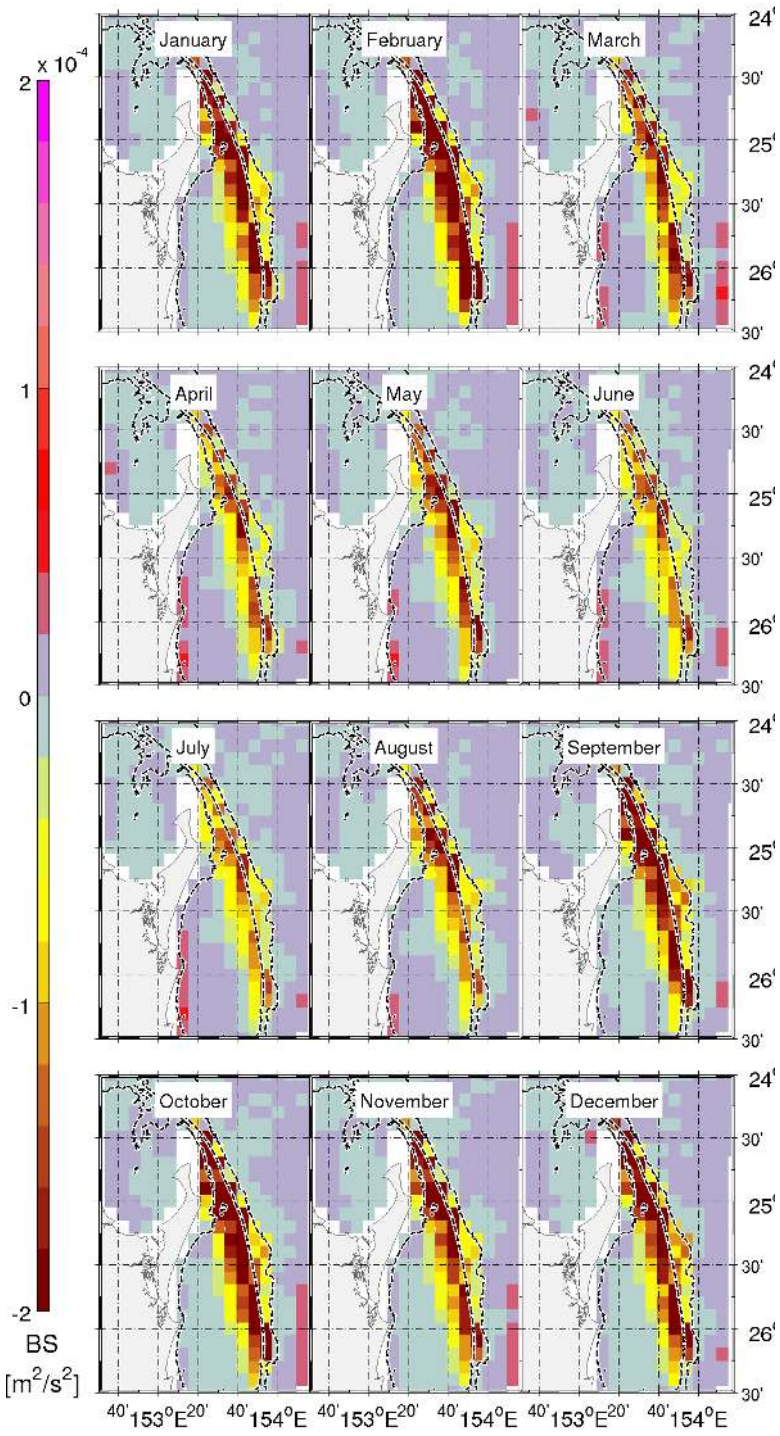

Figure 4.10: Monthly average of bottom stress estimated from BRAN3.5.

Extending the bottom stress analysis along the east coast of Australia highlights three main areas (figure 4.11). The three main areas from north to south include, Fraser Island (25°S), Cape Byron (29°S) and Smoky Cape (31°S) which are all exposed to intense EAC-shelf interaction. Smoky Cape was previously described by Oke and Middleton (2001), where the bottom stress in the area results in the uplifting of deep water over the shelf. Oke and Middleton (2001)'s first figure of SST illustrated two points of upwelling, these are labelled: Cape Byron Upwelling and Laurieton Upwelling. The two points of upwelling are the same as the last two places previously identified as high bottom stress zones. These have a stronger west-east component than the zone off Fraser Island. However, the magnitude and the south-north component of the high bottom stress zones are higher off Fraser Island. The shape of P2 Chla events follows a similar path to Fraser Island high bottom stress areas, located near to the shelf break. The agreement between the location of the two most southerly high bottom stress zones, from BRAN3.5, with the two upwelling systems identified by Oke and Middleton (2001) validates the use of BRAN3.5. Additionally, the first zone of high bottom stress off Fraser Island, agrees with patterns of high Chla concentration, in particular P2 events.

Bottom stress is dominant in P1 and P2 events as is shown in tables 4.1 and 4.2, where bottom stress is always negative (upwelling favourable), with the exception of 2012. Aforementioned tables show that the bottom stress is stronger for P2 (-5.74m^2/s^2) than P1 (-3.3m^2/s^2) events. Table 4.3 shows that the number of days during P1 events with favourable bottom stress is approximately 68%, whilst for P2 it is approximately 87%. 21% of P1 days under both stresses suppressing upwelling point to a physical mechanism that is not included in the analysis summarised in the aforementioned tables.

The application of maximum cross-correlation to a P2 composition and the average bottom stress off Fraser Island results in a minimum value of -0.58. At a value of -0.58 the Chla is high and the bottom stress is strong and negative (poleward direction), leading to a negative or inverse correlation. From this correlation, the assumption can be made that bottom stress plays a role in P2 events. Based on this assumption it can be concluded that water lifted by the bottom Ekman transport tends to move on average 0.15 degree latitudinally poleward and 0.03 degrees longitudinally westward as it moves to the surface. The horizontal displacement is referred to as "average" as each pattern is constructed using averaged data. In conclusion, when the maximum correlation is raised, the

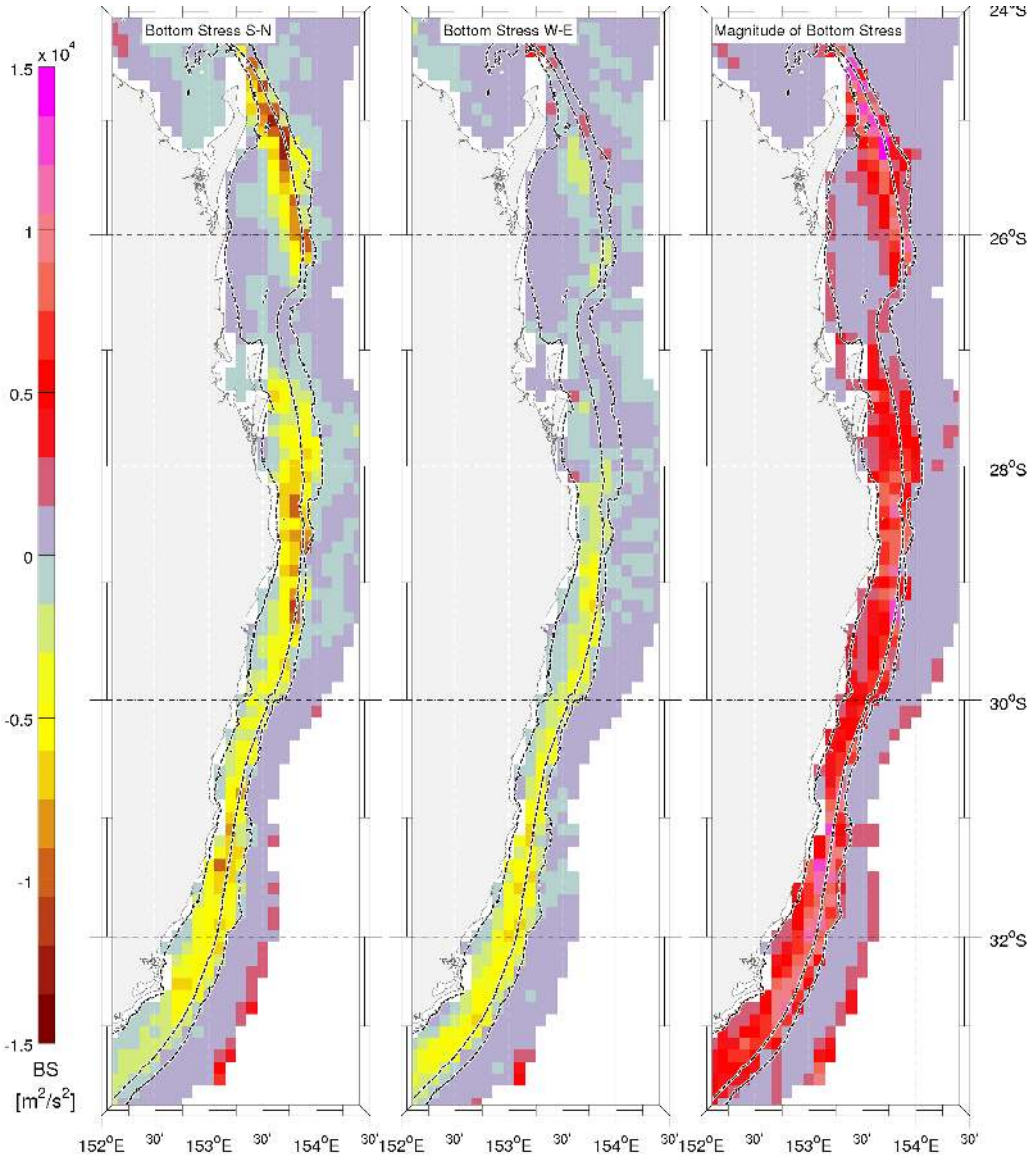

Figure 4.11: Average bottom stress along the east coast of Australia (left side) to highlight areas where it is stronger. In the right side is the accumulation of bottom stress off Smoke Cape where Middleton et al. (1994) describe the role of bottom stress in uplifting water from the shelf break.

water displacement is around $16km$, mostly poleward, from the bottom to the surface.

Fourier analysis for bottom stress indicates that the main frequencies occur at 3.67×10^{-4}days^{-1} (2724.79 days or 7.4 years period), 2.6856×10^{-3}days^{-1} (372.4 days or about a year) and 8.18×10^{-3}days^{-1} (122 days). The highest frequency is in agreement with the literature discussing a 90-120 day oscillation of the EAC. The last two frequencies agree with the annual fluctuation of the EAC, discussed in Chapter 2, as well as the 90-120 days oscillation. The wavelet analysis extends the information regarding the highest frequency, showing it in a range of 3 to 7 years periodically. The harmonic analysis shows that BRAN3.5 is reproducing the main oscillation of the EAC.

4.5 Discussion

The annual variability in the background values of Chla follows the variability in mixing layer thickness. In the Austral Spring and Summer seasons the mixing layer is thinner (Condie and Dunn, 2006), this is in agreement with the monthly average Chla values decreasing in the open ocean ($<0.25mg/m^3$). In Autumn and Winter, the background values of Chla raises the maximum average values in the open ocean, reaching values of $0.4mg/m^3$ (July in figure 4.1). The aforementioned variability leads to the conclusion of an annual oscillation in the Chla captured in the monthly averages. Chla annual variability has an amplitude of approximately $0.15mg/m^3$ resulting from mixing layer thickness' variability. Chla values over $0.5mg/m^3$ are considered to be unrelated to the aforementioned variability.

The observation and definition, of the two main patterns, P1 and P2, in the daily estimations of Chla is supported by the Chla monthly averages as well as the classification of the P1 and P2 Chla blooms. The average and classification analyses agrees with the annual variability of P1 and P2. The inverse relation of SST and Chla supports the idea of deep water with lower heat content and higher nutrient concentrations being uplifted to the surface, resulting in upwelling events. P1 events are concentrated in the Austral Winter and Autumn, whilst P2 are more frequent in Austral Spring and Summer. The blooms of Chla classified as P1 and P2 events are present throughout the analysed years (2000-2012), these are identified in this research as upwelling systems. In this study they are referred to as the SCUS (P1 events) and the SFIUS (P2 events).

To support the two proposed upwelling systems in the SQCMZ, two physical mechanisms potentially related to their formation are explored. The explored physical mechanisms are wind and bottom stresses. Wind stress is known to be a main factor in the Eastern Boundary Upwelling System, whilst bottom stress has been reported to play an important role in upwelling events, off New South Wales.

Australian BOM stations and SeaWinds data show that average winds and, therefore, wind stress mostly favours downwelling in a climatology year. In both databases, three main periods can be identified: January to April, May to September and October to December. The particular wind features for each period are related to the seasonal displacement of the Subtropical Ridge. The May-September wind period agrees with the P1 period of highest event concentration. In this period, the wind has a component (east-west) flowing to the East, resulting in a northward transport, which could support a cyclonic circulation over the shelf. However, the blooms of Chla classified as P1 events, which have their Chla gradient seen across the shelf (characteristic of P1 events) are not driven by wind stress which suppresses upwelling events from May to September. The October-December wind stress period agrees with the period of highest P2 event concentration. It is in this October-December period the wind has a small component flowing South, compared to a strong component flowing West. The small component flowing South favours upwelling and the resulting wind vector is parallel to the east coast of Fraser Island. The wind direction indicates the potential existence of a correlation between wind behaviour in the study area and the morphology of Chla blooms (second and third yearly wind periods). The absence of Chla blooms agrees with the January-April wind period. The identified correlation means that wind has a role to play in upwelling events off Fraser Island and defines the morphology of the Chla blooms resulting from these upwelling events. However, there is no clear reason for the difference in the magnitude of the two types of Chla blooms.

Estimations of bottom stress based on BRAN3.5 show a clear annual fluctuation. The annual fluctuation comes from the EAC and passes to the bottom stress when it interacts with the shelf. Along the east coast of Australia, analysis highlighted three main areas of high bottom stress. The two areas farthest south, off New South Wales, have been associated with upwelling events. Bottom stress was part of the physical dynamic used to explain the uplifting of waters seen in these areas of upwelling (Oke and Middleton, 2001). The zone of high bot-

tom stress farthest North, is located off Fraser Island. As mentioned in Chapter 2, high bottom stress areas result in an intrusion of deep water over the shelf. The high variability in bottom layer velocity (described in Chapter 2), as well as high variability of the EAC-shelf interaction supports the idea that the impact of the shutdown process is diminished by this variability. The annual variability of bottom stress (strongest in spring-summer) and the locations of P1 and P2, can explain the differing Chla magnitudes seen between these P1 and P2 events. The greater Chla magnitude seen in P2 events relates to the proximity of the P2 events to the shelf break. It is at the shelf break where the intrusion of deep water, by bottom stress, is stronger than on the inner shelf. The horizontal distance covered by the transported deep water over the shelf is captured in the maximum cross-correlation between the P2 composition and the high bottom stress area, off Fraser Island ($\sim 16km$). The maximum correlation value of -0.53 demonstrates this similitude; the lag agrees with a poleward transport of the lifted waters, which is observed in the evolution of P2 events throughout time.

The wind stress influences the morphology of the Chla blooms off Fraser Island. In the January-April period the wind mostly suppresses upwelling events. The bottom stress results in the intrusion of water over the shelf, which has an annual fluctuation following that of the EAC behaviour. Bottom stress has a strong influence on Chla bloom magnitude. Wind potentially triggers upwelling events which leads to enhanced Chla blooms, this in addition to bottom stress features are sufficient to explain the blooms of Chla, off Fraser Island, which are classified as P2 events. However, the Chla blooms classified as P1 events are not explained by wind, which suppresses upwelling in the months of maximum P1 event concentration. The aforementioned features are summarised in table 4.3. Days of P2 events are mostly (approx. 87%) under favourable current-driven conditions, (south-north bottom stress component, $\tau_{yb} < 0$) with approximately 67.5% of these days being under wind-driven upwelling conditions (south-north wind stress component, $\tau_{yw} < 0$). The percentages do not consider a lag between the stresses and the Chla blooms. Figure 4.12 illustrates these percentages with a time series of wind and bottom stress, highlighting periods of P2 events. Similarly, approximately 69% of day during P1 events are under wind-driven downwelling conditions, (south-north wind stress component, $\tau_{yw} > 0$) with $\sim$30% of this selection of days being under current-driven downwelling conditions (south-north bottom stress component, $\tau_{yb} > 0$). However, approximately 68% of day during P1 events are under upwelling favourable current-driven conditions. Due to the shape and evolution of P1 events resembling those of wind driven upwelling events,

the wind was studied as a possible physical mechanism. However, the months and percentage of days of P1 events under downwelling wind conditions leads to the conclusion that net surface Ekman transport by wind stress is not the physical mechanism behind P1 upwelling events. Furthermore, the high percentage of days (21%) with both stresses suppressing upwelling points to the involvement of another physical mechanism in P1 upwelling events, which is not bottom stress or wind stress. Considering the fact that both stresses play a role in P2 events, it is possible to estimate the percentage of days that are under favourable upwelling conditions for one of the stresses, whilst the other shows unfavourable conditions. From table 4.3, the condition where the stresses have different signs (direction) in the P2 events show a difference of approximately 27% (28.38%-1.37% in scenario 1 and 28.39%-1.47% in scenario 2), where the bottom stress is dominant.

Relying on estimations of Chla based on remote sensing has its limitations. The impact of cloud cover on the data set used is significant (described in section 4.2) and the quantification of P1 and P2 events is affected by this limitation. However, the analysis of Chla events was developed in this study, under the assumption that the impact on the annual variability is not significant. Other factors potentially impacting the analysis method are the sensitivity of Chla estimation to bottom albedo and sediment in the water (see chapter 2 for a longer list of features to which the Chla estimation is sensitive). Both examples result in over estimations of Chla. An example of Chla over estimation in the study area is at the north of Sandy Cape, Fraser Island. Breaksea Spit is an area of shallow water, with a depth of only a few meters, similar to the channel between Fraser Island and the coastline. In the monthly averages (figure 4.1) these areas are always around $2mg/m^3$; figures 4.2 and 4.4 illustrate identical values in the same areas, however, the temperature shows a clear annual variability which is not observed in the Chla. In these areas the methodology applied in this study is not appropriate as it does not consider shallow optical depth, which is defined as water shallower than $40m$. This $40m$ depth is obtained from the analysis of the remote sensing product K-490. K-490 can be used to estimate the optical depth of water, measuring the depth to which the light can penetrate the water and be reflected (see chapter 3 for the estimation of $40m$). On the open ocean, the optical depth has its maximum values, approximately $40m$. This depth will be less if the water increases its sediment concentration, this is usually observed in coastal areas. These limitations will exclude zones where the method cannot differentiate between "real events" and overestimations due to the water's optical properties.

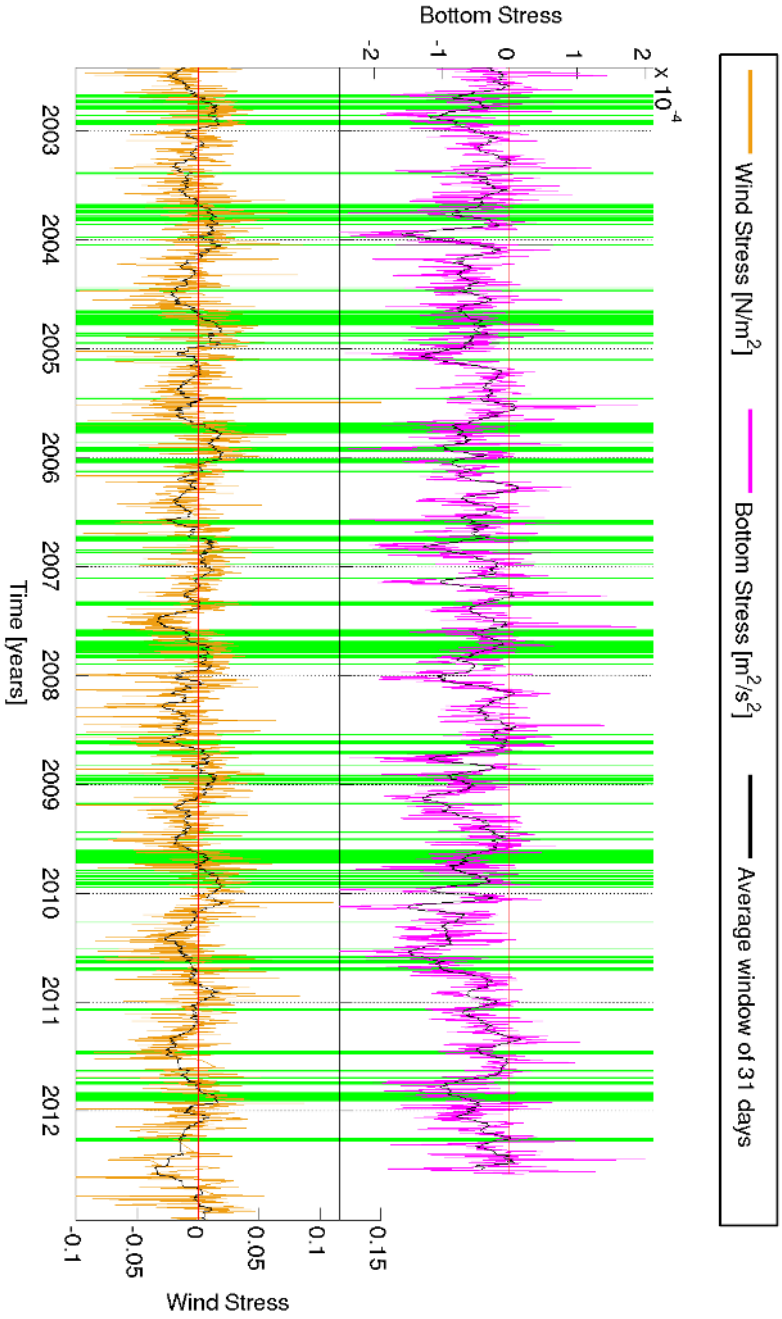

Figure 4.12: Bottom stress, wind stress and high Chla concentrations (green areas) classified as P2 events, off Fraser island. This figure was published by Brieva et al. (2015)

4.6 Summary and Conclusion

Events of high Chla concentration are observable off Fraser Island, their patterns can be classified into two main types. Classification is done according to the length of the coastline involved in the pattern (longer or shorter than $\sim 50km$). P1 events involve a long section of the coast line. From March to July, P1 shows it highest concentration and is, therefore, more likely to be identified. P1's Chla distribution resembles wind-driven upwelling events. A Chla gradient across the shelf, points to an offshore transport of shelf water. P2 events involve a short section of the coastline (<50km), with August to December being when P2 events show their highest concentration. Due to its shape P2 could be identified as a filament, located near to or over the shelf break a majority of the time. The values of Chla are higher in P2 events than P1.

The blooms of Chla classified as P1 and P2 events are proxies of upwelling systems named the SCUS and the SFIUS. The examination of wind stress shows that the SCUS is not a wind-driven upwelling system based on the surface Ekman transport. However, wind stress has a role to play in the SFIUS. Simultaneously, the SFIUS is located over a region of high bottom stress, creating the conditions for upwelling, by uplifting slope water over the shelf. Bottom stress has a stronger role to play than wind stress by approximately 27% based on the number of days showing favourable upwelling conditions for both stresses.

In conclusion the examination of Chla blooms, wind stress and bottom stress lead to:

1. Identifying, naming and characterising the SFIUS, which is mainly driven by bottom stress as well as wind stress, with the latter having only a minor impact ($\sim$27% less impact). The number of Chla blooms in the upwelling system increases with the intensification of the EAC and the displacement of the pattern shows a poleward transport.

2. Identifying, naming and characterising the behaviour of the SCUS. This upwelling system is not driven by surface Ekman transport resulting from the wind stress. The system is associated with the weakening of the EAC and the average wind heading north, with a small eastward component. The displacement of the pattern shows an offshore transport. However, no physical mechanism was associated with this upwelling system.

3. Identifying the Fraser Island high bottom stress zone. This is part of a set of three high bottom stress zones along the eastern coast of Australia and has the strongest bottom stress magnitude values.

4. Identifying three annual periods in the wind stress. The first and second are unfavourable to upwelling whilst the third is favourable. The period in the middle of the year results in a net surface transport northward, which could enhance or create the relaxation of the EAC in this period.

Chapter 5

Eddies of the Southern Queensland Marine Coastal Zone

This chapter discusses the results of the first study regarding near-coastal eddies in the SQCMZ, based on a database created with Halo et al.'s (2014b) eddy detection and tracking tool. Dambacher et al. (2012) suggest transient eddies as a possible mechanism related to the upwelling off Fraser Island. The examination of animation B.2 reveals eddies entraining water from the shelf, resulting in blooms of Chla, classified as P1 events. The first section in this chapter describes a particular eddy event that took place in June-July 2012. Its description shows for the first time in the SQCMZ, the generation of an upwelling event by the entrainment of water resulting from a near coastal eddy, in 2012. Additionally, for the first time the increment of the eddy's vorticity due to the coastal features and physical mechanisms forcing it to reduce its size, is described. The extension of the analysis using the eddy detection and tracking tool for the period of 1993 to 2015, which was restricted to near-coastal eddies, is discussed in the second section of this chapter. The first climatology description of near-coastal eddies along the southern section of the east coast of Australia, results in an agreement with previous descriptions of the EAC in the same area. Finally, the potential of near-coastal eddies to entrain shelf water resulting in upwelling events, the annual periodicity in the eddy activity and the type of eddies that characterise the SQCMZ, lead to the suggestion that near-coastal eddies are a key physical mechanism driving the SCUS.

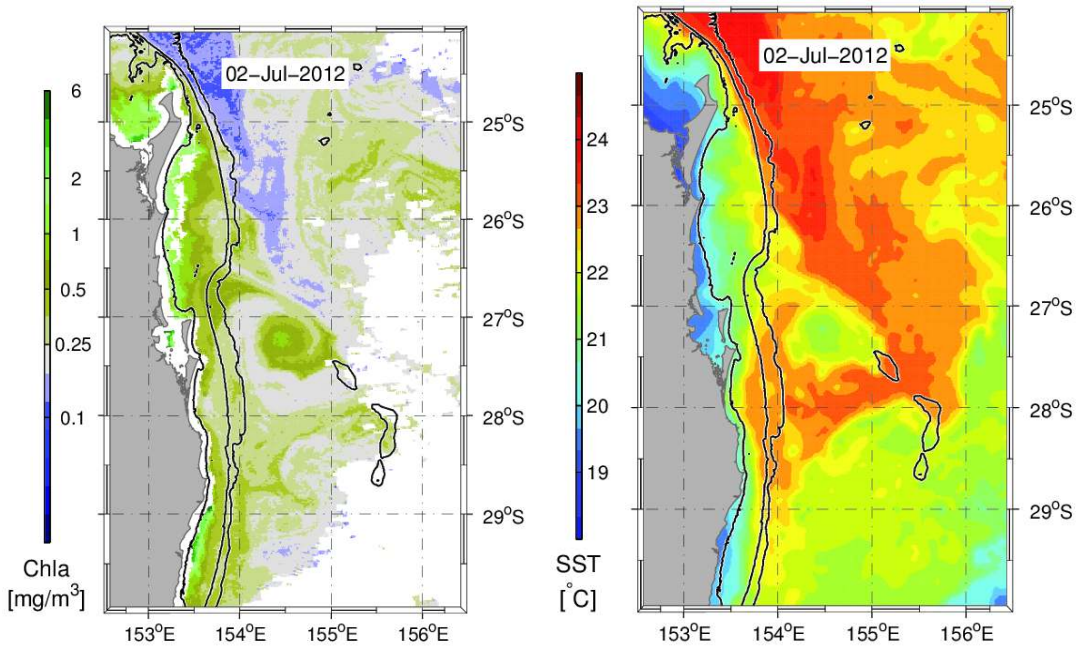

Figure 5.1: Eddy June-July 2012. Left panel shows Chla concentration from IMOS. Right panel shows Sea Surface Temperature from NASA (Jet Propulsion Laboratory).

5.1 Eddy eventin June, 2012

In June 2012 an eddy took place off the SQCMZ. Figure 5.1 shows distribution of Chla and SST for the 2nd of July when the 2012 NCE is observed. Its core can be estimated for the highest value of Chla in the middle of a quasi-circular shape ($>1mg/m^3$), at approximately 154.5°E and 27°S. The eddy is connected to the shelf by a filament with high values of Chla ($>0.5mg/m^3$). In the same figure, SST values show that the water within the 2012 NCE is cold (∼21.5°C) in comparison to the EAC waters (∼23.5°C). From the Chla and SST, it is observable that the entire coast between 25°S and 27°S shows a pattern related to the SCUS. The trigger of the observed upwelling event is the 2012 NCE, which creates an entrainment of shelf water through the filament. Annually from 2012 to 2015 an eddy with similar features is observable in the Chla database between June and July. This research describes the 2012 NCE due to the availability of data from Chla, SST, a set of moorings located off Brisbane, BRAN3.5 and SSHa. The moorings capture changes in the vertical water properties caused by the eddy, as described in the following section.

5.1.1 Near-coastal eddy in mooring observations

Approximately 16 months of data was collected by 5 moorings off Brisbane (section 3.1.2), which covers the period of the aforementioned 2012 NCE in the SQCMZ. The data allows for the vertical impact of an NCE to be described in the study area. The vertical heat distribution of moorings 3 and 4 is strongly impacted by the eddy as its core passes between them, as is shown in figure 5.2. A lifting of the isotherms observed at the moorings in July indicates a change in their profile temperature (figure 5.2). Moorings 1 and 2 show the same behaviour in the isotherms, however, the process is more gradual, with no peak being observed early in July. Mooring 5 shows little disturbance for the same period, demonstrating it is the mooring least affected by the eddy. With the exception of mooring 5, all moorings show a deepening of the isotherms following the dissipation of the eddy. In particular at moorings 3 and 4, the influence of the eddy is observed at depths of approximately $800m$, where cooler and deeper water has been uplifted.

Observed salinity in moorings 3 and 4 (figure 5.2) show a classical vertical distribution. The salinity decreases from the surface ($35.6psu$-$35.2psu$) to approximately $900m$ ($34.45psu$), continuing on from there the salinity increases moderately, remaining stable at approximately $34.7psu$. Due to the vertical salinity distribution, any upwelling or uplifting of water to the surface is expected to result in a decrease of salinity values in the first $1000m$. The salinity time series at moorings 3 and 4 (figure 5.2) show a decrease in the magnitude of the values from early to mid-June. Mooring 3 shows a drop, early in July, of about $0.4psu$ at depths of $\sim 161m$ and $460m$. However, at depths of approximately $2468m$ and $3986m$, the salinity is stable and does not show a reaction to the passage of the eddy. Measurements at approximately $967m$ show a slight increase in the values ($\sim 0.002psu$), contrasting with the salinity drop measured by the two instruments nearest the surface, from early June to mid-July. The small increase in salinity could be explained by the measurements being taken at a depth where the salinity shifts from decreasing to increasing (34.45-$34.7psu$). A similar decreasing to increasing pattern in salinity is observed in the first $800m$ of mooring 4, with a gradient greater ($0.5psu$) than mooring 3 (0.4 or $0.3psu$).

At moorings 3 and 4, their velocity profiles capture the passage of a cyclonic eddy. The u-velocity component (west-east) at mooring 3 shows, in late June, a negative direction (westward transport), indicating it is the southern sec-

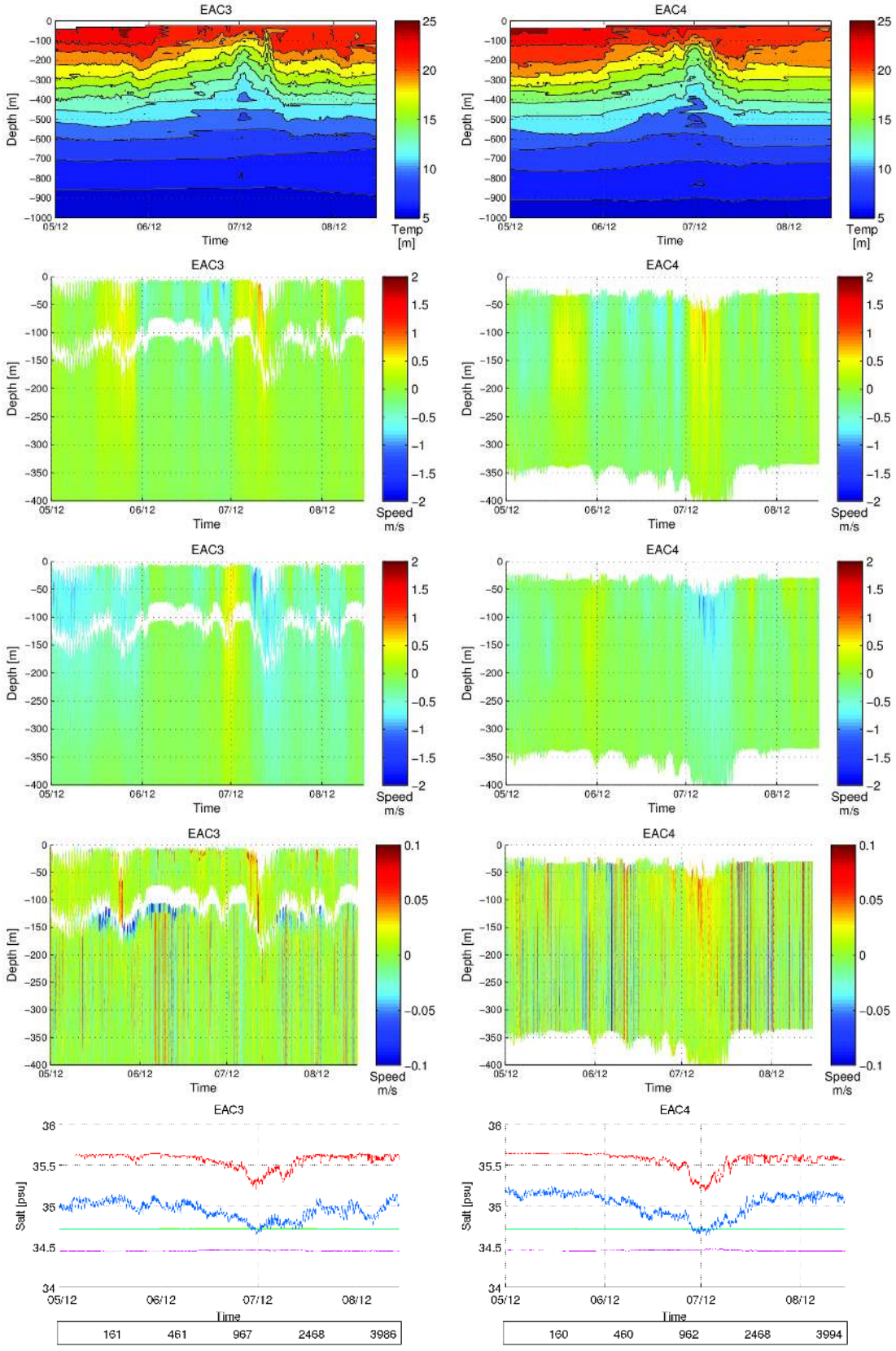

Figure 5.2: Data from mooring 3 and 4 on the left and right, respectively. From top to bottom, temperature, U (east-north), V (south-north) and W (bottom-top) velocity components and salinity.

tion of the cyclonic eddy. Early in July the direction shifts to positive (eastward transport). This is the northern section of the cyclonic eddy which has a poleward displacement. The velocity profiles demonstrate that this behaviour persists to depths of $400m$. The v-velocity component (south-north) shows that mooring 3 has a strong positive value (northward transport) during the transition from June to July. The aforementioned period is when the u-velocity shifts from negative to positive in both moorings (3 and 4). The period of transition should be when the eddy's core passes between moorings 3 and 4. The v-velocity at mooring 4 is negative throughout the entire period of the eddy's passage, meaning this mooring is located to the east side of the cyclonic eddy. The information presented points to the core of the eddy passing between moorings 3 and 4 in late June or early July. When considering the vertical component, mooring 4 has one of the strongest positive vertical velocities (upward transport), so the core should be closest to mooring 4.

5.1.2 Near-coastal eddy in BRAN3.5

BRAN product, version 3.5, is an additional database used to describe the 2012 NCE. BRAN 3.5 also represented an eddy for the same period and location as the 2012 NCE (figure 5.3). The represented eddy was observed to have similar propagation features to the NCE. Figure 5.3 shows, for the 2nd of July, the 2012 NCE to be in a similar location to that of the Chla in figure 5.1. The BRAN3.5 representation is in agreement with both remote sensing data (Chla and SST described before) and observations from the moorings. Agreement between the observations and the BRAN3.5 representation validates its use in the examination of the 2012 NCE genesis. BRAN3.5 surface temperature defines the EAC as a corridor, from north to south, located near the coast (figure 5.3). BRAN3.5 illustrates that the EAC is not always upon the shelf break from June to July. It is when the EAC separates from the shelf break that the eddy is able to begin its formation (14th of June 2012, figure 5.3). It is early in June when the EAC main stream is observed heading east at approximately 25°S. It is plausible that a lee effect in the turning point of the EAC, is hosting a quasi-circular cold mass of water (at approximately 154.5°E and 25.5°S, see figure 5.3 on the 5th of June 2012), which could be the formation of the eddy. From mid-June onward the EAC is returning to its normal position, bringing with it the eddy (25th of June 2012 in figure 5.3). The eddy is forced to move closer to the shelf, where it encroaches

and drafts shelf water offshore. The transport of water results in the enhanced nutrients and cold water observed in figure 5.2 as well as on the 4th of July 2012 in figure 5.3. Finally, the eddy is trapped between the EAC and the shelf at approximately 28°S, where it proceeds to dissipate. This is observed on the 6th, 9th and 11th of July 2012 in figure 5.3.

BRAN3.5 provides sufficient information for the quantification of the offshore water transport, which resulted from the 2012 Eddy encroaching the shelf. Features of the off shore transport were quantified from the 17th June to the 9th July. The average velocity of the offshore transport is approximately 0.03 m/s. The average vertical section area at 154°E involved in the offshore transport was approximately $2.7\times10^7 m^2$. The average flux through the previous area was approximately $9.5\times10^5 m^3/s$ ($0.95Sv$) and the offshore transport was completed in a range of 20 to 25 days. The latitude of maximum offshore transport moves poleward from 26.7°S to 27.6°S. The maximum offshore transport occurs between the 25th June and the 1st July. The period of maximum offshore transport agrees with the sharp increase in eddy vorticity, displacement speed as well as amplitude, estimated using SSHa (section 5.1.3). A rough estimation of the volume of water transported inshore and offshore by the eddy, at 154.3°E, between 27.9°S and 26.1°S, in the aforementioned period, in the first $100m$, resulted in a difference of $1.6\times10^{10} m^3$ offshore transport. An estimation of the volume of water over the shelf between 25°S and 27.5°S, and from $15m$ to $1000m$ depth is $2.5\times10^{10} m^3$. The 64% of renewed water over the shelf due to eddy water entrainment explains the observation of Chla blooms along the majority of the SQCMZ's coast. The percentage increases to almost 100% if the total volume of water off Southern Queensland is estimated between $15m$ and $500m$ depth, instead of $1000m$.

5.1.3 Detection and characterisation of 2012 NCE in the Sea Surface Height

SSHa shows negative values when and where the eddy is located off southern Queensland, Australia. The negative values agree with the concept of cyclonic eddies uplifting water at their core (see figure 5.4). Figure 5.4 illustrates negative SSHa where the eddy, with a poleward displacement, is observable in the SQCMZ, as seen in the BRAN3.5 representation and interpretation of mooring velocity behaviour. The highest amplitude is reached as the eddy approaches 27.5°S, this peak occurs in around the first week of July. The eddy quickly dissipates after

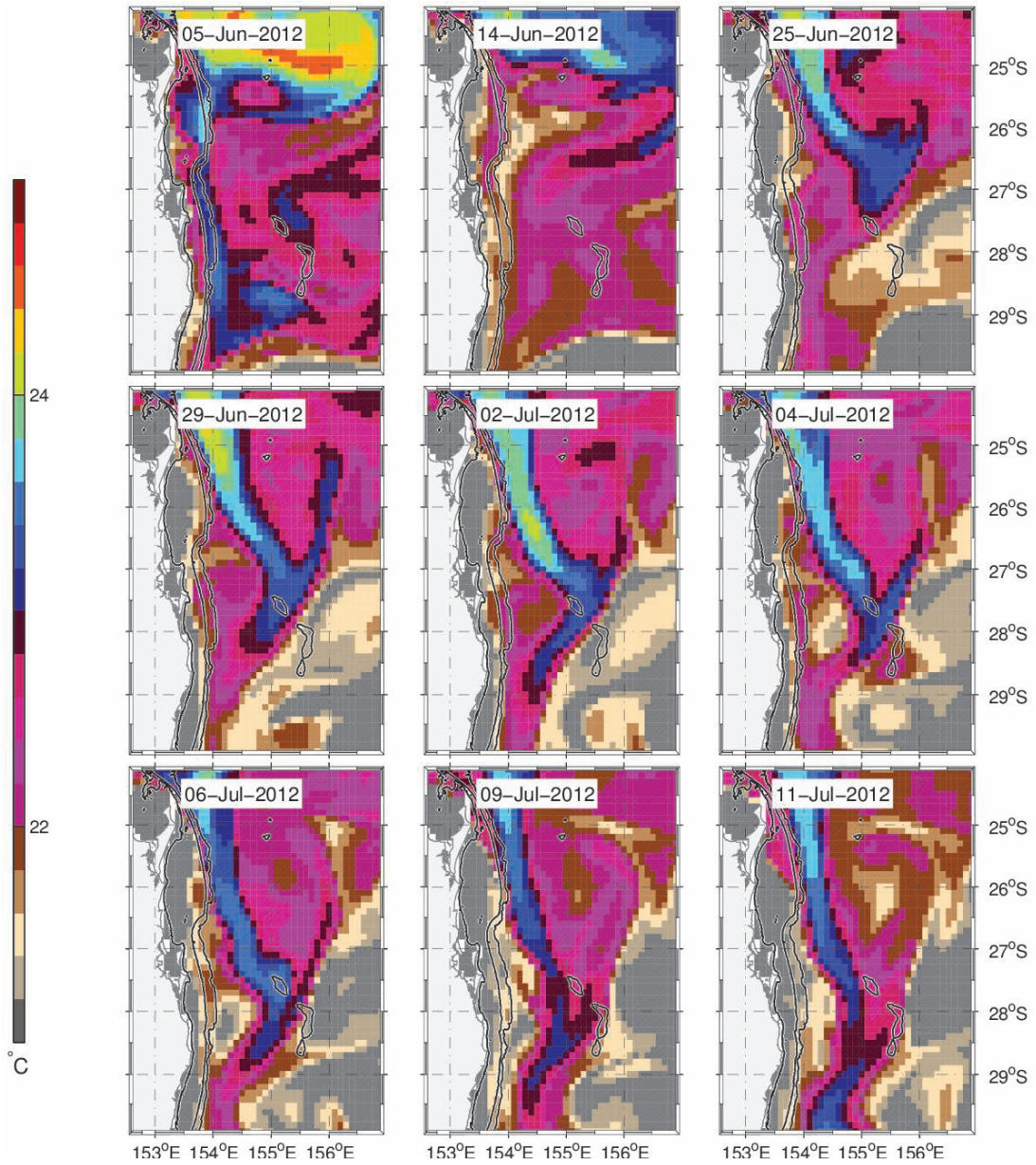

Figure 5.3: The simulated surface temperature from BRAN3.5. The illustrated days are part of the 2012 NCE. Three isolines of bathymetry are represented by constant black lines. From west to east the lines represent the depths $40m$, $200m$, and $1000m$.

reaching its maximum amplitude. The quick dissipation of the eddy agrees with the numerical representation. BRAN3.5 shows the eddy being trapped between the EAC and the shelf, where it is forced to reduce its size. The amplitude of SSHa, which is a proxy of eddy energy, decays as the eddy enters shallower waters in a wider shelf section (∼28°S, see bathymetry in figure 1.1). The eddy dissipates as it experiences strong interactions with the shelf, the bathymetry becomes more shallow and the EAC prevents it from taking an eastward displacement. These aforementioned restrictions force the eddy to reduce its size, similarly it can be assumed that the rotational speed of the eddy increases due to energy conservation. The assumption regarding its rotational speed can be quantified using the implementation of an eddy detection and tracking tool, which estimates the eddy vorticity (Halo et al., 2014b).

The eddy detection and tracking tool developed by Halo et al. (2014b), detects and tracks the 2012 eddy, based on SSHa observations. Figure 5.5 illustrates a selection of the eddies features quantified by the tool. The eddy is first detected late in May, throughout June and early in July. In the first half of its lifespan, the eddy has a stable amplitude, displacement speed and vorticity, which is negative for cyclonic eddies (figure 5.5 from late May until the 22nd of June). In figure 5.5, the extracted SST values for the averaged eddy coordinates decreased by 1°C, between the 31st of May and the 1st of June. The stability of the eddy features seen in the first three weeks of June are disrupted in the last week, when its amplitude and vorticity suddenly increase. The displacement speed of the eddy accelerates, as well as travelling in a straight poleward direction (figure 5.4). SST values decrease by a further degree and the Chla values raise their magnitude simultaneously, as illustrated by figure 5.5 (from the 27th to the 29th of June). Once maximum vorticity is reached (figure 5.5) the eddy rapidly dissipates in the following two weeks. The maximum vorticity period is in agreement with the period when entrainment of shelf water is strongest, according to BRAN3.5, this is also confirmed by the clear signal printed in the Chla and SST. The sudden change in the vorticity and its ability to extract water results in the formation of an upwelling event (figure 5.1), which forms part of the SCUS (P1 event according to Chapter 4).

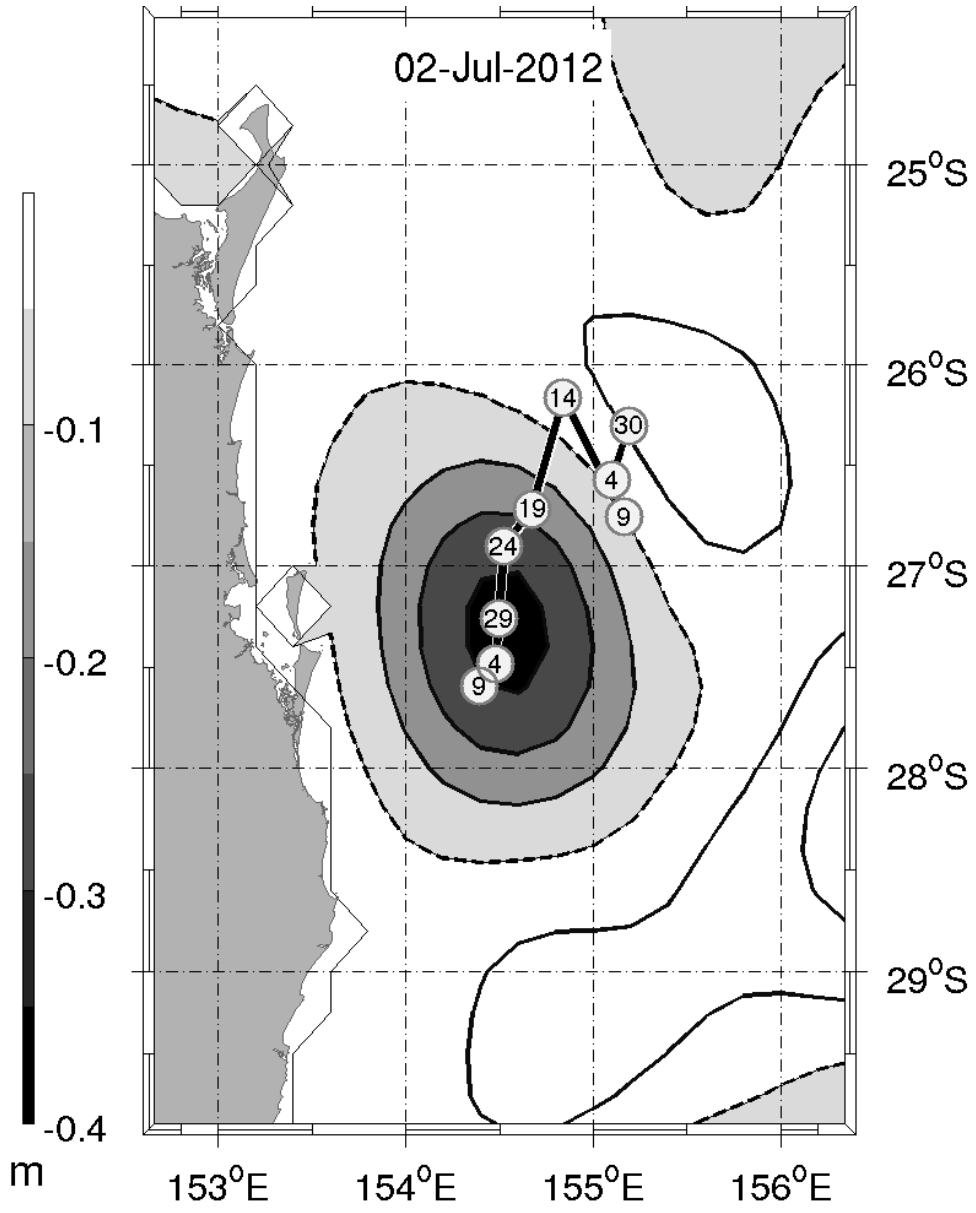

Figure 5.4: Sea Surface Height anomaly (SSHa) for the days where the 2012 NEC is present in the SQCMZ. Shading areas are <0 and the contour interval is $0.05m$. The line representing $0m$ is a dash line. White areas are $>0m$. The numbers within a circle illustrate the average location of the eddy for the day indicated by the number. The first location of the eddy is the 30th of May (30 within a circle) and the last location of the eddy is on the 9th of July (9 within a circle). The location of the eddy is according to the results of eddy detection and tracking tool (Halo et al., 2014b)

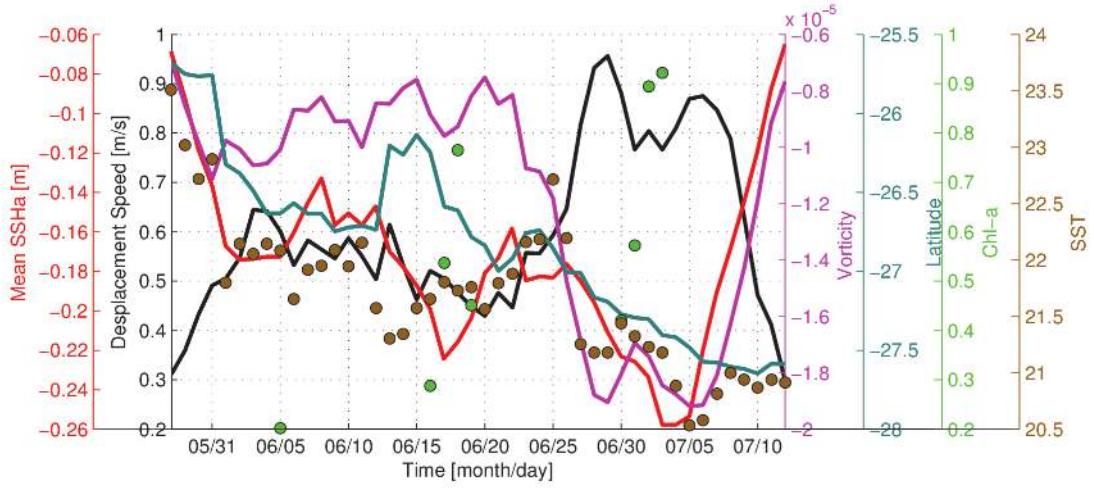

Figure 5.5: 2012 Eddy features from Halo et al.'s (2014b) code. Dots are Chla (green) and SST (brown) extraction at the eddy coordinates calculated by the Matlab code from IMOS Chla data base and NASA SST data base.

5.2 Eddy Climatology Description

The application of the aforementioned eddy detection and tracking tool (Halo et al., 2014a) to the whole period of available SSHa data, results in a climatology view of eddy features, both in the study area and along the east coast of Australia. Similar studies describe the eddies based on existing eddy census data. These are restricted to the parameters applied in the detection and tracking processes. In the case of this research, after the detection and tracking processes, a filter of a minimum seven-day day life span is applied. The filter is included in the analysis of the small NCEs, which may potentially have a similar impact to the eddy mentioned in section 5.1.

The eddy study has been restricted to two corridors. The corridors western boundary is the coast line, whilst their eastern boundaries are defined, for the purpose of this research, at $100km$ and $600km$, respectively, offshore from a constant depth (bathymetry isoline) of $100m$ (see section 2.2.3.2 to discuss the reasons behind these distances). The widest corridor will be used as a comparison against other studies. The narrowest corridor is used to describe the features of the NCEs along the southern section of the east coast of Australia. Detected eddies as well as eddy events were included in this analysis (see section 3.2.1.3 for further details). The eddy events used in this analysis, are those with a life span longer than seven days. A detected eddy results from the analysis of a single sample of SSHa, the detected eddy is part of an eddy event with a life span

greater than seven days. To validate the results, the same analysis was restricted to eddy events with a minimum life span of twenty eight days. The change in the restricted lifespan allows for comparisons to be made with studies based on the eddy census carried out by Chelton et al. (2011).

5.2.1 Validation of the eddy census based on the eddies within the 600km corridor

Figure 5.7 displays the latitudinal concentration of detected eddies for both corridors. Three zones delimit the areas in which the concentration is approaching a normal distribution of data based on the results from the 100km corridor. The boundaries are located in areas of minimum concentration. These three zones are named Zone 1, Zone 2 and Zone 3, listed from north to south (see figure 5.6). Figure 5.7 illustrates that the number of cyclonic and anticyclonic eddies is similar along the coast, however, there are a greater number of cyclonic eddies occurring in the three zones (figure 5.7). Zone 1 shows a low variability in latitudinal distribution. Zone 2 shows a quasi-normal distribution, where the peak is mainly associated with the increase of short life eddies (gray bars), with a greater increase in the number of anticyclonic eddies. The increase could be due to the Tasman Front and the separation of the EAC. The number of detected eddies increases poleward in Zone 3, with two peaks being identified in this zone. The first peak is located at approximately 35°S and is related to an increase in long life eddies. The second peak is located at approximately 36°S and is associated with an increase in short life cyclonic eddies. Generally, the long life eddies are found to be more dominant in this corridor.

The combination of Zone 2 and Zone 3 includes the Eddy Avenue, described by Everett et al. (2012). Similarly, combining Zone 1, Zone 2 and Zone 3 includes the area described by Pilo et al. (2015). Both studies use the eddy census created by Chelton et al. (2011), which analysed SSHa over a shorter time period than used in this study, it involved a lower time resolution (this study uses every two days and after 2011 daily again every seven days) as well as lower spatial resolution (this study 0.2 degrees resolution SSHa again a 0.25 degrees resolution). Pilo et al. (2015) also applied an additional filter with a minimum life span of ten weeks. Considering the aforementioned differences, the results show that the proportion of cyclonic and anticyclonic eddies is similar. In this study, cyclonic eddies are ∼51.7% of the total eddies detected (from table 5.1), in Everett et al. (2012) the

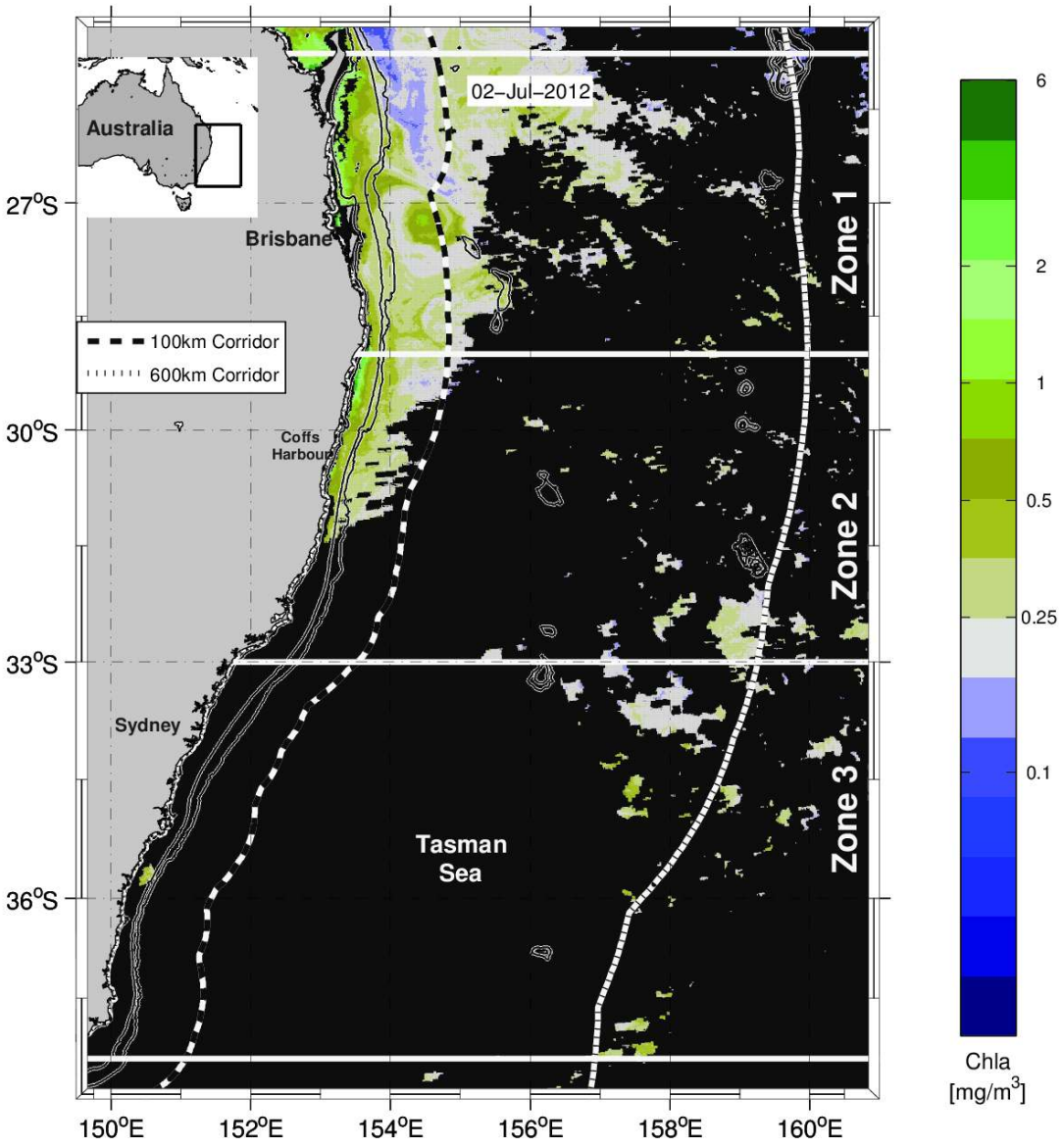

Figure 5.6: Chla along the eastern coast of Australia, black represents areas covered by clouds. 2012 NCE is observable as in the figure 5.1. Coloured dots represent the moorings. Horizontal lines delimited the three zones defined according to the NCEs features. Dash lines represent the eastern boundaries of the $100km$ and $600km$ corridors, left and right lines respectively.

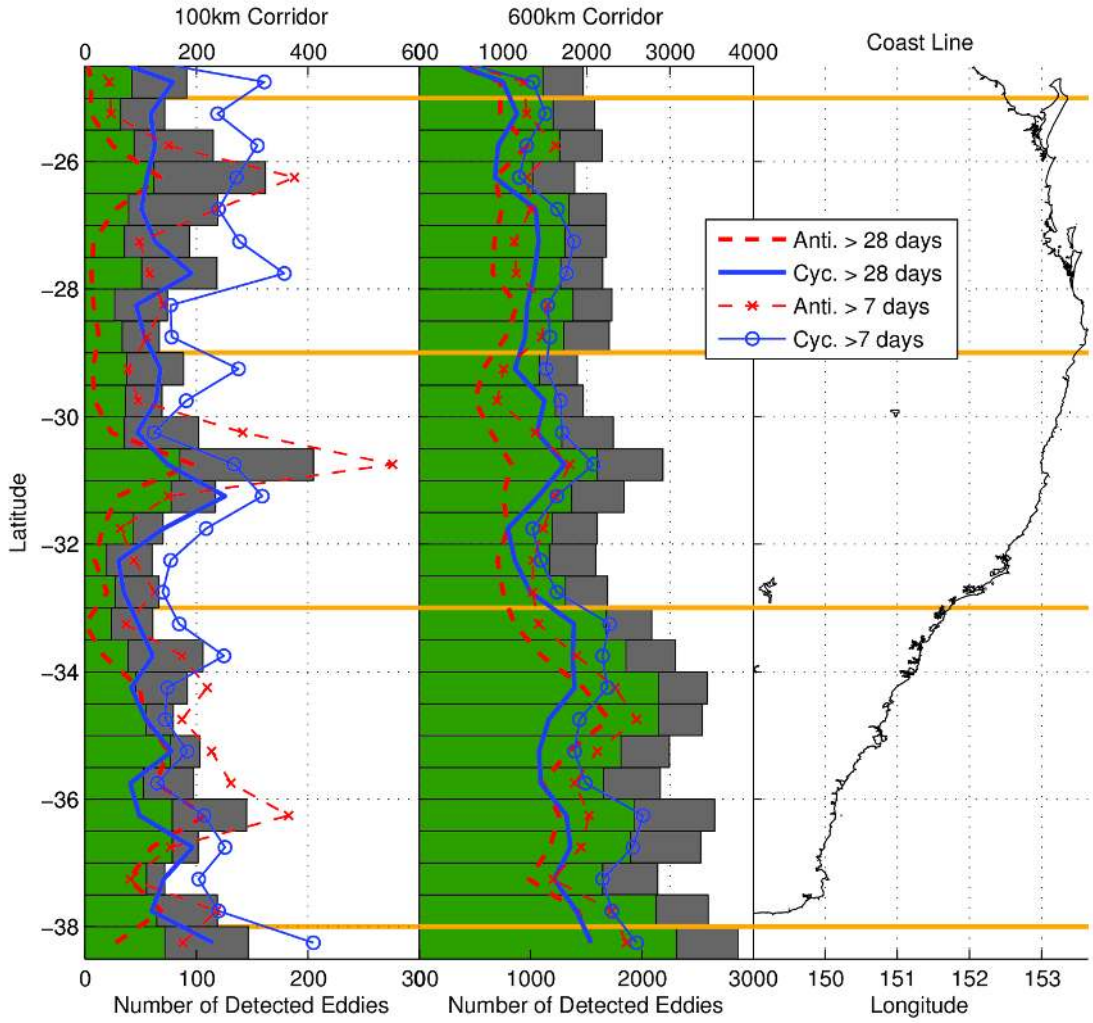

Figure 5.7: Distribution of eddies along the coast for $100km$ and $600km$ corridors. Histograms (bars) are scaled at the top axis and the time series (lines) are scales at the bottom axis.

proportion is ∼50.3% and in Pilo et al. (2015) it is 51%. The average eddy radius is smaller in this study with: $74km$ and $77km$ for Cyclonic Eddies (CEs) and Anti-Cyclonic Eddies (ACEs) respectively, compared to $92km$ and $95km$ in Eddy Avenue (Everett et al., 2012) and $83.4km$ and $82.7km$ in Coral Sea and Tasman Sea, respectively (Pilo et al., 2015). The proportion of ACEs a few kilometres larger than the CEs is observed by Everett et al. (2012), however, in Pilo et al. (2015) cyclonic eddies show the largest average radius. Differences in the average radius magnitude could be due to the higher spatial resolution used, allowing for the detection of smaller eddies.

The magnitude of the average amplitude is in the range of the Eddy Avenue (CE $22cm$ and ACE $21cm$ again CE $23cm$ and ACE $24cm$ from Eddy Avenue). However, this magnitude is significantly larger if compared with eddies in the open ocean, which are less energetic, Pilo et al. (2015) describes values of $9.2cm$ (CE) and $8.6cm$ (ACE). In Zone 2 highly energetic short eddies occur, resulting in larger magnitudes of rotational speed (CE $64cm/s$ and ACE $59cm/s$) than those described by Everett et al. (2012, CE $45cm/s$ and ACE $50cm/s$) and Pilo et al. (2015, CE $21.1cm/s$ and ACE $20.1cm/s$). Pilo et al. (2015) describe the propagation speeds in both the Coral Sea (3-$6cm/s$), which includes Zone 1 (CE $2.7cm/s$ and ACE $2.4cm/s$), as well as the Tasman Sea (1-$1.5cm/s$), which includes Zone 2 and Zone 3 (CE $1.8cm/s$ and ACE $1.5cm/s$). Eddies have a slower propagation in the Tasman Sea than in the Coral Sea, as captured in the results of this study. In summary, this study tends to capture a large number of eddies smaller and more energetic (larger amplitude) than those described by Everett et al. (2012) and Pilo et al. (2015). In conclusion, this study shows main features similar to those described by Everett et al. (2012) and Pilo et al. (2015). These main features are: the largest number of cyclonic eddies, similar proportion between cyclonic (∼51%) and anti-cyclonic eddies (∼49%) and a slower propagation speed in the Tasman Sea rather than in the Coral Sea.

5.2.2 Characterisation of near-coastal eddies

The detected eddies latitudinal distribution in the narrowest corridor (figure 5.7, left histogram) shows both greater variability and proportion of short-lived eddies when compared to the wider corridor. Cyclonic eddies are dominant in Zone 1 and Zone 2 (blue lines), whilst in Zone 3 the number of cyclonic and anti-cyclonic eddies are similar. There is a main peak in Zone 1 and Zone 2, whilst Zone 3

Table 5.1: Climatology features of eddies in $100km$ corridor based on the selected eddy tracking tool. These features are for eddies with a lifespan of 7 days or more and no minimum radius was used, which results in the minimum radius of about $22km$ ($21.967km$).

Features	Zone 1		Zone 2		Zone 3	
	Cyclonic	Anticy.	Cyclonic	Anticy.	Cyclonic	Anticy.
Number of eddy events	153	138	121	127	151	150
Daily abundance of eddy events	0.018	0.017	0.015	0.015	0.018	0.018
Number of detected eddies	1003	640	840	719	968	985
Daily abundance of detected eddies	0.121	0.08	0.101	0.087	0.116	0.119
Percentage from total detected eddies	61.05	38.95	53.88	46.12	49.56	50.44
Radius average $[km]$	59.99	55.38	57.19	52.99	51.61	53.18
Amplitude average $[m]$	0.099	0.051	0.132	0.061	0.116	0.128
Area average $[km^2]$	11887.3	10117.6	10894.9	9339.2	8784.3	9493.1
Mean SSH $[m]$	-0.124	0.097	-0.165	0.166	-0.123	0.189
Mean Velocity of displacement $[m/s]$	0.055	0.045	0.046	0.017	0.036	0.026
Mean Rotational Speed $[m/s]$	0.435	0.294	0.528	0.349	0.467	0.504
Number of detected eddies available at the Chla database	318	198	279	235	314	287
Number of detected eddies with quantification of Chla gradient	287	178	238	222	255	253
Mean Chla $[mg/m^3]$	0.18	0.11	0.22	0.14	0.43	0.26
Chla gradient or anomaly average $[10^{-4}mg/m^3]$	-16.7	-113.8	-60.6	-185.4	188.3	-274.4
Number of detected eddies available at the SST database	740	452	652	507	623	680
Number of detected eddies with quantification of SST gradient	740	452	652	507	580	656
Mean Temp [°C]	24.08	24.63	23.13	23.03	20.24	20.45
Temp gradient or anomaly average [°C]	-0.05	0.032	-0.058	0.021	-0.171	0.021

Table 5.2: Percentages of the total number of detected eddies per zone for the cases listed in the highlighted left columns. The results from the analysis of the 100km corridor show the two most dominant cases (bold percentages) that characterise each zone. The top half section of the table is the analysis for eddies with radius $> 22.5km$, whilst the bottom half section for eddies with radius $>45km$.

radius $>22.5km$		Z1		Z2		Z3	
		Short Lived	Long Lived	Short Lived	Long Lived	Short Lived	Long Lived
100km	CEs [%]	**31.35**	**29.7**	20.85	**33.03**	18.74	**30.82**
	ACEs [%]	29.15	9.8	**32.58**	13.53	22.94	**27.5**
600km	CEs [%]	11.12	**42.12**	9.76	**44.73**	12.25	**40.25**
	ACEs [%]	11.7	**35.06**	14.77	**30.74**	8.41	**39.09**
radius $>45km$		Z1		Z2		Z3	
		Short Lived	Long Lived	Short Lived	Long Lived	Short Lived	Long Lived
100km	CEs [%]	**32.82**	**36.74**	21.03	**41.2**	24.36	**26.01**
	ACEs [%]	23.15	7.29	**29.83**	7.94	17.07	**32.56**
600km	CEs [%]	13.5	**40.72**	13.38	**42.74**	14.03	**35.24**
	ACEs [%]	16.38	**29.4**	15.61	**28.27**	9.95	**40.78**

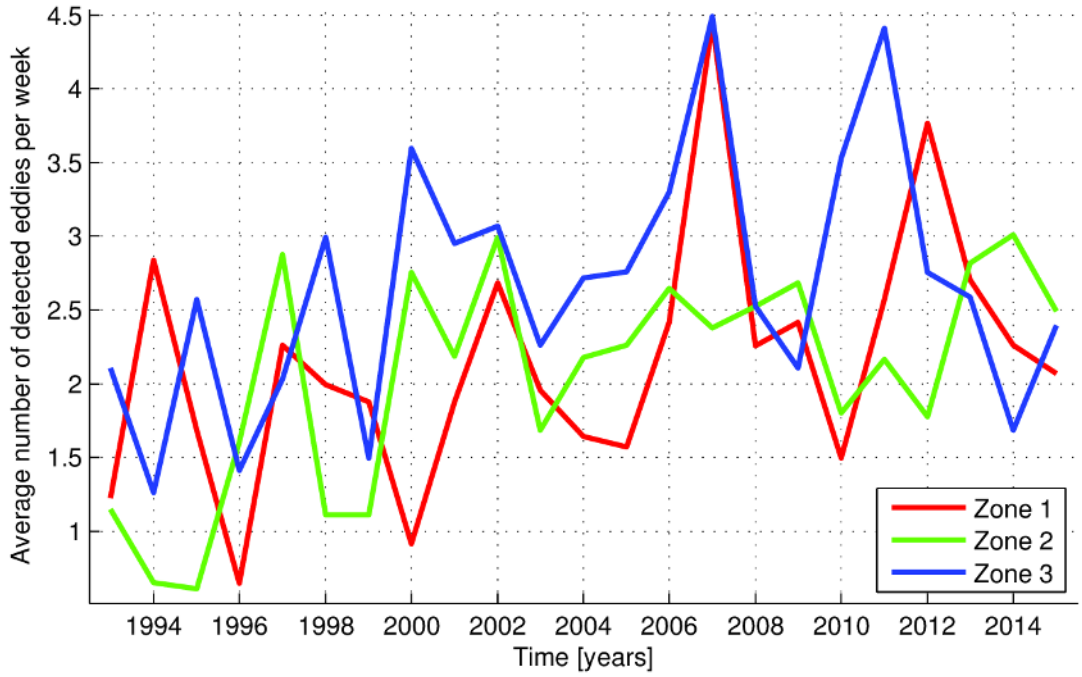

Figure 5.8: As the temporal resolution of Sea Surface Height database changes from data every two days to daily data in 2011, lines represent the average of detected eddies per week for each year, considering this changes in temporal resolution. The line colours represent the three zones.

contains multiple peaks. The peaks in Zone 1, Zone 2 as well as a single one in Zone 3 are mainly created by a sharp increase in anti-cyclonic short lived eddies (∼26°S, ∼31°S and ∼36°S). The two other peaks observed in Zone 3 are associated with a sharp increase in cyclonic short-lived eddies (∼34°S and ∼38°S). Figure 5.8 illustrates the number of eddies detected, per day, for each year of the analysed period. Zone 1 and Zone 2 have similar magnitudes, with Zone 3 having the largest concentration of eddies per day, as it is the largest of the three zones. A linear trend is observed, as the number of eddies tends to increase in time. The linear trend to increase is observed when short-lived eddies are included (<24 days and >7 days). For long-lived eddies, the average number of eddies, per day, in each year shows a stable variability.

The maximum peak in the latitudinal distribution is located in Zone 2. In the narrowest corridor, Zone 2 is dominated by long-lived cyclonic eddies (> 24 days) and short-lived anti-cyclonic eddies (table 5.2). The dominant features are the same if the analysis does not consider eddies with a radius smaller than $45km$ (table 5.2). Anticyclonic eddies are the smallest eddies in Zone 2, as their percentages show the largest decrease when the minimum radius is $45km$ (table 5.2).

The higher percentage associated with short-lived cyclonic eddies is mainly due to their peak in Zone 2. The peak's location is consistent with the EAC separation point, described by Ridgway and Dunn (2003) and discussed by Cetina-Heredia et al. (2014).

The second maximum peak is located in Zone 1. Similarly to the peak in Zone 2, this peak is due to an increase in short-lived anti-cyclonic eddies. However, the two dominant features in Zone 1 are short-lived cyclonic eddies and long-lived cyclonic eddies (5.2). If eddies with a radius smaller than $45km$ are not considered, then the percentages for the four types of eddies are similar, however, the two dominant features shift positions, resulting in long-lived cyclonic eddies being the most dominant. The shift in the position of dominance between the types of eddies in Zone 1, shows that smaller eddies tend to be short-lived and cyclonic. Zone 1 shows the lowest percentage in table 5.2 for long-lived anticyclonic eddies, these are inhibited in Zone 1 as well as being slightly inhibited in Zone 2. This inhibition is also observed in the amplitude of eddies. Table 5.1 lists small amplitude averages ($<0.1m$) in Zone 1, for anti-cyclonic and cyclonic eddies. Zone 2 has a smaller amplitude average for anti-cyclonic eddies. Figure 5.9 illustrates these small amplitudes, showing that anticyclonic eddies have smaller amplitudes in Zone 1 and Zone 2. In Zone 3, the anticyclonic eddies increase their amplitude to a range similar to that of cyclonic eddies. At the same time, the amplitude of the cyclonic eddy magnitude increases in Zone 1, remaining stable around $12cm$. EAC intensification occurring in Zone 1 and the formation of cyclonic eddies in that zone could be the reason for this quasi-linear increase of cyclonic eddy amplitude. Similarly, the inhibition of anti-cyclonic eddies by the EAC explains the small amplitudes in Zone 1 and Zone 2.

Table 5.1 lists the features of the eddies whose estimated coordinates fall within the $100km$ corridor. The largest percentage difference between cyclonic and anticyclonic eddies occurs in Zone 1 (22%), where a larger number of cyclonic eddies were detected. Cyclonic eddies are larger than anticyclonic eddies in Zone 1 and Zone 2, whereas, anticyclonic eddies are larger in Zone 3. This supports the idea of the EAC suppressing anti-cyclonic eddy formation and shortening their life span in Zone 1 and Zone 2, when the EAC is near the shelf. The mean radii of cyclonic and anti-cyclonic eddies in Zone 3 is greater for anti-cyclonic eddies, with a difference of $\sim 2km$. Zone 1 and Zone 2 show a difference of $\sim 4km$, where cyclonic eddies have the greatest radii. The similarity and difference between the two types of eddies also relates to their rotational speed in the three defined zones.

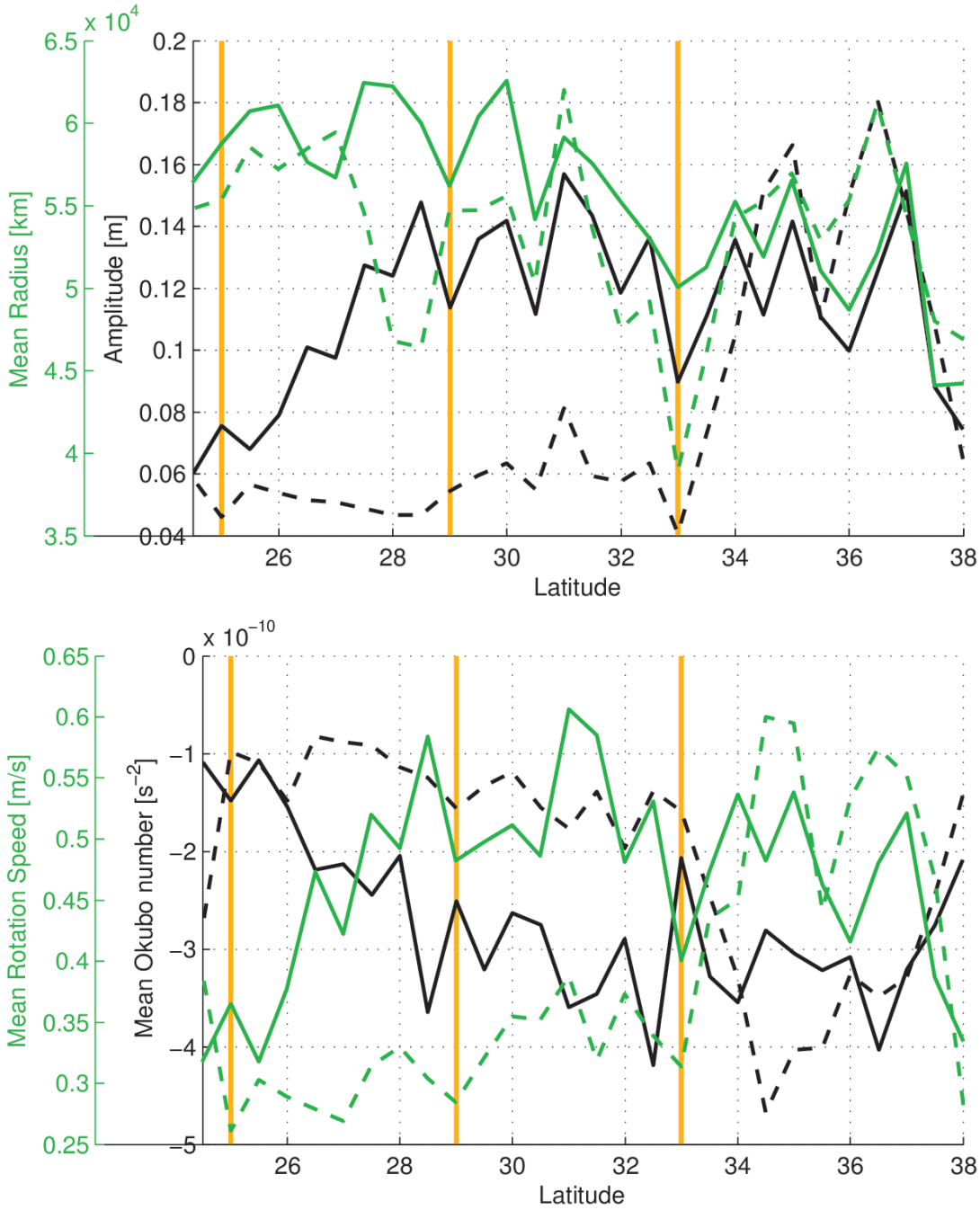

Figure 5.9: Latitudinal average of eddy features from the 100km corridor. Constant lines represent cyclonic eddies and dashed lines anticyclonic eddies. Yellow lines (vertical lines) delimited Zone 1, Zone 2 and Zone 3 from left to right.

Zone 1 and Zone 2 have faster rotational speeds for CE's in comparison to AE's, whilst Zone 3 shows similar values for both. However, in general, anti-cyclonic eddies show faster rotational speeds in Zone 3. The largest difference in average displacement speed is observed in Zone 2 ($\sim 0.03 m/s$), where Zone 1 and Zone 3 have a difference of $0.01 m/s$ and $0.006 m/s$, respectively. Zone 3, again, shows the greatest similarity in features between CEs and AEs. These features allow it to be concluded that the EAC restricts the formation of near-coast AEs, whilst enhancing the formation of near-coast CEs in Zone 1 and Zone 2.

Mean Chla at the averaged eddy coordinates shows greater values for CEs than for AEs (table 5.1), which agrees with the idea of CEs uplifting water in their core. Average values of Chla for CEs per zone is largest in Zone 3 and smallest in Zone 1. The magnitude in Zone 1 is around the normal open ocean value for winter or the usual value over the shelf. The average background value is around $0.2 mg/m$ in winter, when the surface mixing layer deepens. Zone 2 is slightly above the average background value and Zone 3 is about $0.2 mg/m^3$ over, for CEs. For ACs both zones have values similar to or lower than the background. Additionally, the gradient is expected to be positive for CEs, as Zone 3 shows, and negative for AEs, as all the zones show. However, the mean Chla anomaly is only positive (greater Chla concentration in the core) in Zone 3 while Zone 1 and Zone 2 show negative values of Chla anomalies, meaning the highest values of Chla are at the edge and not the core of the eddy. Anomalies of SST show similar features to Chla, with SST anomalies showing greater contrast between CEs than AEs, allowing for a more clear definition of the two. Nevertheless, the magnitude of the anomalies is small in Zone 1 and Zone 2 (~ 0.05). All the values in both zones are in a similar order of magnitude, including the AEs in Zone 3. CEs in Zone 3 are the exception, showing a mean anomaly one order of magnitude larger (-0.17). Anomalies in the three zones are, negative for CEs and positive for AEs. Averages of SST are slightly less in CEs than in AEs, with the exception of Zone 2.

. A large number of CEs are observed along the latitude 23°S, which agrees with the rotational direction (cyclonic) and position (mouth of Capricorn Channel) of the Capricorn Eddy (Weeks et al., 2010). This concentration mainly consists of cyclonic and short-lived eddies. The Capricorn eddy is reported by the literature and called a quasi-stationary eddy, explaining the large number of detected eddies in that area (quantify the number of eddies per day). This additional information contributes to validate the analysis of eddies in the $100 km$

corridor.

5.3 Discussion

The examination of observations and numerical representations of an eddy event, in June-July 2012 (2012 NCE), shows its impact on the circulation and shelf-water properties. The 2012 NCE finds its origin in what could be a lee effect, resulting from the EAC separating from the coast and interacting with Fraser Island. The formation of the eddy takes place in late May. A detection and tracking tool based on SSHa captures the 2012 eddy, quantifying its poleward displacement. The eddy's characteristics show little change throughout early June, however, in late June and early July these characteristics show a drastic change. The vorticity as well as displacement velocity suddenly increases. Simultaneously, the EAC moves back to its usual position upon the shelf break following its separation in late May and early June. The return of the EAC near to the coast encapsulates the eddy against the shelf, forcing the eddy to reduce its size and to encroach on the shelf. Considering the conservation of energy, the eddy should increase its rotational speed as it reduces its size, meaning an increment of vorticity previously captured by the detection and tracking tool. As the eddy is encroaching the shelf, shelf-water is transported offshore, resulting in an offshore Chla filament of cold water connected to the edge of the eddy, as captured by remote sensing. The extraction of water by the eddy results in a coastal bloom of Chla characterised by cold water as the eddy travels poleward. The pattern of the Chla bloom agrees with the characteristics associated with the SCUS (P1 event described in Chapter 4). The net volume of shelf-water transported off shore is roughly $1.6\times10^{10}m^3$. This is transported over a range of 20 to 25 days at $\sim$0.03 m/s. The amount of water transported offshore is about 64% of the total water volume over the shelf (between Fraser Island and Moreton Island and between the $15m$ and $1000m$ bathymetry isolines, $2.5\times1010m^3$). The impact on larvae concentrations upon the shelf should be significant if the shelf water is renewed at this level. However, to confirm this, it is necessary to describe the larvae distribution before and after the eddy takes place in the SQCMZ, which is not done in this study. Finally, late in July the eddy dissipates, potentially due to the dissipation of energy by its interaction with the shelf.

Reports or studies regarding potential sporadic separations of the EAC off

Fraser Island (∼25°S) have not been found to date. The shelf narrows at this point, presenting a possible explanation for the EAC separation, as discussed by Cetina-Heredia et al. (2014). Additionally, it may be related to the weakening of the EAC in Austral autumn and winter, or to the wind stress that results in a northward net Ekman transport during this period (May to September). At this point the assumption of the separation of the EAC being a driver of eddy formation off Fraser Island is made. Once the eddies are trapped between the EAC and the coast they extract water from over the shelf. As the EAC "forces" them to reduce their size the volume of shelf water extracted increases. NCEs show their highest concentration in winter. In winter, particularly June-July, remote sensing has captured eddies off Southern Queensland having similar impacts over the shelf from 2012 to 2015. At this point it is possible to state that eddies in this region play a role in upwelling events, supporting the suggestion of Dambacher et al. (2012), that transient eddies are possible drivers of upwelling events. In the case of this research, the resulting upwelling events are part of the SCUS.

Eddies within the $600km$ corridor show similar general features to those mentioned in previous studies. Applying a minimum radius of $45km$, which is near to the minimum radius of Chelton et al.'s (2011) database ($\sim 40km$), allows for the comparison of values. This demonstrates that Everett et al.'s (2012) eddy detection tool detects more small eddies, due to the higher spatial resolution of the SSHa. The ratio between cyclonic and anticyclonic eddies are the same (Everett et al., 2012; Pilo et al., 2015). The difference between the propagation speed in the Coral Sea and the Tasman Sea (Pilo et al., 2015) is also captured using the detection and tracking tool selected for this study. These congruences support the use of the selected eddy detection and tracking tool.

The narrowest corridor focuses on NCEs potentially impacting the shelf circulation. The study area (Zone 1 in the narrowest corridor) holds the second maximum peak of latitudinal eddy concentration. The hypothesis of sporadic separations of the EAC off Fraser Island explains the peak in Zone 1, which mainly consists of short-lived anti-cyclonic eddies. The hypothesis is suggested in this study as the main eddies are cyclonic in the SQCMZ (Zone 1) and the peak steps out of the norm. The same is observed in the separation of the EAC, where the peak of AEs steps out of the normal dominance by CEs. EAC-Fraser Island interaction results in a lee effect, where the radius of the eddies starts to increase poleward in Zone 1. The interaction could be the formation of eddies, as was shown in the 2012 NCE. Nevertheless, no formal reports were found regarding a

separation of the EAC in this area. Ridgway and Dunn (2003) suggest a secondary point of separation for the EAC in Zone 1.

The three zones, initially defined according to the latitudinal distribution of their eddies, show particular features that define and characterise each zone individually. Characterisation by the two most dominant types of eddies is what defines each zone. The four defined types of eddies are: short-lived cyclonic eddies (SCE), long-lived cyclonic eddies (LCE), short-lived anti-cyclonic eddies (SACE) and long-lived anti-cyclonic eddies (LACE). The characterisation results in Zone 1 having SCE and LCE as the two most dominant features, Zone 2 with LCE and SACE and Zone 3 having LCE and LACE. This characterisation remains the same if small eddies (radius$<45km$) are not considered in the analysis. However, the characterisation changes for the widest corridor where all zones are dominated by the LCE and LACE. In this case, the three zones are not distinguishable from each other as is the case in the $100km$ corridor.

In terms of eddy amplitude, Zone 1 has CEs which increase their amplitude poleward, in a quasi-linear trend, as well as ACEs with a small amplitude ($<0.06m$). Zone 2 has CEs with average amplitudes around $0.13m$ and ACEs which oscillate around $0.06m$. In Zone 3, both eddies (CEs and ACEs) have a similar amplitude, with ACEs sharply increasing between 33°S and 35°S. The increase in the average amplitude in Zone 1 agrees with the EAC intensification zone defined by Ridgway and Dunn (2003). Regarding the eddy latitudinal distribution, the number of total CEs in Zone 1 is around 300 every 0.5°S, while ACEs show a quasi-normal distribution centred at approximately 26°S. Along Zone 2, CEs and ACEs show quasi-normal distributions centred at 31.5°S and 31°S, respectively. Finally, along Zone 3, CEs and ACEs show a trend increasing poleward, with ACEs displaying a maximum peak at approximately 36°S.

Additional features of the study area (Zone 1) show that it is strongly dominated by eddies with a life span of seven to twenty four days (short-lived eddies). The maximum peak is formed mostly by short-lived AEs (difference between red lines in figure 5.7), with short-lived CEs making up more than half of the total of CEs (difference between blue lines in figure 5.7). This research attributes the formation of CE's to the lee effect (EAC-Fraser Island interaction), whilst attributing the formation of ACEs to the twisted remains of the EAC. Following the examination of the 2012 NCE, CEs in this zone are mechanisms that entrain shelf water. NCEs can be a mechanism to trigger upwelling if the

volume of entrained shelf water is significant in relation to the volume of water over the shelf, as was seen in the 2012 NCE. The resulting upwelling is connected to the analysis of patterns described in Chapter 4, in which the first pattern defined (P1) has a similar period of maximum monthly concentration, including the minimum month (May). The maximum concentration period is from March to July, with a low concentration in May, which is the month where Zone 2 has a significantly lower concentration of cyclonic eddies. May is between two periods of maximum concentration in Zone 2. A similar pattern is observed in Zone 1, with the minimum month between the maximum periods being in April. These concentrations of eddies in Zone 1 and Zone 2 are for cyclonic eddies.

5.4 Summary and Conclusion

The examination of the eddy census carried out in this research agrees with general features described in two studies off the east coast of Australia (Everett et al., 2012; Pilo et al., 2015). These similar features are the decrease in propagation speed from the Coral Sea to the Tasman Sea, a larger number of CEs and the proportion between CEs and AEs. These common features validate the results from the eddy detection and tracking tool. Additionally, the analysis of NCEs ($100km$ corridor) is validated by the agreement of the features listed below:

1. The increase of the mean latitudinal radii in Zone 1, with the definition of the EAC intensification zone by Ridgway and Dunn (2003).

2. The AEs concentration peak within a normal distribution in Zone 2, with the definition of the area of the EAC separation zone (Cetina-Heredia et al., 2014; Ridgway and Dunn, 2003).

3. The dominance of CEs between the EAC and the coast in Zone 1 and Zone 2, with the direction of the EAC that dissipates and suppresses the formation of AEs when it is near the coast.

4. Similarity in the number of CEs and AEs in zone 3, where the EAC is no longer upon the shelf break, with a balance of both type of eddies in Eddy Avenue (Everett et al., 2012). NCEs in the SQCMZ (Zone 1) create the SCUS by entraining water. The 2012 NCE is an example of their impact upon the shelf and how the EAC plays its role, by propelling the

eddies upon the shelf break. As the eddy reduces its size and increases its vorticity the volume of shelf water extracted is larger, resulting in a stronger upwelling. Through the examination of the eddies in the SQCMZ (Zone 1), it is proposed that there is an area of sporadic EAC separation in this zone. The proposed separation point is supported by the description of the 2012 NCE and the peak of AEs stepping out of the normal dominance by CEs.

In conclusion, this chapter describes the analyses that have led to the following results.

1. The first description of an NCE "forced" to reduce its size and increment its vorticity, resulting in an enhanced entrainment of shelf water by the 2012 NCE.

2. The first climatology assessment of NCEs in the southern section of the east coast of Australia. The results lead to the definition of three zones according to the latitudinal distribution of NCE's. The features of the three defined zones agree with the description of the EAC.

3. The first examination of the eddies in the SQCMZ's circulation that led to the identification of their key role in the circulation. The SCUS is associated to CEs, found more frequently in the SQCMZ than AEs.

4. The discussion of evidence supporting a sporadic separation point of the EAC in the SQCMZ. The separation of the EAC was previously suggested by Ridgway and Dunn (2003)

5. The presentation of results supporting the suggestion of Dambacher et al. (2012), that eddies are a physical mechanism creating upwelling events.

Chapter 6

A Circulation Model of the Southern Queensland Coastal Marine Zone

This chapter discusses the integration of the features of the SQCMZ's circulation, which is the first model proposed for the general shelf circulation in this zone. Chapters 4 and 5 examine and describe upwelling events in the SQCMZ, as well as the physical mechanisms associated with them. The SFIUS and the SCUS are defined using the morphology of their Chla blooms, their annual variability and the physical mechanisms associated with each of them. The SFIUS is related to Chla blooms originating in the northern section of Fraser Island and extending along the shelf break. The Chla blooms are most frequently observed with the intensification of the EAC (spring-summer). Bottom stress is the main physical mechanism behind upwelling events, closely followed by wind stress. The SCUS is associated with Chla blooms originating in a long section of the coast ($>50km$), with an eastward transport. Winter is the season exhibiting the highest frequency of Chla blooms associated with cyclonic eddies which encroach upon the shelf. Near-coastal cyclonic eddies are the physical mechanism behind the aforementioned upwelling system.

Observations provided the main basis for the analyses and are complemented by calculations of numerical models. This chapter discusses the performance of BRAN3.5 in describing general features including temperature, salinity and velocity field at 27°S based on mooring data. Following the successful reproduction of some known features of the SQCMZ's circulation and the mooring data

by BRAN3.5, the analysis of BRAN3.5 is used to describe the marine circulation in the SQCMZ. Additionally, these were used to contextualise the findings of chapters 4 and 5 in a formulated conceptual-physical model of the SQCMZ's circulation. An implementation of ROMS for the SQCMZ extends the examination of the general circulation to sub-mesoscale features, highlighting a key geophysical feature in the formation of the SFIUS. A final discussion focuses on the formulated conceptual-physical model of the SQCMZ's circulation addressing the role of the findings from chapters 4 and 5.

Section 6.1 describes the observations of SST and from the moorings at approximately ∼27°S (Sloyan et al., 2016), defining reference points which are compared with BRAN3.5. Section 6.2 describes the circulation based on BRAN3.5. Section 6.3 extends the research to submesoscale features represented by the implementation of ROMS for the SQCMZ, showing the key role of Breaksea Split in the SFIUS. The final discussion (section 6.4) incorporates the information and findings from chapters 4 and 5 in the description of the general circulation based on numerical results. The final discussion ends linking into a proposed model the features and physical mechanisms addressed in this research and related to the SQCMZ's circulation.

6.1 BRAN3.5 versus observation in the study area

Monthly averages of SST show the annual temperature fluctuation of the EAC (figure 6.1). The maximum values off Fraser Island occurred in February, at approx. 28°C, whilst the minimum values occur in August, at approx. 22.5°C. The intrusion of the EAC's warm mass of water is captured in the orientation of the SST gradients (isotherms), from west to east. The expected orientation is north-south, as the temperature decreases poleward. Throughout the months in figure 6.1, the temperature of the shelf water is approx. 1.5°C cooler than the EAC. A particular feature is a cold mass of water off Gold Coast, (∼28°S) from November to January. Particularly in December, the cold water shows a trace of being transported farther north than 27°S. The northward transport of a cold mass of water could be associated to the River of Sand (see section 2.2.3).

From EACM1213, which are observations collected at approximately 27°S

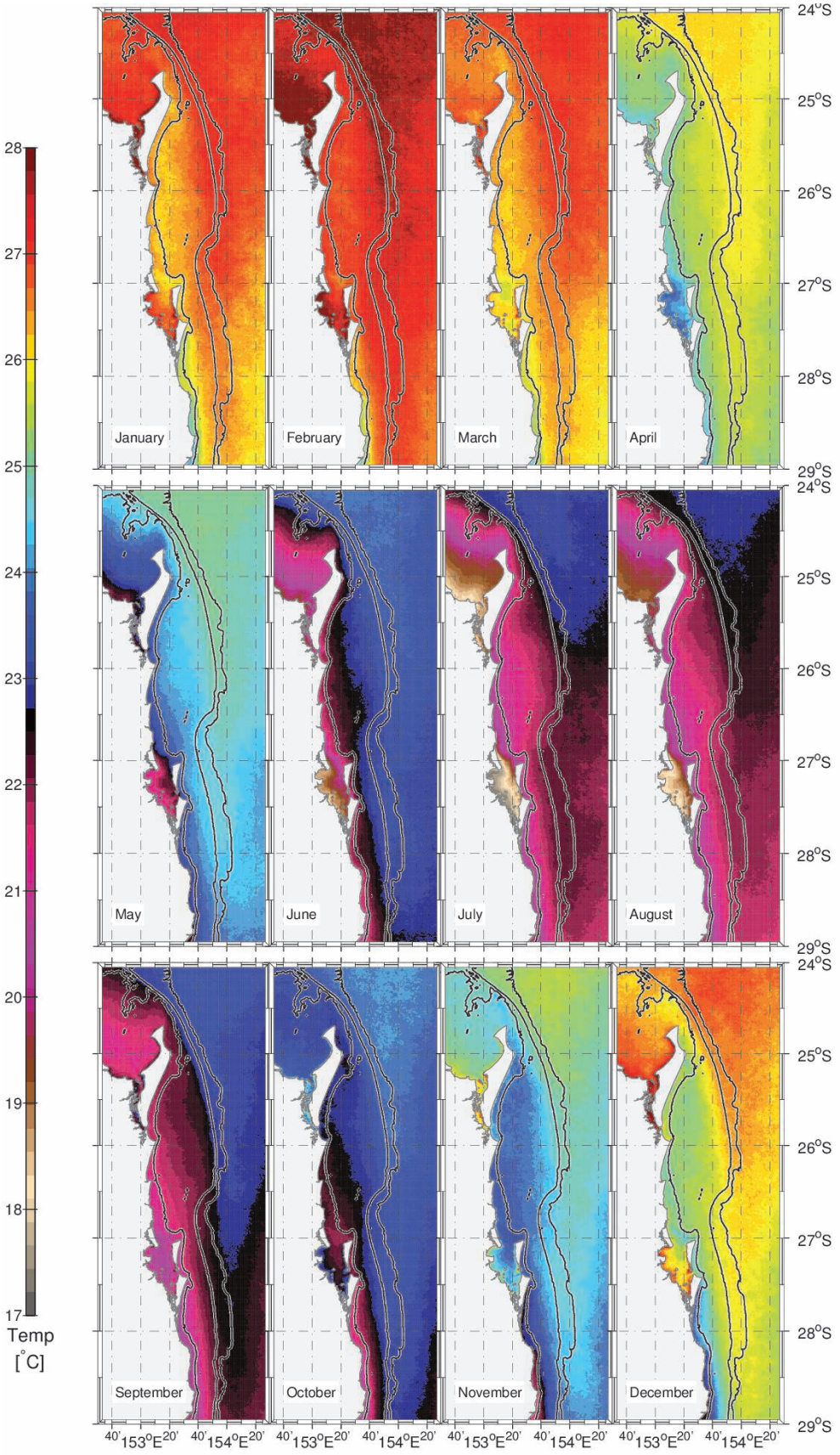

Figure 6.1: Monthly averages of SST based on IMOS data (section 3.1.1)

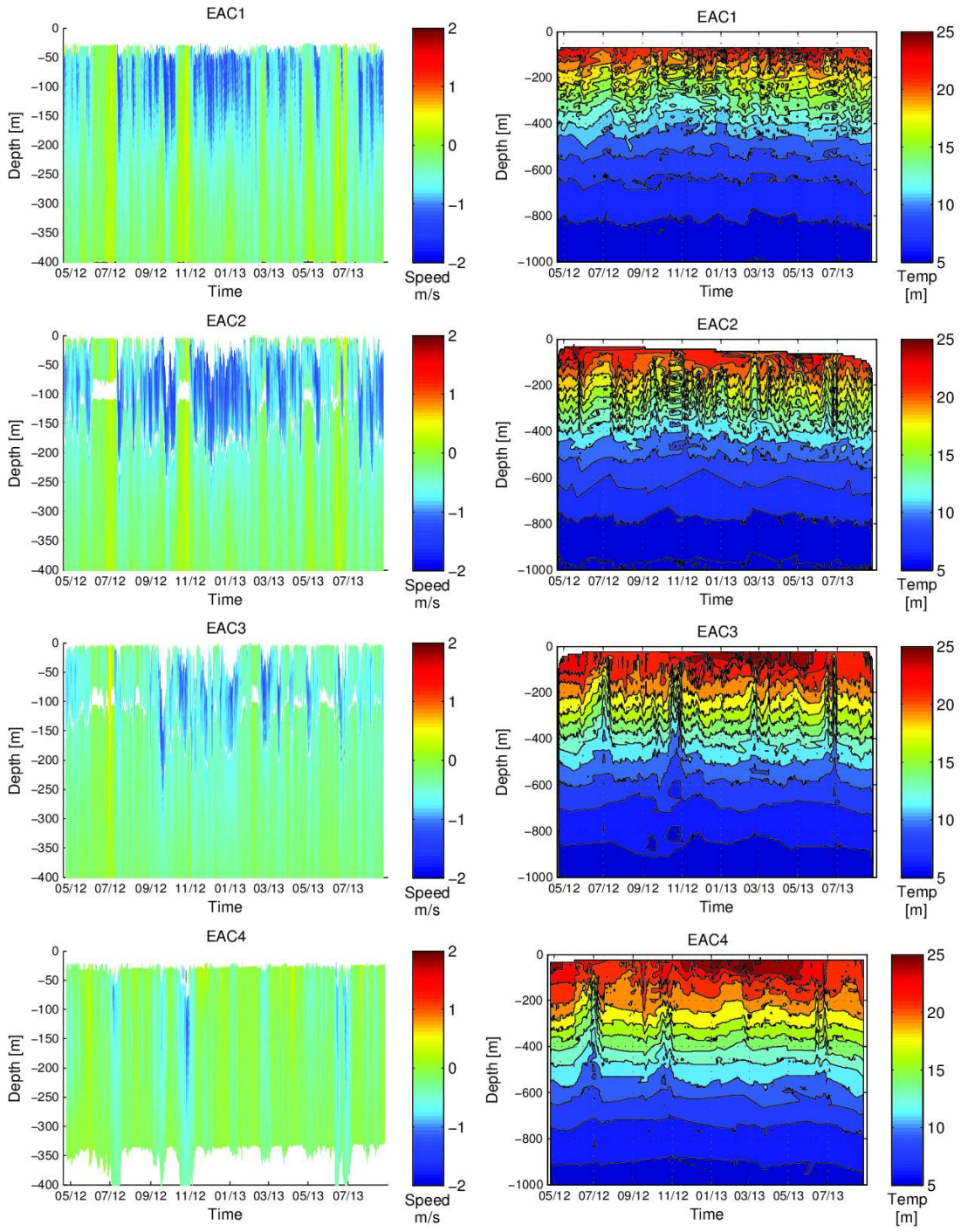

Figure 6.2: v-velocity component and temperature recorded at 4 moorings from 2012-2013. See figure 3.1 for location.

(figure 6.2, see section 3.1.2 data description), temperatures reach the maximum values in February-March. The maximum values are around 25°C, at 30m depth. The largest vertical gradient of temperature is in the first 400m. The vertical velocity profiles in the three moorings nearest to the coast show the v-velocity component strongly dominated by a poleward current. This is the EAC. The velocity range of this poleward current in the three closest moorings to the coast is from -0.5 to -1.5m/s. The velocity of the poleward current in mooring 4 (EAC4) decreases to a range of 0 to -0.5m/s. Individual events show sporadic increases in the v-velocity component, which are associated to the uplifting of the isotherms in the EAC4. The relationship between sporadically strong negative v-velocity and the uplifting of the isotherms is a specific feature of the EAC4. However, the uplifting of the isotherms in the EAC4 are simultaneously observed in the EAC3. Nevertheless, no significant impact is observed in the v-velocity (figure 6.2) of the EAC3, as the EAC is present through most of the observed period. The simultaneous uplifting of the isotherms in the EAC3 and the EAC4 means that it is a result of the same physical mechanisms involving both moorings (e.g. NCE described in chapter 5). The EAC1 and the EAC2 show a weaker uplifting of isotherms, whilst the EAC4 clearly captures the uplifting of the isotherms. Figure 6.2 illustrates that the moorings highly influenced by the EAC are the two located nearest to shore (EAC1 and EAC2). The poleward current in the two moorings nearest to the shore is faster and the surface vertical mixing is more intense than the other moorings. Ganachaud et al. (2014) quantify the poleward transport above 2000m from the moorings data in $\sim$22.1Sv. The difference in the poleward transport and the net transport over 2000m was $\sim$6.3Sv.

Figure 6.3 illustrates the temperature at approximately 2.5m, where the vertical coordinate nearest to the surface is located in BRAN3.5. The annual variability of the temperature has its lowest values in August and the highest in February, as is seen in the SST and the mooring data. The representation of salt concentration (figure 6.4) also exhibits an annual variability, with an inverse relationship with the month of maximum and minimum heat content (temperature). In terms of salinity, the annual variability ranges from 35.2psu to 35.5psu in the EAC and 35.5psu to 35.6psu over the shelf in the monthly averages illustrated in figure 6.4. The range of salinity data agrees with the observation in the EAC1 (near the shelf) and the EAC3 (near the EAC core). The aforementioned features confirm that the EAC is less dense in the summer (minimum in February) and most dense in winter (maximum in August). The annual variability in the EAC strength is illustrated by figure 6.5. The monthly averaged v velocity component

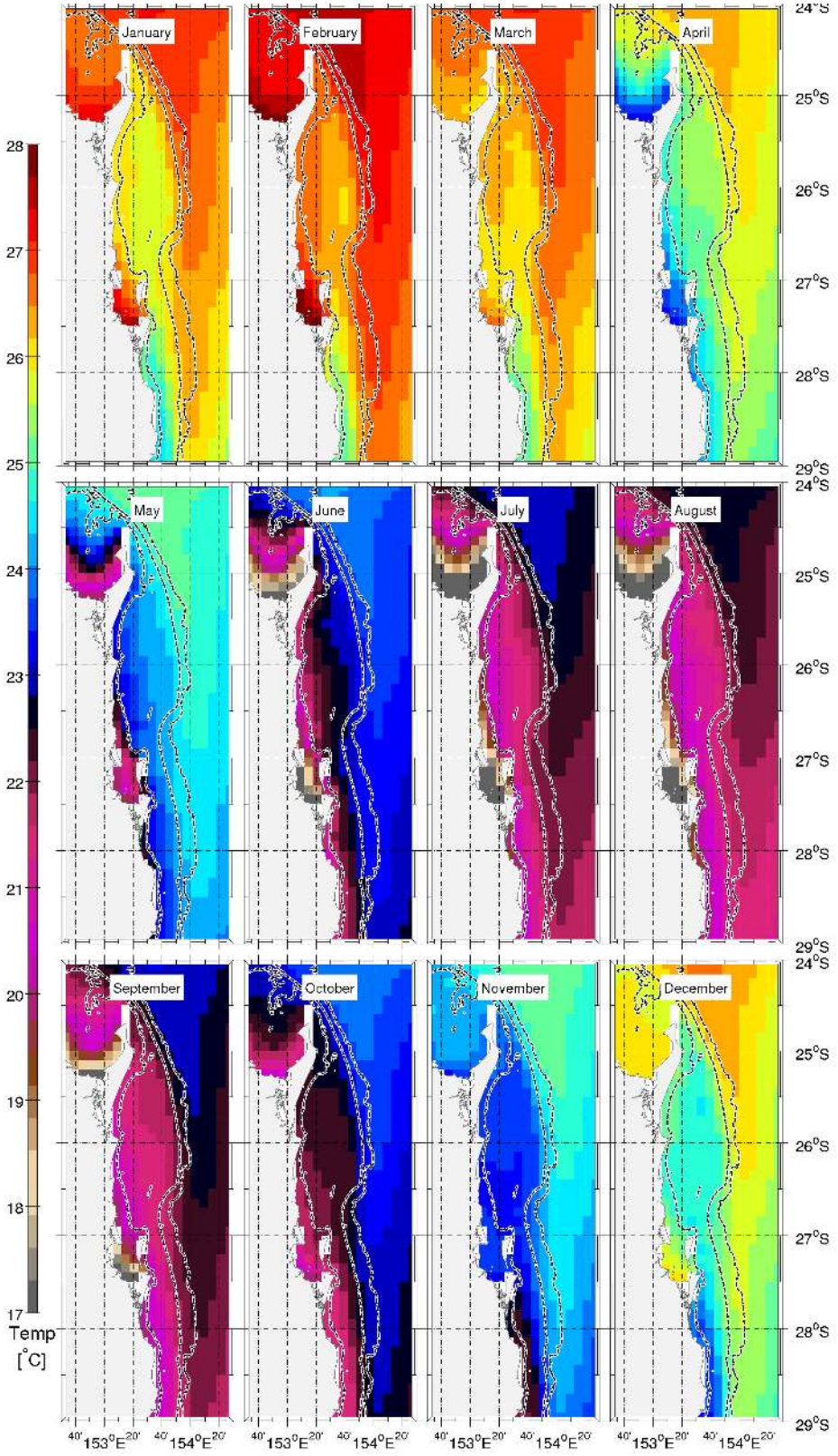

Figure 6.3: Monthly averages temperature in the nearest vertical coordinate to the surface from BRAN3.5 which reproduces the marine circulation from 1993 to 2012.

near the surface reaches values of $0.8m/s$. The strongest and weakest values are observed in February and July respectively.

Table 6.1 lists the south-north transport in the cross section along the SQCMZ. The dominant transport is poleward due to the EAC, as the net-transport shows negative values. In general, an intensification of transport exists when the estimations of the poleward transport from farthest north and south cross-sections are compared, -32.2Sv and -35.7Sv respectively. The northward transport in the first 2000m shows an intensification in the northern section of the SQCMZ, which then decays in the southern section. At 27°S the BRAN3.5's poleward transport is -32.4Sv and has a difference of 10.6Sv with the net transport, against the -22.1Sv of poleward transport and 6.3Sv of the difference with the net transport described by Ganachaud et al. (2014).

Temperature values compared with mooring observations at ∼27°S shows that at 300m the temperature at the EAC3 is similar to BRAN3.5 (approx. 15-16°C). The EAC1 and the EAC2 which are located on the shelf slope show, at 300m, water 1 to 2°C colder than the mooring farther off shore. BRAN3.5 represents the uplifting of the isotherms near the shelf slope, as is illustrated in figures A.2 to A.8. Salinity values at the EAC3 and the EAC4 range from 35.6 at ∼160m to 34.9psu at ∼460m. In the monthly average cross section at ∼27°S, BRAN3.5 shows values of ∼35.6psu at 160m (154.45°E) and values around 35.1psu at the same depth closer to the shelf break (153.8°E) where the water is uplifted. Comparisons of BRAN3.5 with observations show an accurate general description of temperature and salinity.

6.2 General circulation in the study area according to BRAN3.5

Two cross sections at 25°S and 26.5°S are described and illustrated in figures A.2 to A.8. The isotherm is uplifted near the shelf in both cross sections, however, the section at 26.5°S shows a stronger uplifting. The minimum temperatures at 25°S are observed in August whilst at 26.5°S the minimum is in July. Comparatively, maximum values are observed in February for both cross sections. The uplifting of the isotherm is in agreement with the intensification of the EAC. From August to February the isotherms rise, for the remainder of the year the isotherms

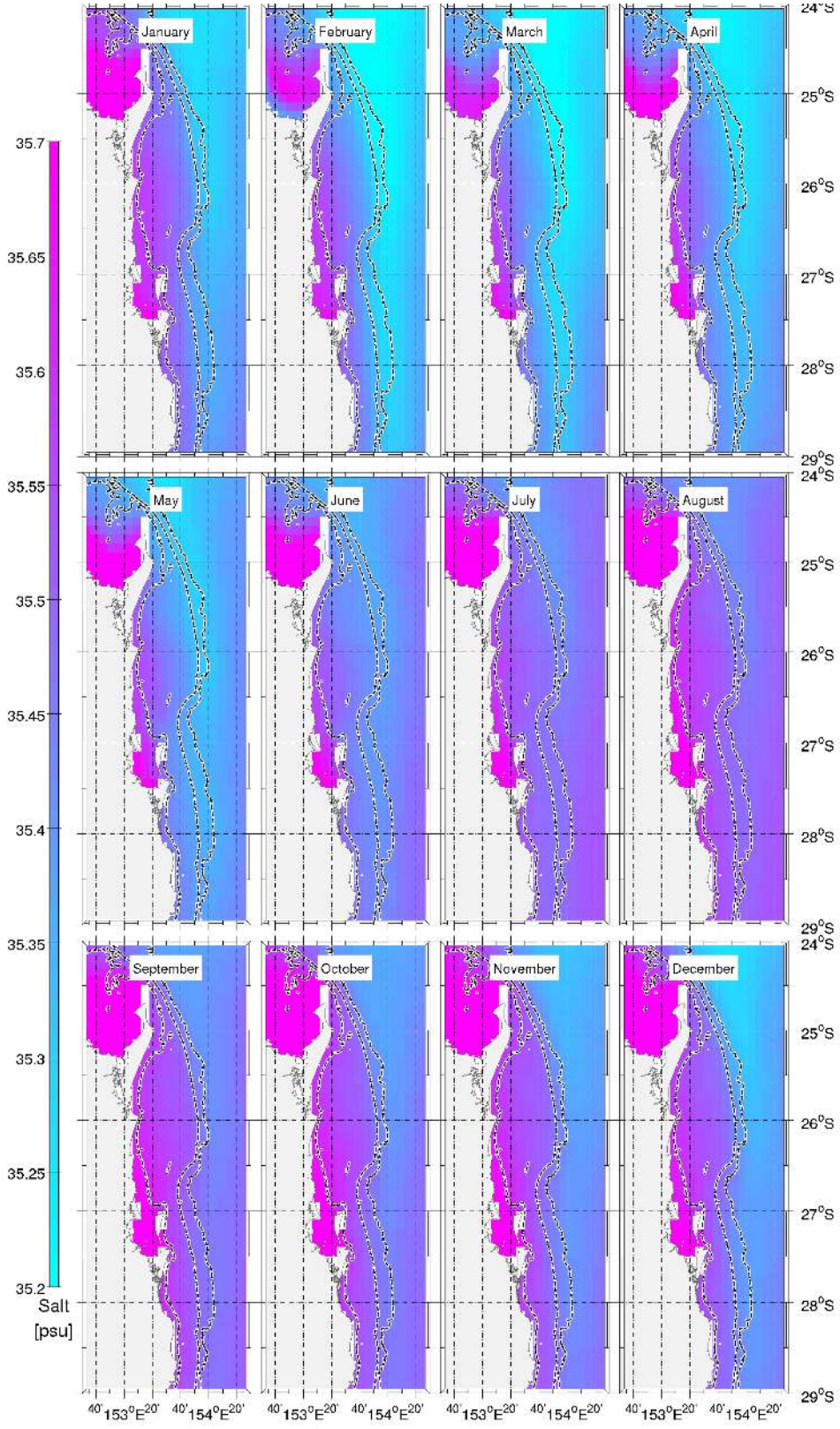

Figure 6.4: Monthly averages of salinity in the nearest vertical coordinate to the surface from BRAN3.5.

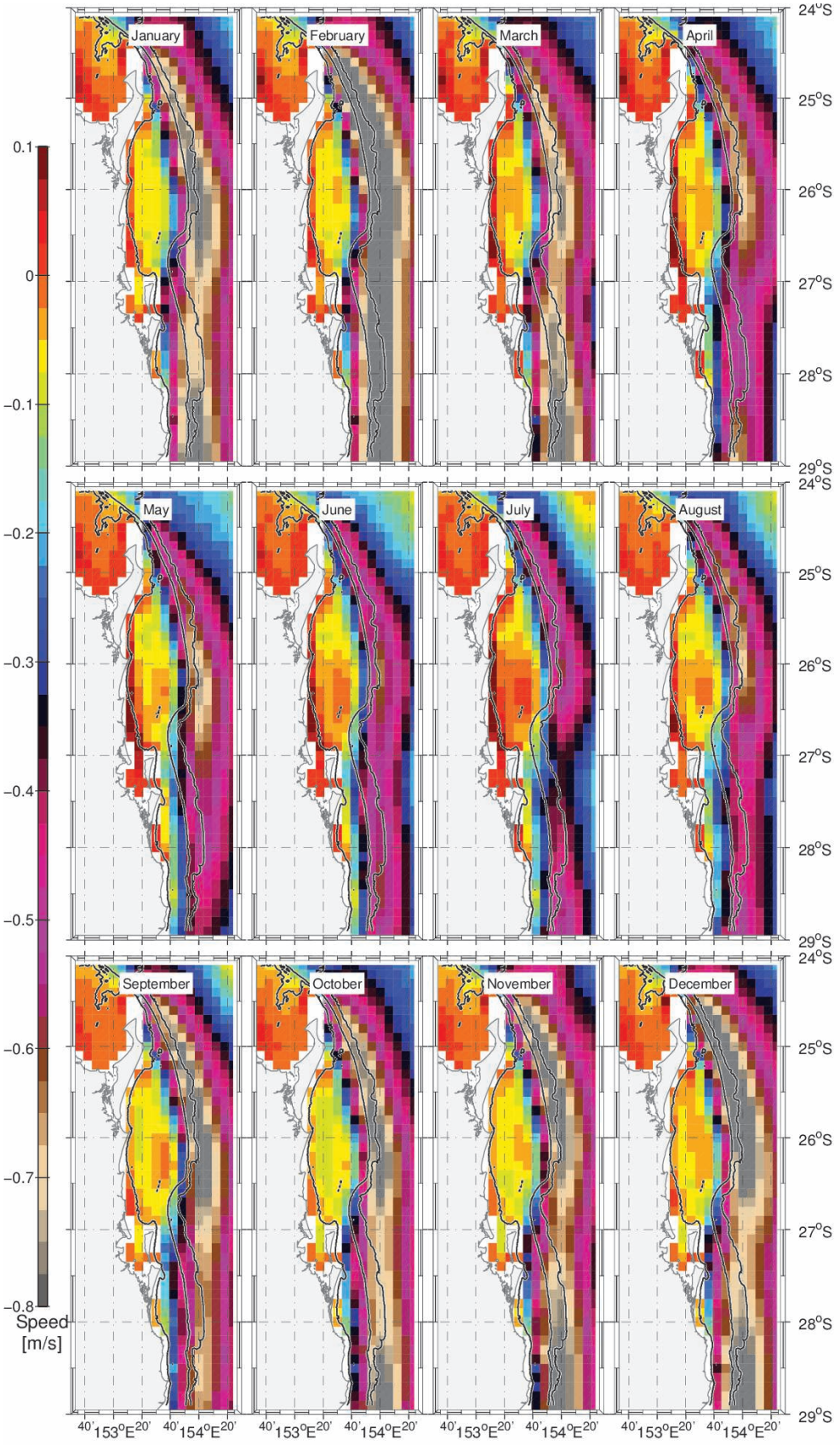

Figure 6.5: Monthly averages of v-velocity component in the nearest vertical coordinate to the surface from BRAN3.5.

Table 6.1: South-north transport in cross sections along the eastern coast of Australia based on BRAN3.5. 1 Sv is equivalent to $10^6 m^3/s$. The highlighted row which indicates the transport at 27°S, is comparable to the transport quantified by Sloyan et al. (2016).

Cross section's latitude	Average of poleward transport $[Sv]$	Average of northward transport $[Sv]$	Average of net transport $[Sv]$
-25	-32.2	9.12	-23.1
-25.5	-32.7	9.41	-23.3
-26	-32.6	10.2	-22.4
-26.5	-32.6	11.2	-21.3
-27	-32.4	10.5	-21.8
-27.5	-31.5	7.11	-24.4
-28	-33.6	6.74	-26.8
-28.5	-35.7	7.52	-28.1

move downwards. The strongest rise appears to occur in November in both cross sections. Similar features are observed in the salinity for both cross sections. In November, at 26.5°S it is possible to observe salinity values next to the shelf at $100m$ depth which correspond to values usually identified at approximately 250-300m.

Figures A.8 and A.9 illustrate the monthly average of the v-velocity component in the cross sections at 25°S and 26.5°S. The maximum average velocity in the south-north direction is observed in two months: December and February. The observation of two periods of the EAC intensification agrees with a similar fluctuation of the Chla monthly averages, in particular related to the P2 events of Chla (see figure 4.1). A larger magnitude is observed at 25°S, however, a strong northward bottom current is observed at 26.5°S. A small current with an opposite direction to the EAC and located over the bottom along the slope can be observed at 26.5°S. Simultaneously, a weak northward current is observed over the shelf, near the shore, which may be associated with the River of Sand (see section 2.2.3). The inner shelf current is not consistently present throughout the whole year in the monthly averages, leading to the conclusion that it is a sporadic current.

Monthly averages of the v-velocity component show an intensification of the EAC between 25°S and 26.5°S, as well as from 28°S southward (figure 6.5). The two sections of intensification take place after the narrowing of the shelf. Upon the shelf, the circulation shows small negative values for the v-velocity component (poleward current $<0.1m/s$). The pixels closest to the shore, illustrated in figure 6.5, show a northward current (positive values) referred to in this study as the ISC. The ISC supports the sand transport named the River of Sand, which has a northward transport (Boyd et al., 2008). The ISC intensifies from February to July, which is the period when the EAC weakens, with maximum values occurring in July. In October, the ISC is not present in the monthly averages of BRAN3.5 representations and the shelf shows a main poleward transport upon the shelf.

The u-velocity component (west to east) of the EAC shows changes in its direction (sign) as the shelf break changes its orientation, demonstrating how the EAC follows the shelf break (figure A.1). From 24°S to 26°S the u-velocity component is positive (eastward/offshore), from 26°S to 27.5°S it is negative (westward/inshore) and from 27.5°S to the southern boundary of our study area

the component is around zero. The direction of the flow upon the shelf is westward ($\sim$0.05 to 0.1m/s) and its strongest period is when the EAC relaxes (March-July). Values are near to zero from September to December, however, a small area at the east of Fraser Island ($\sim$25.5°S) shows negative monthly averages throughout the year.

6.3 Features of the general circulation based on a submesoscale resolving model

The implementation of ROMS with a greater grid resolution than BRAN3.5 adds finer details to the description of the marine circulation. A resolution of approximately 2km allows for dynamics to be observed at a submesoscale level. The first configuration of the model was completed to obtain a stable numerical simulation with climatology boundary conditions based on BRAN3.5. The second configuration was initiated from the stable state of the first configuration as well as with boundary conditions interpolated from the resolved 2010 year in BRAN3.5. There are two main contributions from the implemented ROMS: the evidence of submesoscale eddies involved in the SFIUS and the demonstration of the key role of the Breaksea Split in defining the source of water of the SFIUS. The following sections discuss the performance of the implemented model, which has completed its first stage to became a downscaling tool for the SQCMZ based on BRAN3.5.

6.3.1 ROMS with climatology boundary conditions

The climatology simulation took about 1 to 2 years of simulation to raise a stable circulation. The kinetic energy, volume of water and heat concentration after one year reached a stable oscillation, whilst the salinity takes 2 years to stabilise. The main issue with this simulation is the temperature and salinity representations, which are underestimated. The issue of underestimation was passed to the ROMS simulation based on the year 2010 of BRAN3,5 and no solution was implemented in this study. Due to this issue, the temperature and salinity values are not used to complement the description of the upon shelf circulation.

6.3.2 ROMS based on year 2010 of BRAN3.5

It has been demonstrated in sections 6.1 and 6.2 that BRAN3.5 reproduces the physical marine features in the SQCMZ and is a valid reference to compare with the results of the implemented model. In following sections the accuracy of ROMS is examined by comparing it with BRAN3.5 and then the circulation of ROMS is described. The main results from ROMS is the identification of Bracksea Split as a key feature defining the source of the water supplying the SFIUS as well as the presentation of evidence demonstrating that submesoscale eddies are part of the aforementioned upwelling system.

6.3.2.1 Accuracy of ROMS representation

Monthly averages of surface salinity in ROMS show values in a range of 35.2-35.7psu off Southern Queensland (Fraser Island to Moreton Island). BRAN3.5 has a similar range, however, the distribution differs (figure 6.3). ROMS shows a mass of fresh water (<35.2psu) off the Gold Coast which is observed in the SST and BRAN3.5. However, ROMS over-represents the impact of this mass of cold water from November to February (see animation C.3 on the 24th of Feb year 2 and 22nd of Nov year 2) which includes the period where is observed in BRAN3.5 and SST. The monthly averages of temperature and salinity are both underestimated when compared with BRAN3.5. The intrusion of the warm EAC is observed in ROMS, however, the transport is inferior to BRAN3.5 (tables 6.1 and 6.2). The best representation of transport in ROMS is at 25°S (first row in tables 6.1 and 6.2), where the SFIUS originates.

The EAC is stronger from August to February, which is the intensification period of the EAC. Another specific feature observed and accepted as an error is the warm mass of water being transported from Hervey Bay to the east side of Fraser Island from December to February (animation B.4 on the 7th of Feb year 2, 20th of Dec year 2 and 8th of Dec year 3). The same feature is not observed in BRAN3.5 and the main difference in this area is the representation of the sand extension at the north of Fraser Island (Breaksea Split). It should be mentioned that the ROMS is considering 5 years for the monthly averages, in comparison BRAN3.5 has ∼20 year of simulation for the monthly averages.

The v-velocity component has a similar surface horizontal distribution in

Table 6.2: Normal transport through cross sections indicated by the latitudes coordinates. Cross sections are rotated with respect to the west-east orientation while the transport in BRAN3.5 is estimated in east-west orientated cross sections. 1 Sv is equivalent to $10^6 m^3/s$.

Cross section's latitude	Average of poleward transport $[Sv]$	Average of northward transport $[Sv]$
-25.0	-31.0	18.80
-25.5	-19.19	13.37
-26.0	-18.01	17.11
-26.5	-15.96	13.16
-27.0	-16.85	14.89
-27.5	-20.64	15.06
-28.0	-17.30	11.58
-28.5	-17.43	11.09

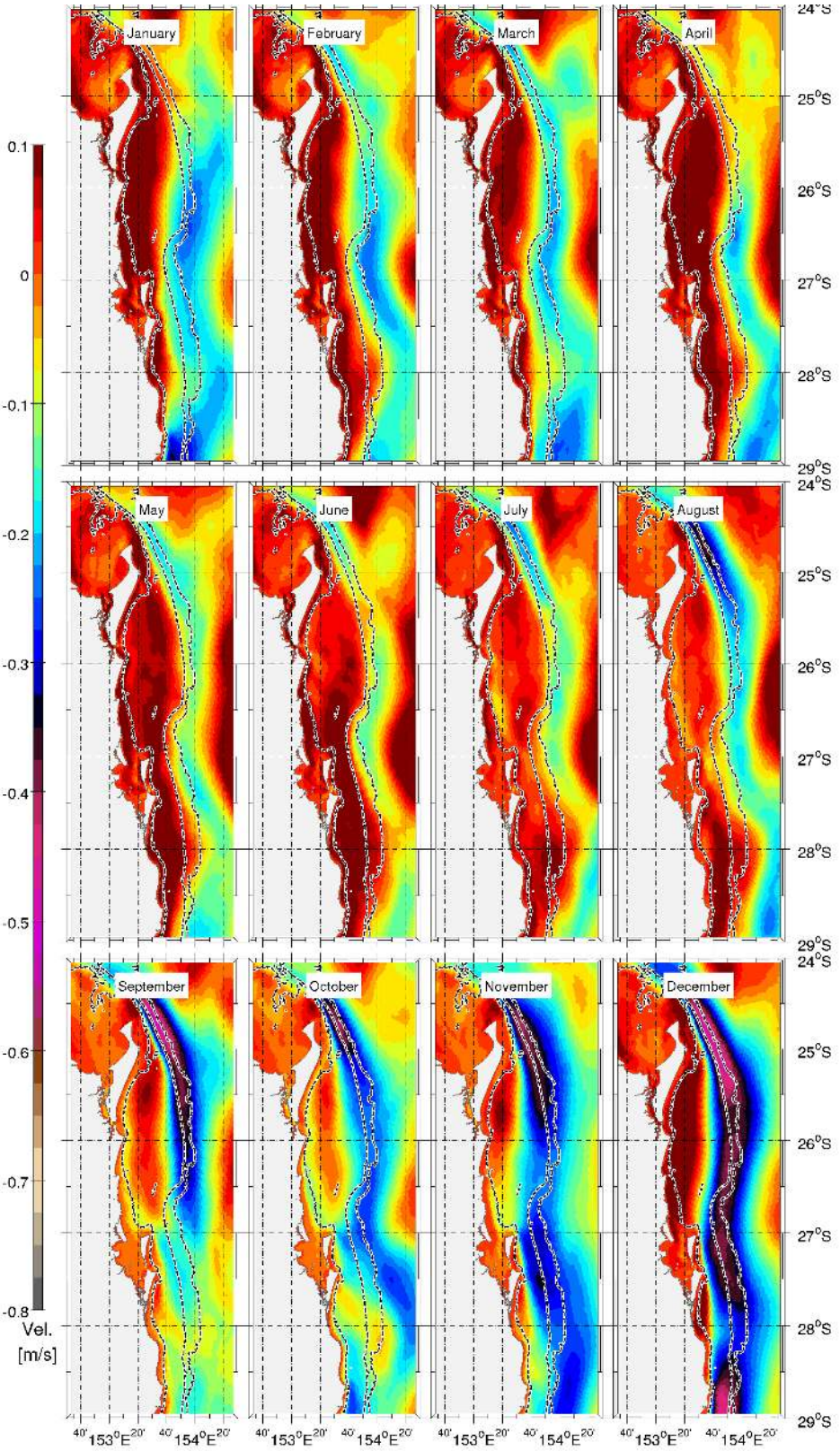

Figure 6.6: Monthly averages of v-velocity component in the nearest vertical sigma coordinate to the surface from ROMS.

BRAN3.5 and ROMS, however, ROMS underestimates the magnitude. In the monthly averages (figure 6.6) ROMS shows magnitudes around $0.5m/s$ off Fraser Island instead of the $0.8m/s$ observed in BRAN3.5 (figure 6.5). However, the transport is similar in BRAN3.5 and ROMS (25°S), as is shown in the first row of tables 6.1 and 6.2. Again, the averages consider 5 years for ROMS and 20 years for BRAN3.5. The path of the EAC is similar in both simulations and agrees with the concept that both follow the shelf break, in particular, the fluctuation at about 27°S.

Animations B.3 and B.4 show that in the vertical, ROMS underestimates the salinity and temperature, however, the intrusion of slope water is reproduced by ROMS and BRAN3.5. Cross sections show that ROMS represents a similar vertical profile of the salinity, however, it underestimates the salt concentration. The lowest salinity at $100m$ depth is $sim34.55psu$ in ROMS, whilst BRAN3.5 shows the lowest salinity at about $150m$ with values of $\sim 35.6psu$. Animations B.3 and B.4 capture the vertical oscillation of the greatest vertical temperature gradient resulting in the intrusion of slope water upon the shelf. The intrusion of slope water occurs when the EAC intensifies, retreating during the relaxation of the EAC. These are the upward and downward oscillations respectively. Temperatures in the cross sections show similar values in the surface from November to March, whilst for the remainder of the year the surface temperature is colder than BRAN3.5. For example, in June, cross section 1, (the section farthest south, see animation B.4) shows ∼3°C of difference between ROMS and BRAN3.5. The temperature difference increases as the cross sections move farther south. This points to the issue of over representation of the northward transport of cold water in the souther section of ROMS. The vertical distributions show that ROMS's temperatures have a higher gradient and a lower minimum temperature than BRAN3.5.

6.3.2.2 ROMS contribution to the description of the marine circulation

Monthly averages of the Okubo-Weiss parameter (W) estimated in BRAN3.5's nearest surface velocity field shows mostly positive results. Positive numbers in the W indicate that deformation is dominant over rotation. BRAN3.5 shows the greatest values related to the EAC, particularly to its western edge. The zone of high positive W values is where the greatest gradient of the v-velocity

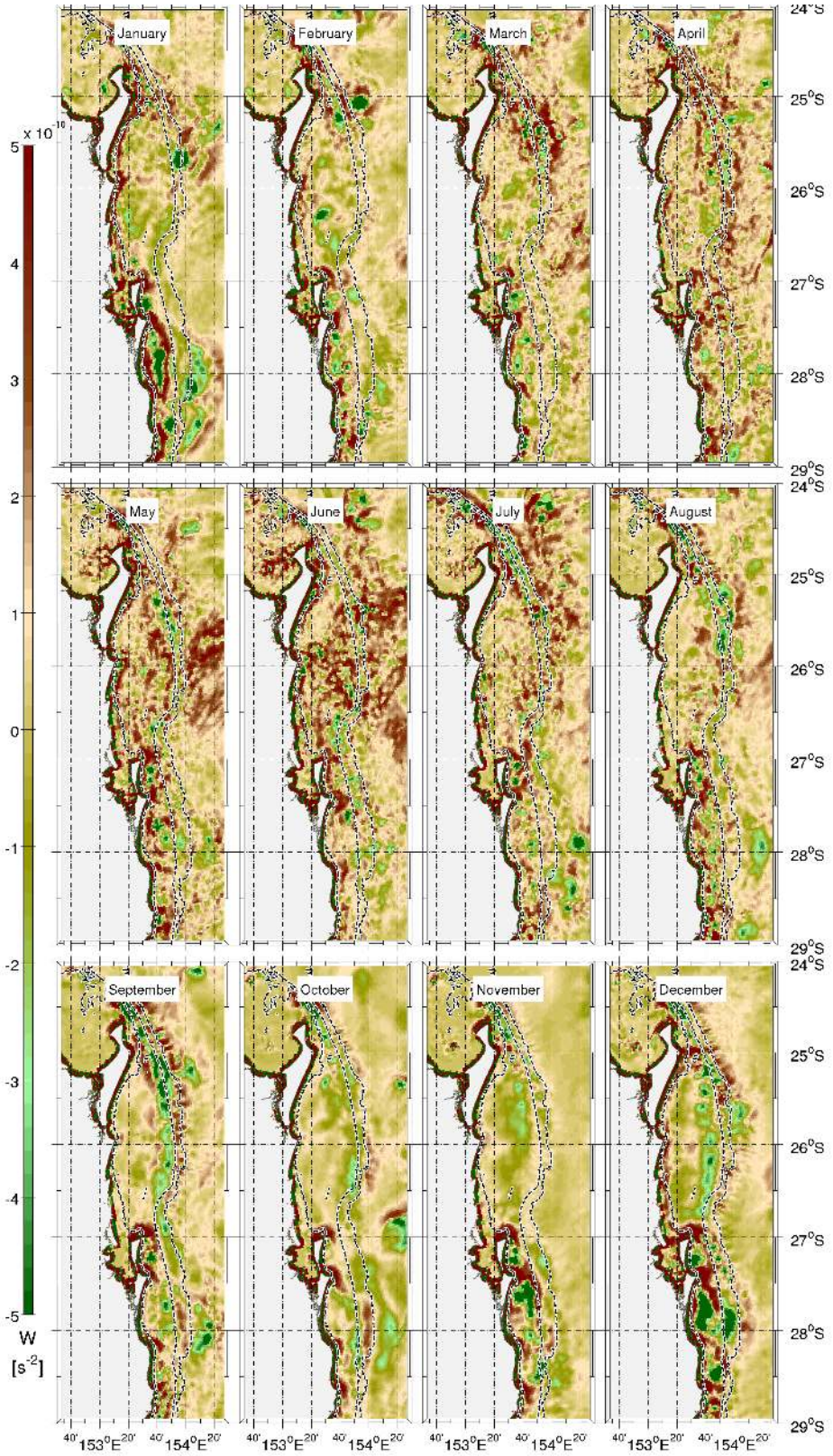

Figure 6.7: Monthly averages of Okubo-Weiss ($1/s^2$) parameter at the nearest sigma layer to the surface from the ROMS_AGRIF, under the 2010 scenario.

component is present. ROMS has positive values of W along the shelf break, however, the values are mixed with negative values. The negative values are particularly present at 25°S (eastern side of Fraser Island), where the poleward transport is similar to BRAN3.5 (see tables 6.1 and 6.2). Monthly averages of W based on ROMS near surface velocity field (figure 6.7) show smaller values in the EAC ($1\times10^{-10}s^{-2}$) than BRAN3.5 ($5\times10^{-10}s^{-2}$). The western edge of the EAC shows zones and periods of negative values, which are associated to vorticity being dominant over deformation. From August to December, the vorticity increases upon the shelf break in response to the EAC intensification.

Similar events to the P2 Chla blooms (see section 4.1) are observed in the surface temperature of ROMS. However, the water is warmer than its surroundings, disagreeing with the cold water of the P2 Chla blooms. The P2 events of high Chla concentration were associated with an upward transport of slope water in zones of high bottom stress. Apart from the significant temperature difference, ROMS does produce a similar pattern in the same area during the period when P2 dominates P1. However, the source is warm water which is transported from Hervey Bay around the north of Fraser Island and finally along the shelf break. This source of water therefore, explains why ROMS fails to reproduce the cold mass of water associated with P2 events. Some examples of the warm mass of water off Fraser Island in animation B.4 are observed on 9th Dec. year 2, 11th Dec. year 3 and 17th Feb. year 5.

The main explanation presented for the temperature difference is related to the minimum depth of $10m$ used in ROMS. Any marine area with water shallower than $10m$ is represented as $10m$ in ROMS. The north sand extension of Fraser Island (Breaksea Split), which is few meters deep is represented as an area that is $10m$ deep. The misrepresentation of Breaksea Split's depth in the ROMS, allows in its calculations the transport of water from the north (Hervey Bay) due to the dynamics (vorticity and lee effect) off eastern Fraser Island. Additionally, the transport of water could be associated to an area of low pressure caused by the narrowing of the shelf as the EAC flowing southwards near Fraser Island. If transport from the north is not allowed in the numerical model, then the low pressure, vorticity and lee effect in the area are restricted to having only slope water as a water source. BRAN3.5 solves this problem, extending the land mask farther north of Fraser Island, including its sand extension. The extension of the land mask upon Breaksea Slipt is a solution to be implemented in future ROMS implementations.

6.4 Final Discussion

This research project was carried out with the aim of expanding knowledge of the marine circulation in the SQCMZ. The initial approach was to examine observations based on remote sensing (Chla, SST and K490), leading to the identification of two upwelling systems. The upwelling system off Fraser Island was initially related to bottom stress and wind stress (chapter 4). The SCUS was defined by the analysis of Chla blooms (chapter 4) and was later related to near-coastal eddies encroaching upon the shelf and extracting shelf water. This chapter extends the list of physical mechanisms associated with the SFIUS, identifying the Breaksea Split as a key feature defining the source of the water for the upwelling systems. In this section, the two upwelling systems identified in the study area are reviewed, integrating the results and information from chapter 5 with those of this chapter. The final section discusses a proposed model summarising the information and knowledge generated by this research project.

6.4.1 The Southeast Fraser Island Upwelling System

Middleton et al. (1994) was the first to report evidences of upwelling off the eastern coast of Fraser Island, however, no conclusive data was found to explain its presence there. Nevertheless, bottom Ekman transport was suggested as a potential physical mechanism behind the observed upwelling. This research's examination of Chla blooms in the same area demonstrates the existence of periodicity in the Chla blooms off Fraser Island. These blooms are more frequent from August to December, which is when the EAC intensifies. The Chla blooms originate in the northern section of the east coast of Fraser Island and propagate along the shelf break. The SFIUS was named the upwelling event with the aforementioned features (Brieva et al., 2015; Dambacher et al., 2012).

The analysis of bottom stress and wind stress demonstrated that both have a role to play in the formation of upwelling events in the SFIUS. The area of upwelling is a zone of high bottom stress. Along the east coast of Australia, three zones of high bottom stress were identified. The two zones farthest south were included in the study carried out by (Oke and Middleton, 2001). The bottom Ekman transport resulting from the bottom stress transports slope water upon the shelf. In this particular area, where the shelf is a few kilometres wide, (considering Breaksea Split) the uplifted slope water can reach the surface. The wind

stress throughout the period exhibiting the greatest number of Chla blooms has a small poleward component as the Subtropical Ridge reaches its point farthest north. The poleward wind component is favourable to upwelling. Considering the number of days with Chla blooms associated to this upwelling system, it is possible to conclude that bottom stress has an influence 27% greater than that of wind stress in the generation of upwelling events (Chla blooms). Evidence showing bottom stress as physical mechanism supports the suggestion of Dambacher et al. (2012) stating that the EAC-shelf interaction is one of the causative mechanisms behind the aforementioned upwelling. The second mechanism proposed by them is transient eddies.

The analysis of eddies in the SQCMZ does not show a direct link with the upwelling system off Fraser Island. However, the period of greatest Chla bloom frequency is associated with a reduction in the mean radii of eddies in the study area. The analysis of the numerical results shows that in BRAN3.5 a westward transport exists in the upwelling area, at approximately 25.5°S. The westward transport is present throughout the entirety of the monthly averages in the aforementioned study area. ROMS improves on this by reproducing mesoscale features (eddies) and showing that the western edge of the EAC is not dominated by deformation alone (positive values of W). Negative and positive values along the western edge of the EAC are mixed, demonstrating that deformation is an important feature of the circulation as well as the vorticity. The vorticity in BRAN3.5 is not as significant as it is in ROMS along the shelf break, the main difference between BRAN3.5 and ROMS is the resolution of the grids. The grid difference leads to the conclusion that the vorticity associated with the EAC edge is dominated by mesoscale features or eddies, which are a mechanism related to the SFIUS. Again, these results support the suggestion of transient eddies by Dambacher et al. (2012).

Finally, the reproduction of the shape of Chla blooms associated with the SFIUS by ROMS shows that the physical mechanisms are solved by ROMS. However, the pattern is created by warm water instead of cold slope water. The minimum depth in ROMS transforms the Breaksea Split into a deeper region, resulting in a wider shelf where the north-south transport is possible. The water extracted from Hervey Bay does not have any limitations to it cross the Breaksea Split in the model representation. However, the observations demonstrate that the water is from the slope. These features lead to the conclusion that Breaksea Split is a key feature in the SFIUS for the extraction of water from the slope and

not from Hervey Bay.

6.4.2 The Sunshine Coast Upwelling System

A different pattern in the Chla blooms to those off Fraser Island was found along the Sunshine Coast. The features of the new Chla blooms are a long connection with the shore ($>50km$), originating near to the coast and showing an eastward transport. The greatest frequency of Chla blooms can be seen from March to July. The values of Chla are smaller than in the SFIUS. The first examination demonstrated that the upwelling events of the SCUS are not generated by Ekman transport due to wind stress. The contribution of bottom stress is the uplifting of slope water upon the shelf. However, it is not sufficient to explain the whole process, as a significant percentage of the Chla blooms are observed in days where both mechanisms (bottom and wind stresses) have conditions unfavourable to upwelling events.

The description and quantification of the impact of NCEs on the shelf circulation, demonstrate that it is a physical mechanism able to reproduce the observed Chla blooms along Sunshine Coast. The EAC plays a key role in propelling the eddies to encroach upon the shelf and force them to reduce their size. The increase in vorticity is an attempt to conserve the energy due to the reduction of size, which results in the increment of water volume entrained from upon the shelf. An enhanced entrainment of shelf water by the eddy can renew over 60% of the shelf water. The configuration of the study area is similar to that of an open bay, where the EAC blocks the across shelf circulation, meaning the source of water to conserve the mass is extracted from the bottom and slope. The resulting dynamic is due to the entrainment of water by NCEs causing Chla blooms similar to those created by wind as both, wind and NCEs extract water off shore from the shelf. The role of the eddies is confirmed by the increment of the mean radii of NCEs during the period of greatest Chla bloom frequency associated with P1 events (see chapter 4). In this study the suggested name for the aforementioned dynamic is Sunshine Coast Upwelling System (SCUS). This name has only been suggested as there remains aspects related to this upwelling dybamic that have not been explored (role of the seasonal fluctuation of the surface mixed layer's thickness and the river discharges among others).

The examination of BRAN3.5 finds that during Winter wind produces a

northward Ekman transport resulting in the relaxation of the EAC. The resulting northward transport enhances the cyclonic circulation upon the shelf, as is observed in the monthly averages of the v-velocity component. The cyclonic circulation facilitates the formation of mesoscale cyclonic eddies and results in the increment of the mean near-coastal eddies radii in the study area. Additionally, along the period of highest Chla bloom frequency, the EAC becomes more dense, with a decrease in the temperature and slight increment in the salinity. The change in density may impact the instability of the interface due to the EAC-shelf water interactions.

As the SCUS is caused by the entrainment of water originating from NCEs, the inner shelf's northward current, which is part of the upon shelf cyclonic circulation, is related to the upwelling system. Both, inner self current and the SCUS, have the same annual variability, with Winter being the most active period. The northward intrusion of cold water from the south along the Gold Coast and Moreton Island, in Spring, together with the inner shelf northward current, in Winter, could transport sand and form part of the River of Sand. As the season of each water transport shows, the transport of sand would occur in two stages in the study area. First, the transportation along the southern section of the SQCMZ reaching the Sunshine coast throughout Spring. Secondly, the sand is transported to Breaksea Split throughout Winter.

6.4.3 A model formulation of the general circulation in the study area

Figure 6.8 illustrates the proposed model of interaction in the SQCMZ. The EAC is located at the centre, acting as a main driver of the circulation and dynamics in the study area. The orange lines are the physical mechanisms resulting from the interactions with the bottom of the shelf, the shelf waters and Fraser Island (Breaksea Split). The first physical mechanism is bottom stress, which results from the interaction of the EAC with the bottom of the shelf, specifically the shelf break. The bottom stress generates an inshore Ekman transport in the bottom layer. The inshore transport supplies nutrients upon the shelf enhancing the primary production. The second physical mechanism is the instability resulting from the interaction between the EAC and shelf waters. Both masses of waters have different densities and velocities creating a zone of high tangential shear. The zone of high instability is a source of sub- and mesoscale eddies. The third

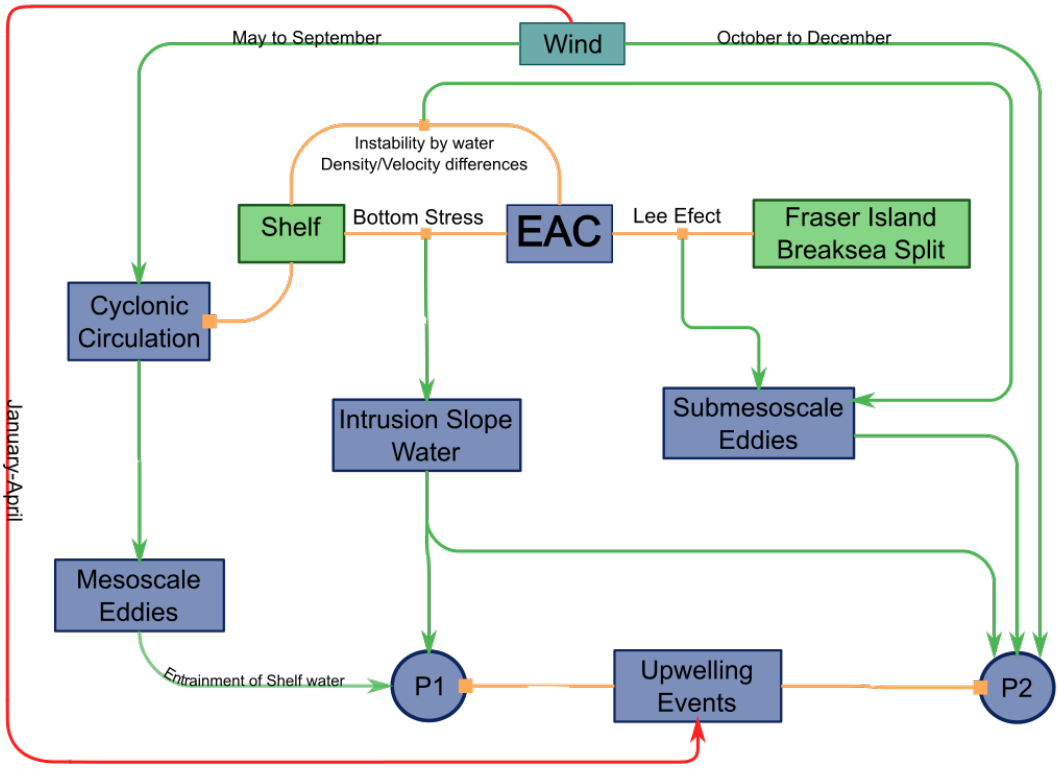

Figure 6.8: Proposed model of the physical mechanisms and features examinated, analysed and described in this research.

physical mechanism is the lee effect, resulting from the interaction of the EAC with Fraser Island. The lee effect results in a zone of low pressure which "attracts" water and is a source of submesoscale eddies, as seen in the zone instability along the self break. The Break Split limits the source of the "attracted" water to slope water, blocking its transport from Hervey Bay.

Wind stress has three annual periods identified. The first is represented by a red line, meaning the wind suppresses any kind of upwelling. The following period enhances the cyclonic circulation upon the shelf, and by that, the formation of mesoscale eddies. The third period of wind supports the formation of upwelling, in particular, the SFIUS.

Shifting the focus to the upwelling events observed in the SQCMZ, two main types of Chla blooms are named as the SFIUS and the SCUS, represented by P2 and P1 respectively in figure 6.8. The SFIUS is the one with more physical mechanisms supporting its formation, including the intrusion of slope water, vorticity related to submesoscale eddies and wind stress. On the other side, the SCUS forms mainly as the result of NCEs which entrain shelf water and is supported by the intrusion of slope water upon the shelf.

Chapter 7

Summary and Conclusions

The results of this study highlighted particular features of the coastal marine dynamics off Southern Queensland, Australia. The EAC is the main driver of these features and its behaviour impacts upon the marine shelf dynamics and circulation. The following sections summarise the findings of this project, addressing each objective describing how each was completed as well as making suggestions for future work.

7.1 Summary

The EAC, its variability as well as wind stress are addressed to examine their impact upon the circulation in the SQCMZ. The EAC intensifies from August to December, relaxing in January, intensifying in February until again relaxing from March to July. This annual variability is described in section 2.2.1. The second relaxation and intensification periods occurring in January and February respectively, were not found in the literature. The EAC intensification period coincides with the Austral Spring (September - November) and Summer (December - February) seasons, when the secondary periods in January and February were excluded. The EAC relaxation coincides with the Austral Autumn (March - May) and Winter (June - August) seasons.

The first analysis of Chla blooms in the SQCMZ led to the identification of the SFIUS and the SCUS. The SFIUS integrates three physical mechanisms identified in this research: bottom stress, wind stress and submesoscale eddies.

A zone of high bottom stress was found on the shelf break off Fraser Island. Bottom stress uplifts slope water upon the shelf, creating the optimal conditions for upwelling events. The uplifting of water is represented along the whole shelf break off the SQCMZ in BRAN3.5 calculations. P2 events characterising the SFIUS are more frequent in the period of the EAC intensification (Spring and Summer). Within the EAC intensification period, a period of wind-driven upwelling exists, which supports the formation of upwelling events. The lee effect and the submesoscale eddies within it are mechanisms that support upwelling. Dambacher et al. (2012) suggest the interaction of the EAC with the shelf and transient eddies as the possible mechanisms. Both suggestions are supported by the results of this research. However, a better representation of the submesoscale features is required to address their impact and role in the SFIUS. Kelvin waves described byKämpf (2006) could be an additional mechanism supporting upwelling in the same area. Finally, the off- and in-shore movement of the EAC could be a potential mechanism supporting and inhibiting upwelling events.

Chla blooms of the SCUS are more frequent in Winter. The surface Ekman transport does not explain the formation of Chla blooms as it is unfavourable to their formation (downwelling wind conditions). The eddy analysis shows that the mean radii of the eddies in the SQCMZ increases along the period of greater Chla bloom frequency in the SCUS. Simultaneously, in the same period, the wind's eastward component results in a northward net Ekman transport, which enhances the cyclonic circulation upon the shelf.

The interaction of the EAC waters with shelf waters results in an unstable interface which is rich in cyclonic eddies, in particular, submesoscale eddies due to the marine dynamic configuration. The close proximity of the EAC to the shelf break enhances cyclonic eddies whilst inhibiting anti-cyclonic eddies. However, two peaks of anti-cyclonic eddies along the coast are the exception to the rule. Sharp increases in the number of anti-cyclonic eddies along the coast are associated with separations of the EAC from the shelf break (e.g.the primary separation zone of the EAC). The latitudinal concentration displays a peak in anti-cyclonic eddies in the primary separation zone, as well as at 26°S, where the shelf narrows resulting in the EAC sporadically detaching from the shelf break for a few kilometres. Additionally, the two peaks in the concentration of anti-cyclonic eddies agree with the cores of the double anti-cyclonic circulation at the east of the EAC described by Ridgway and Dunn (2003). The separation of the EAC farther south results in an increase in the number of near-coastal anticyclonic eddies, as

the EAC is not present. The number of eddies with a radius larger than $45km$ shows a stable variability from 1993 to 2014 in Southern Queensland. For the same period, when smaller eddies which have radii larger than the minimum that can be detected are included ($\sim 22km$, section 3.2.1.3), the distribution of eddies throughout time shows an increasingly linear trend. The linear trend could be associated with improvements made to the measurements and algorithms used in obtaining the SSH. Alternatively, it may be related to a strengthening of the EAC resulting in an increase in small mesoscale eddies. The final hypothesis agrees with the scenario of global warming, which forecasts an intensification of the EAC.

The results of the BRAN3.5 and ROMS analyses confirmed that submesoscale activity, in particular eddies, is high within the lee effect as a result of the interaction of the EAC and Fraser Island. ROMS represents a weak poleward current. However, the analysis of deformation and vorticity shows that the surface area over the shelf break has well defined areas in which the vorticity or deformation dominates. BRAN3.5 does not reproduce submesoscale features due to its resolution ($\sim 10km$), whilst the Okubo-Weiss parameter shows deformation to be dominant over vorticity without exception in BRAN3.5 calculations. The western edge of the EAC is where the greatest longitudinal gradient of the v-velocity component is located (SS, Halo et al. 2014b). Comparing BRAN3.5 and ROMS, it is possible to observe the number of submesoscale eddies increasing during the intensification period of the EAC. In an inverse relationship, the number of mesoscale eddies increases during the relaxation of the EAC. The detection of mesoscale eddies shows that cyclonic eddies decrease their number from July to December. However, the sharp increase in January then proceeds to decrease from February.

BRAN3.5 reproduces an inner-shelf northward current. The current is illustrated in the v-velocity component monthly averages. The inner-shelf northward current is represented along the coast in the two pixel nearest to the shore. Its annual variability has an inverse relationship with that of the EAC. The intensification period of this current is from March to August. It is in the same period that the middle of the shelf moves to a near zero value for v-velocity component, potentially indicating equal southward and northward velocities. Simultaneously, the cyclonic circulation upon the shelf reaches its maximum velocities. The increase in the number of mesoscale eddies (larger eddies than in Spring-Summer) could stimulate the cyclonic circulation or visa versa. This inner-shelf current

could be the River of Sand, characterised by its poleward transport of sand.

The northward transport of sand by the inner-shelf current ends at the north of Fraser Island. According to Boyd et al. (2008) a balance exists between tides and waves, creating the sand extension at the north of Fraser Island (Breaksea Spit). The sand accumulation extends to the shelf break, which is where the sand falls. The depth of the Breaksea Spit is a few meters, it is a natural barrier which significantly inhibits the transport of water in the south-north orientation. This inhibition leaves just the slope water as the source of water in the SFIUS. ROMS represents the sand extension at the north of Fraser Island as water having a depth of $10m$. In animation 6.2, it is possible to see warm water off Hervey Bay being transported around the North of Fraser Island and finally along the shelf break. The resulting pattern of warm water is similar to P2 Chla bloom events. The main difference between ROMS and Chla observations is the source of water creating the particular signal in the surface. ROMS represents the source of the water as Hervey Bay, whilst Chla and SST observations lead to the conclusion that the source is deep water from the shelf break. The conclusion reached by examining the observations is the one proposed by this research leading to the affirmation that Breaksea Split is a key geography feature defining the source of water for the SFIUS, due to the implications observed in ROMS (warm water instead of cold water). BRAN3.5 manages this feature by simply extending the land mark upon the sand extension, thus preventing any transport through this area. The BRAN3.5 solution will be implemented in future improvements of the downscaling model.

Based on the circulation and dynamics proposed in this study, the following inferences should be true:

1. The suggested intensification of the EAC under global warming implies that P1 upwelling events will have a reduction in their frequency, whilst P2 will increase. The intrusion of slope water will be stronger, resulting in more fertile shelf water.

2. The increasing amplitude of EAC variability will increase both P1 and P2 upwelling events, resulting from a rise in sub- and mesoscale eddies. The intrusion of slope water will be stronger during the EAC intensification period, resulting in greater shelf water fertility.

3. The decreasing strength of the EAC implies a greater number of P1 events

as well as a reduced number of P2 events, which is a result of the decrease in submesoscale eddies and increase in mesoscale eddies. The intrusion of slope water will decrease, resulting in reduced shelf water fertility.

Finally, the description summarised in this section achieved the objectives proposed in chapter 1. Additionally, using the results from this research, it is possible to propose future research work (see section 7.3), this will endeavour to expand the current understanding of marine dynamics and circulation in the study area. Areas suggested for improvement are on-site observations in particular locations, numerical simulation activities for the downscaling model and addressing unanswered questions.

7.2 Achievement of the objectives

In chapter 1 three objectives were listed. The results from this research are sufficient to complete the aim and the objectives proposed for this research project. These results provide a basis for the proposed dynamics and circulation summarised in section 7.1. The first objective was completed by examining Chla blooms, which were used as a proxy of upwelling events. The examination resulted in the quantification of Chla blooms which characterise the SFIUS and the SCUS. Bottom and wind stresses were studied and found to play a role in the SFIUS. The detection and quantification of near coastal eddies provided the basis for their description, which included their spatial distribution along the coast, distribution in time, and the spacial variability of their physical features along the coast. These results highlighted that the SCUS is associated with the entrainment of water by NCEs. The final objective was completed through the construction of a model describing the interconnectivity of the aforementioned features in the SQCMZ. This was achieved by analysing the numerical results from BRAN3.5 and ROMS. Below the activities related to the completion of each objective are listed.

1. To analyse and characterise the upwelling events in the SQCMZ and to propose possible physical mechanisms driving these events (results are presented in chapter 4).
    - The classification of Chla blooms into two patterns resulting in a close relationship with the annual variability of the EAC.

- The analysis of SST, supporting the theory that Chla blooms are intrusions of slope or deeper water upon the shelf.
- The correlation of high bottom stress zones with Chla blooms, classified as P2.
- The demonstration of wind as a possible trigger for P2 Chla blooms as well as being an inhibitor of P1 upwelling events, despite P1 Chla blooms resembling wind-driven upwelling.

2. To quantify, analyse and describe NCEs, including their potential impact upon the shelf circulation (results are presented in chapter 5).

   - The implementation of an eddy detection and tracking tool based on Sea Surface Height.
   - The development of a method to filter eddies within a near-coastal corridor.
   - The description of a single NCE and its impact upon the shelf circulation, representing the potential impact of NCEs.
   - The climatology description of NCEs including their temporal and spatial distribution, as well as the spatial variability of some of their physical features.

3. To analyse and examine the general circulation of the SQCMZ based on BRAN3.5 and the implementation of a numerical model, as well as to design a model showing how the described features are interconnected by physical mechanisms (results are presented in chapter 6).

   - The implementation of ROMS_AGRIF with a grid of $\sim 2km$ resolution upon the shelf. The spatial resolution allows the representation of submesoscale features which were not solved by the $\sim 10km$ grid of BRAN3.5.
   - The numerical implementation identifies issues with climatology boundary conditions.
   - The identification of Breaksea Spit (northern extension of Fraser Island) as a crucial point inhibiting the transport of water from Hervey Bay to the east side of Fraser Island.
   - The representation of submesoscale eddies as part of the lee effect resulting from the interaction of the EAC with Fraser Island. The description of the annual variability in the inner shelf northward current,

which is inversely related to periods of intensification and relaxation in the EAC.

- Characterisation of the EAC by the Okubo-Weiss parameter and its components (deformation and vorticity).
- The description of high submesoscale activity in the period of the EAC intensification.
- The construction of a model describing how the aforementioned features are interconnected based on the physical mechanisms observed.

7.3 Recommendations for future work

The current data available was sufficient to address the questions of this research, however, it is not possible address certain topics due to the lack of observations in the Southern Queensland Coastal Marine Zone. IMOS was a great system for accessing the majority of the satellite data. On-site observations of the physical variables (salinity and temperature) and velocity field will contribute greatly to understanding as well as supporting (or changing) the circulation proposed here. Particular areas of interest include the areas off north-east Fraser Island (eddy activity), along the shelf break from Fraser Island to 25°S (lee effect and submesoscale eddies) and within $\sim 10km$ from the shore (inner shelf northward current). The use of radar to characterise the activities and dynamics off east Fraser Island and upon the shelf break will contribute highly relevant data.

This thesis and Brieva et al. (2015) already initiated new research (Tran et al., 2015), however, other questions remain to be answered. Below is a list of improvements suggested for this research work:

- General Circulation: Apply an orthogonal analysis to study the main modes of oscillation in the velocity field represented by BRAN3.5.
- Upwelling: To study the role and impact of Kelvin waves, submesoscale eddies and the EAC off- and in-shore movement in upwelling events off Southern Queensland.
- Upwelling: To use fluorescence line height following the work of Kämpf (2015) to improve the representation and analysis of Chla blooms.

- Eddy analysis: To improve the method used in the estimation of Chla and SST gradients, defining the radius of the inner area and the ring in proportion to the radius of the eddy.

- Eddy analysis: To extend the description of a single eddy to other events, examining trends in their impact upon the shelf circulation.

- Eddy analysis: To extend the analysis of the numerical results with BRAN3.5 to estimate the impact of the eddies in the SQCMZ, as well as using ROMS to estimate the role of sub-mesoscale eddies.

From the downscaling model implemented for this research it was concluded that future numerical activities needed the following improvements. First, to extend the land mask farther north of Fraser Island to also represent the role of the Breaksea Split in the Southeast Fraser Island Upwelling System, as BRAN3.5 does. An alternative solution is to nest a grid with a lower number of sigma layers to solve that particular section with a minimum depth less than $10m$. This solution will better represent the role of shallow waters in the circulation. Second, to study a smoother transition from BRAN3.5 data to the boundary condition. For example, grid's boundaries with a similar resolution to BRAN3.5, increasing the resolution near the SQCMZ, to implement a different interpolation method, to implement the same resolution grid as BRAN3.5 and to nest a grid on top of the SQCMZ, among others. These improvements will result in a more accurate representation of the circulation in SQCMZ. Third, to move to a surface forcing that is similar to or the same as BRAN3.5.

Bibliography

Abraham, E. R. and Bowen, M. M. (2002). Chaotic stirring by a mesoscale surface-ocean flow. *Chaos: An Interdisciplinary Journal of Nonlinear Science*, 12(2):373–381.

Abraham, E. R., Law, C. S., Boyd, P. W., Lavender, S. J., Maldonado, M. T., and Bowie, A. R. (2000). Importance of stirring in the development of an iron-fertilized phytoplankton bloom. *Nature*, 407(6805):727–730.

Anderson Jr, J. D. (2005). Ludwig Prandtl's boundary layer. *Physics Today*, 58(12):42–48.

Andreu-Burillo, I., Brassington, G., Oke, P., and Beggs, H. (2010). Including a new data stream in the BLUElink Ocean Data Assimilation System. *Australian Meteorological and Oceanographic Journal*, 59:77–86.

Andrews, J. C. and Gentien, P. (1982). Upwelling as a source of nutrients for the Great Barrier Reef ecosystems: a solution to Darwin's question? *Marine Ecology - Progress Series*, 8(3):257–269.

Aryal, R., Kandel, D., Acharya, D., Chong, M. N., and Beecham, S. (2012). Unusual Sydney dust storm and its mineralogical and organic characteristics.

Bakun, A. (2006). Fronts and eddies as key structures in the habitat of marine fish larvae: opportunity, adaptive response and competitive advantage. *Scientia Marina*, pages 105–122.

Benthuysen, J., Thomas, L. N., and Lentz, S. J. (2015). Rapid Generation of Upwelling at a Shelf Break Caused by Buoyancy Shutdown. *Journal of Physical Oceanography*, 45(1):294–312.

Bowen, M. M., Emery, W. J., Wilkin, J. L., Tildesley, P. C., Barton, I. J., and Knewtson, R. (2002). Extracting Multiyear Surface Currents from Sequential Thermal Imagery Using the Maximum Cross-Correlation Technique. *Journal of Atmospheric and Oceanic Technology*, 19(10):1665–1676.

Bowen, M. M., Wilkin, J. L., and Emery, W. J. (2005). Variability and forcing of the East Australian Current. *Journal of Geophysical Research*, 110(C03019).

Boyd, R., Ruming, K., Goodwin, I., Sandstrom, M., and Schröder-Adams, C. (2008). Highstand transport of coastal sand to the deep ocean: A case study from fraser Island, southeast Australia. *Geology*, 36:15–18.

Brassington, G. B., Pugh, T., Spillman, C., Schulz, E., and Beggs, H. (2007). BLUElink> Development of Operational Oceanography and Servicing in Australia. *Journal of Research and Practice in Information Technology*, 39(2):151–164.

Brieva, D., Ribbe, J., and Lemckert, C. (2015). Is the East Australian Current causing a marine ecological hot-spot and an important fisheries near Fraser Island, Australia? *Estuarine, Coastal and Shelf Science*, 153:121 – 134.

Brown, O. B. and Minnett, P. J. (1999). MODIS Infrared Sea Surface Temperature Algorithm. Technical report, NASA.

Cannizzaro, J. P. and Carder, K. L. (2006). Estimating chlorophyll a concentrations from remote-sensing reflectance in optically shallow waters. *Remote Sensing of Environment*, 101(1):13–24.

Cetina-Heredia, P., Roughan, M., Van Sebille, E., and Coleman, M. A. (2014). Long-term trends in the East Australian Current separation latitude and eddy driven transport. *Journal of Geophysical Research: Oceans*, 119(7):4351–4366.

Chaigneau, A., Eldin, G., and Dewitte, B. (2009). Eddy activity in the four major upwelling systems from satellite altimetry (1992-2007). *Progress in Oceanography*, 83(1-4):117–123.

Chelton, D. B., Schlax, M. G., and Samelson, R. M. (2011). Global observations of nonlinear mesoscale eddies. *Progress in Oceanography*, 91(2):167–216.

Chenillat, F., Franks, P. J. S., Rivière, P., Capet, X., Grima, N., and Blanke, B. (2015). Plankton dynamics in a cyclonic eddy in the Southern California Current System. *Journal of Geophysical Research: Oceans*, pages n/a—-n/a.

Chin, T. M., Vazquez, J., and Armstrong, E. (2013). Algorithm Theoretical Basis Document: A multi-scale, high-resolution analysis of global sea surface temperature. Version 1.3. Technical report, NASA.

Claustre, H. and Maritorena, S. (2003). The Many Shades of Ocean Blue. *Science*, 302(5650):1514–1515.

Coles, R. G., Rasheed, M. A., McKenzie, L. J., Grech, A., York, P. H., Sheaves, M., McKenna, S., and Bryant, C. (2015). The Great Barrier Reef World Heritage Area seagrasses: Managing this iconic Australian ecosystem resource for the future. *Estuarine, Coastal and Shelf Science*, 153:A1 – A12.

Combes, V., Hormazabal, S., and Di Lorenzo, E. (2015). Interannual variability of the subsurface eddy field in the southeast Pacific. *Journal of Geophysical Research: Oceans*, pages n/a—-n/a.

Condie, S. A. and Dunn, J. R. (2006). Seasonal characteristics of the surface mixed layer in the Australasian region: implications for primary production regimes and biogeography.

Corredor-Acosta, A., Morales, C. E., Hormazabal, S., Andrade, I., and Correa-Ramirez, M. A. (2015). Phytoplankton phenology in the coastal upwelling region off central-southern Chile (35ÂřS–38ÂřS): Time-space variability, coupling to environmental factors, and sources of uncertainty in the estimates. *Journal of Geophysical Research: Oceans*, pages n/a—-n/a.

Cresswell, G. (2001). East Australian Current. In Sciences, E.-i.-C. J. H. S. B. T. E. o. O., editor, *Encyclopedia of Ocean Sciences*, pages 783–792. Academic Press, Oxford.

Dambacher, J. M., Hosack, G. R., and Rochester, W. A. (2012). *Ecological Indicators for the Exclusive Economic Zone of Australia's East Marine Region*. A report prepared for the Australian Government Department of Sustainability, Environment, Water, Population and Communities. CSIRO Wealth from Oceans Flagship, Hobart.

Daubechies, I. (1990). The wavelet transform, time-frequency localization and signal analysis. *IEEE Transactions on Information Theory*, 36(5):961–1005.

Debreu, L., Marchesiello, P., Penven, P., and Cambon, G. (2011). Two-way nesting in split-explicit ocean models: algorithms, implementation and validation. *Ocean Modelling*, 49-50:1–21.

Ekman, V. W. (1905). On the influence of the earth\'s rotation on ocean currents. *Ark. Mat. Astron. Fys.*, 2:1–53.

Everett, J. D., Baird, M. E., Oke, P. R., and Suthers, I. M. (2012). An avenue of eddies: Quantifying the biophysical properties of mesoscale eddies in the Tasman Sea. *Geophysical Research Letters*, 39(16):n/a—-n/a.

Everett, J. D., Baird, M. E., Roughan, M., Suthers, I. M., and Doblin, M. A. (2014). Relative impact of seasonal and oceanographic drivers on surface chlorophyll a along a Western Boundary Current. *Progress in Oceanography*, 120(0):340–351.

Everett, J. D., Baird, M. E., and Suthers, I. M. (2011). Three-dimensional structure of a swarm of the salp Thalia democratica within a cold-core eddy off southeast Australia. *Journal of Geophysical Research: Oceans (1978–2012)*, 116(C12).

Everett, J. D., Macdonald, H., Baird, M. E., Humphries, J., Roughan, M., and Suthers, I. M. (2015). Cyclonic entrainment of pre-conditioned shelf waters into a frontal eddy. *Journal of Geophysical Research: Oceans*.

Gabric, A. J., Cropp, R. A., McTainsh, G. H., Johnston, B. M., Butler, H., and Tilbrook, B. (2010). Australian dust storms in 2002-2003 and their impact on Southern Ocean biogeochemistry. *Global Biogeochemical Cycles*, 24:1–17.

Ganachaud, A., Cravatte, S., Melet, A., Schiller, A., Holbrook, N. J., Sloyan, B. M., Widlansky, M. J., Bowen, M., Verron, J., Wiles, P., Ridgway, K., Sutton, P., Sprintall, J., Steinberg, C., Brassington, G., Cai, W., Davis, R., Gasparin, F., Gourdeau, L., Hasegawa, T., Kessler, W., Maes, C., Takahashi, K., Richards, K. J., and Send, U. (2014). The Southwest Pacific Ocean circulation and climate experiment (SPICE). *Journal of Geophysical Research: Oceans*, 119(11):7660–7686.

Gill, A. E. (1982). *Atmosphere-Ocean Dynamics*. International Geophysics Series. Academic Press.

Griffies, S. M., Gnanadesikan, A., Dixon, K. W., Dunne, J. P., Gerdes, R., Harrison, M. J., Rosati, A., Russell, J. L., Samuels, B. L., Spelman, M. J., Winton, M., and Zhang, R. (2005). Formulation of an ocean model for global climate simulations. *Ocean Science*, 1(1):45–79.

Griffin, D. A., Middleton, J. H., and Bode, L. (1987). The tidal and longer-period circulation of Capricornia, Southern Great Barrier Reef. *Marine and Freshwater Research*, 38(4):461–474.

Gruber, N., Lachkar, Z., Frenzel, H., Marchesiello, P., Munnich, M., McWilliams, J. C., Nagai, T., and Plattner, G.-K. (2011). Eddy-induced reduction of biological production in eastern boundary upwelling systems. *Nature Geosci*, 4(11):787–792.

Halo, I., Backeberg, B., Penven, P., Ansorge, I., Reason, C., and Ullgren, J. E. (2014a). Eddy properties in the Mozambique Channel: A comparison between observations and two numerical ocean circulation models. *Deep Sea Research Part II: Topical Studies in Oceanography*, 100(0):38–53.

Halo, I., Penven, P., Backeberg, B., Ansorge, I., Shillington, F., and Roman, R. (2014b). Mesoscale eddy variability in the southern extension of the East Madagascar Current: seasonal cycle, energy conversion terms, and eddy mean properties. *Journal of Geophysical Research: Oceans*, 119(10):7324–7356.

Hamon, B. V., Godfrey, J. S., and Greig, M. A. (1975). Relation between mean sea level, current and wind stress on the east coast of Australia. *Marine and Freshwater Research*, 26(3):389–403.

Hamon, B. V. and Kerr, J. D. (1968). Time and space scales of variations in the East Australian Current, from merchant ship data. *Marine and Freshwater Research*, 19(2):101–106.

Harris, P. T., Tsuji, Y., Marshall, J. F., Davies, P. J., Honda, N., and Matsuda, H. (1996). Sand and rhodolith-gravel entrainment on the mid- to outer-shelf under a western boundary current: Fraser Island continental shelf, eastern Australia. *Marine Geology*, 129(3-4):313–330.

Henson, S. A. and Thomas, A. C. (2008). A census of oceanic anticyclonic eddies in the Gulf of Alaska. *Deep Sea Research Part I: Oceanographic Research Papers*, 55(2):163–176.

IMOS (2014a). Chlorophyll-a concetration (OC3) (accessed Feb. 2015).

IMOS (2014b). Five moorings extending from the continental slope to the abyssal waters off Brisbane (Nov. 2014).

IMOS (2015a). Gridded sea level anomaly (accessed Mar. 2015).

IMOS (2015b). Sea Surface Temperature (SST) estimation (accessed Feb. 2015).

Isern-Fontanet, J., García-Ladona, E., and Font, J. (2006). Vortices of the Mediterranean Sea: An Altimetric Perspective. *Journal of Physical Oceanography*, 36(1):87–103.

Jia, Y., Calil, P. H. R., Chassignet, E. P., Metzger, E. J., Potemra, J. T., Richards, K. J., and Wallcraft, A. J. (2011). Generation of mesoscale eddies in the lee of the Hawaiian Islands. *Journal of Geophysical Research: Oceans*, 116(C11):n/a—-n/a.

Kämpf, J. (2006). Transient wind-driven upwelling in a submarine canyon: A process-oriented modeling study. *Journal of Geophysical Research: Oceans*, 111(11).

Kämpf, J. (2012). Lee effects of localized upwelling in a shelf-break canyon. *Continental Shelf Research*, 42(0):78–88.

Kämpf, J. (2015). Phytoplankton blooms on the western shelf of Tasmania: evidence of a highly productive ecosystem. *Ocean Science Discussions*, 11(5):2173–2204.

Kämpf, J. and Kaempf, J. (2009). On the Interaction of Time-Variable Flows with a Shelfbreak Canyon. *Journal of Physical Oceanography*, 39(1):248–260.

Kim, S. Y., Terrill, E. J., Cornuelle, B. D., Jones, B., Washburn, L., Moline, M. A., Paduan, J. D., Garfield, N., Largier, J. L., Crawford, G., and Kosro, P. M. (2011). Mapping the U.S. West Coast surface circulation: A multiyear analysis of high-frequency radar observations. *Journal of Geophysical Research: Oceans*, 116(C3):n/a—-n/a.

Kowalik, Z. and Murty, T. S. (1993). *Numerical Modeling of Ocean Dynamics*. Advanced Series on Ocean Engineering. World Scientific.

Lévy, M., Iovino, D., Resplandy, L., Klein, P., Madec, G., Tréguier, A.-M., Masson, S., and Takahashi, K. (2012). Large-scale impacts of submesoscale dynamics on phytoplankton: Local and remote effects. *Ocean Modelling*, 43:77–93.

Lévy, M., Resplandy, L., and Lengaigne, M. (2014). Oceanic mesoscale turbulence drives large biogeochemical interannual variability at middle and high latitudes. *Geophysical Research Letters*, 41(7):2467–2474.

Liu, X. and Levine, N. M. (2016). Submesoscale frontal dynamics enhances phytoplankton chlorophyll in the North Pacific Subtropical Gyre. *Geophysical Research Letters*, 43(4):n/a—-n/a.

Mahadevan, A. and Tandon, A. (2006). An analysis of mechanisms for submesoscale vertical motion at ocean fronts. *Ocean Modelling*, 14(3):241–256.

Marchesiello, P. and Middleton, J. H. (2000). Modeling the East Australian Current in the Western Tasman Sea. *Journal of Physical Oceanography*, 30(11):2956–2971.

Mason, E., Pascual, A., and McWilliams, J. C. (2014). A New Sea Surface Height-Based Code for Oceanic Mesoscale Eddy Tracking. *Journal of Atmospheric and Oceanic Technology*, 31(5):1181–1188.

Mata, M. M., Tomczak, M., Wijffels, S., and Church, J. A. (2000). East Australian Current volume transports at 30ÂřS: Estimates from the World Ocean Circulation Experiment hydrographic sections PR11/P6 and the PCM3 current meter array. *Journal of Geophysical Research: Oceans*, 105(C12):28509–28526.

Matano, R. P. and Palma, E. D. (2008). On the Upwelling of Downwelling Currents. *Journal of Physical Oceanography*, 38(11):2482–2500.

Middleton, J. H., Coutis, P., Griffin, D. A., Macks, A., McTaggart, A., Merrifield, M. A., and Nippard, G. J. (1994). Circulation and water mass characteristics of the southern Great Barrier Reef. *Marine and Freshwater Research*, 45(1):1–18.

Morlet, J., Arensz, G., Fourgeau, E., and Giard, D. (1982). Wave propagation and sampling theory-Part II: Sampling theory and complex waves. *Geophysics*, 47(2):222–236.

Mueller, J. L. and Lange, R. E. (1989). Bio-optical provinces of the Northeast Pacific Ocean: A provisional analysis. *Limnology and Oceanography*, 34(8):1572–1586.

Mühlhäusler, P. and Peace, A. (2001). Discourses of ecotourism: the case of Fraser Island, Queensland. *Language & Communication*, 21(4):359–380.

Mullaney, T. J. and Suthers, I. M. (2013). Entrainment and retention of the coastal larval fish assemblage by a short-lived, submesoscale, frontal eddy of the East Australian Current. *Limnology and Oceanography*, 58(5):1546–1556.

Nagai, T., Gruber, N., Frenzel, H., Lachkar, Z., McWilliams, J. C., and Plattner, G.-K. (2015). Dominant role of eddies and filaments in the offshore transport of carbon and nutrients in the California Current System. *Journal of Geophysical Research: Oceans*, 120(8):5318–5341.

Nencioli, F., Dong, C., Dickey, T., Washburn, L., and McWilliams, J. C. (2010). A Vector Geometry-Based Eddy Detection Algorithm and Its Application to a High-Resolution Numerical Model Product and High-Frequency Radar Surface Velocities in the Southern California Bight. *Journal of Atmospheric and Oceanic Technology*, 27(3):564–579.

Oke, P. R., Brassington, G. B., Griffin, D. A., and Schiller, A. (2008). The Bluelink ocean data assimilation system (BODAS). *Ocean Modelling*, 21(1-2):46–70.

Oke, P. R. and Middleton, J. H. (2000). Topographically Induced Upwelling off Eastern Australia. *Journal of Physical Oceanography*, 30(3):512–531.

Oke, P. R. and Middleton, J. H. (2001). Nutrient enrichment off Port Stephens: the role of the East Australian Current. *Continental Shelf Research*, 21(6-7):587–606.

Oke, P. R., Sakov, P., Cahill, M. L., Dunn, J. R., Fiedler, R., Griffin, D. A., Mansbridge, J. V., Ridgway, K. R., and Schiller, A. (2013). Towards a dynamically balanced eddy-resolving ocean reanalysis: BRAN3. *Ocean Modelling*, 67(0):52–70.

Oke, P. R., Schiller, A., Griffin, D. A., and Brassington, G. B. (2005). Ensemble data assimilation for an eddy-resolving ocean model of the Australian region. *Quarterly Journal of the Royal Meteorological Society*, 131(613):3301–3311.

Okubo, A. (1970). Horizontal dispersion of floatable particles in the vicinity of velocity singularities such as convergences. *Deep Sea Research and Oceanographic Abstracts*, 17(3):445–454.

O'Reilly, J. and coauthors, . (2000). SeaWiFS Postlaunch Calibration and Validation Analyses, Part 3. *NASA Tech. Memo. 2000-206892*, Vol. 11, S:49 pp.

Penven, P., Debreu, L., Marchesiello, P., and McWilliams, J. (2006). Evaluation and application of the ROMS 1-way embedding procedure to the central california upwelling system. *Ocean Modelling*, 12:157–187.

Penven, P., Marchesiello, P., Debreu, L., and Lefevre, J. (2007). Software tools for pre- and post-processing of oceanic regional simulations. *Environ. Model. Softw.*, 23:660–662.

Pilo, G. S., Mata, M. M., and Azevedo, J. L. L. (2015). Eddy Surface properties and propagation at Southern Hemisphere western boundary current systems. *Ocean Science Discussions*, 12(1):135–160.

Reynolds, R. W., Smith, T. M., Liu, C., Chelton, D. B., Casey, K. S., and Schlax, M. G. (2007). Daily High-Resolution-Blended Analyses for Sea Surface Temperature. *Journal of Climate*, 20(22):5473–5496.

Ribbe, J. (2006). A study into the export of saline water from Hervey Bay, Australia. *Estuarine, Coastal and Shelf Science*, 66(3-4):550–558.

Ridgway, K. and Sloyan, B. (2012). ss2012_v01 Voyage: Sustained Monitoring of the East Australian Current: Mass, Heat and Freshwater Transports. Technical report, CSIRO, Marine National Facility.

Ridgway, K. and Sloyan, B. (2013). SS2013_v05 Voyage: Sustained Monitoring of the East Australian Current: mass, heat and freshwater transport. Technical report, CSIRO, Marine National Facility.

Ridgway, K. R. and Dunn, J. R. (2003). Mesoscale structure of the mean East Australian Current System and its relationship with topography. *Progress In Oceanography*, 56(2):189–222.

Ridgway, K. R. and Godfrey, J. S. (1997). Seasonal cycle of the East Australian Current. *Journal of Geophysical Research*, 102(C10):22921–22936.

Rochford, D. J. (1991). 'Upwelling': Does it need a stricter Definition? *Marine and Freshwater Research*, 42(1):45–46.

Rossi, V., López, C., Hernández-García, E., Sudre, J., Garçon, V., and Morel, Y. (2009). Surface mixing and biological activity in the four Eastern Boundary Upwelling Systems. *Nonlinear Processes in Geophysics*, 16(4):557–568.

Rossi, V., Schaeffer, A., Wood, J., Galibert, G., Morris, B., Sudre, J., Roughan, M., and Waite, A. M. (2014). Seasonality of sporadic physical processes driving temperature and nutrient high-frequency variability in the coastal ocean off southeast Australia. *Journal of Geophysical Research: Oceans*, 119(1):445–460.

Roughan, M., Macdonald, H. S., Baird, M. E., and Glasby, T. M. (2011). Modelling coastal connectivity in a Western Boundary Current: Seasonal and interannual variability. *Deep Sea Research Part II: Topical Studies in Oceanography*, 58(5):628–644.

Roughan, M. and Middleton, J. H. (2002). A comparison of observed upwelling mechanisms off the east coast of Australia. *Continental Shelf Research*, 22(17):2551–2572.

Roughan, M., Morris, B. D., and Suthers, I. M. (2010). NSW-IMOS: An Integrated Marine Observing System for Southeastern Australia. *IOP Conf. Series: Earth and Environmental Science*, 11:012030.

Schaeffer, A., Roughan, M., and Morris, B. D. (2013). Cross-Shelf Dynamics in a Western Boundary Current Regime: Implications for Upwelling. *Journal of Physical Oceanography*, 43(5):1042–1059.

Schaeffer, A., Roughan, M., and Wood, J. E. (2014). Observed bottom boundary layer transport and uplift on the continental shelf adjacent to a western boundary current. *Journal of Geophysical Research: Oceans*, 119(8):4922–4939.

Schröder-Adams, C. J., Boyd, R., Ruming, K., and Sandstrom, M. (2008). Influence of sediment transport dynamics and ocean floor morphology on benthic foraminifera, offshore Fraser Island, Australia. *Marine Geology*, 254(1-2):47–61.

Sloyan, B. M., Ridgway, K. R., and Cowley, R. (2016). The East Australian Current and Property Transport at 27 S from 2012-2013. *Journal of Physical Oceanography*.

Smith, S. D. (1980). Wind Stress and Heat Flux over the Ocean in Gale Force Winds. *Journal of Physical Oceanography*, 10(5):709–726.

Smith, W. H. F. and Sandwell, D. T. (1997). Global Sea Floor Topography from Satellite Altimetry and Ship Depth Soundings. *Science*, 277(5334):1956–1962.

Stewart, R. H. (2009). *Introduction to Physical Oceanography*. Orange Grove Books.

Suthers, I. M., Young, J. W., Baird, M. E., Roughan, M., Everett, J. D., Brassington, G. B., Byrne, M., Condie, S. A., Hartog, J. R., Hassler, C. S., Hobday, A. J., Holbrook, N. J., Malcolm, H. A., Oke, P. R., Thompson, P. A., and Ridgway, K. (2011). The strengthening East Australian Current, its eddies and biological effects - an introduction and overview. *Deep Sea Research Part II: Topical Studies in Oceanography*, 58(5):538–546.

Tomczak, M. and Godfrey, J. S. (2003). *Regional Oceanography: an Introduction*. Daya Publishing House, Delhi, 2nd improv edition.

Torrence, C. and Compo, G. P. (1998). A Practical Guide to Wavelet Analysis. *Bulletin of the American Meteorological Society*, 79(1):61–78.

Tran, D. V., Gabric, A., and Cropp, R. (2015). Interannual variability in chlorophyll-a on the southern Queensland continental shelf and its relationship to {ENSO}. *Journal of Sea Research*, 106:27–38.

Tranter, D. J., Carpenter, D. J., and Leech, G. S. (1986). The coastal enrichment effect of the East Australian Current eddy field. *Deep Sea Research Part A. Oceanographic Research Papers*, 33(11-12):1705–1728.

Trees, C. C., Clark, D. K., Bidigare, R. R., Ondrusek, M. E., and Mueller, J. L. (2000). Accessory pigments versus chlorophyll a concentrations within the euphotic zone: A ubiquitous relationship. *Limnology and Oceanography*, 45(5):1130–1143.

Valla, D. and Piola, A. R. (2015). Evidence of upwelling events at the northern Patagonian shelf break. *Journal of Geophysical Research: Oceans*, 120(11):7635–7656.

Ward, T. and Staunton-Smith, J. (2002). Comparison of the spawning patterns and fisheries biology of the sardine, Sardinops sagax, in temperate South Australia and sub-tropical southern Queensland. *Fisheries Research*, 56(1):37–49.

Ward, T. M., Staunton-Smith, J., Hoyle, S., and Halliday, I. A. (2003). Spawning patterns of four species of predominantly temperate pelagic fishes in the subtropical waters of southern Queensland. *Estuarine, Coastal and Shelf Science*, 56(5-6):1125–1140.

Waugh, D. W., Abraham, E. R., and Bowen, M. M. (2006). Spatial Variations of Stirring in the Surface Ocean: A Case Study of the Tasman Sea. *Journal of Physical Oceanography*, 36(3):526–542.

Weeks, S. J., Bakun, A., Steinberg, C. R., Brinkman, R., and Hoegh-Guldberg, O. (2010). The Capricorn Eddy: a prominent driver of the ecology and future of the southern Great Barrier Reef. *Coral Reefs*, 29(4):975–985 LA – English.

Weiss, J. (1991). The dynamics of enstrophy transfer in two-dimensional hydrodynamics. *Physica D: Nonlinear Phenomena*, 48(2):273–294.

Whiteway, T. (2009). Australian Bathymetry and Topography Grid. Technical report, Geoscience Australia Record 2009/21, Australian Government.

Wolanski, E. and Pickard, G. L. (1983). Upwelling by internal tides and kelvin waves at the continental shelf break on the Great Barrier Reef. *Marine and Freshwater Research*, 34(1):65–80.

Wood, J. E., Roughan, M., and Tate, P. M. (2012). Finding a proxy for wind stress over the coastal ocean. *Marine and Freshwater Research*, 63(6):528–544.

Wood, J. E., Schaeffer, A., Roughan, M., and Tate, P. M. (2016). Seasonal variability in the continental shelf waters off southeastern Australia: Fact or fiction? *Continental Shelf Research*, 112:92–103.

Zhang, Z., Wang, W., and Qiu, B. (2014). Oceanic mass transport by mesoscale eddies. *Science*, 345(6194):322–324.

Zhao, H., Han, G., and Wang, D. (2013). Timing and magnitude of spring bloom and effects of physical environments over the Grand Banks of Newfoundland. *Journal of Geophysical Research: Biogeosciences*, 118(4):1385–1396.

Appendix A

Extra figures supporting the analysis described in chapter 6

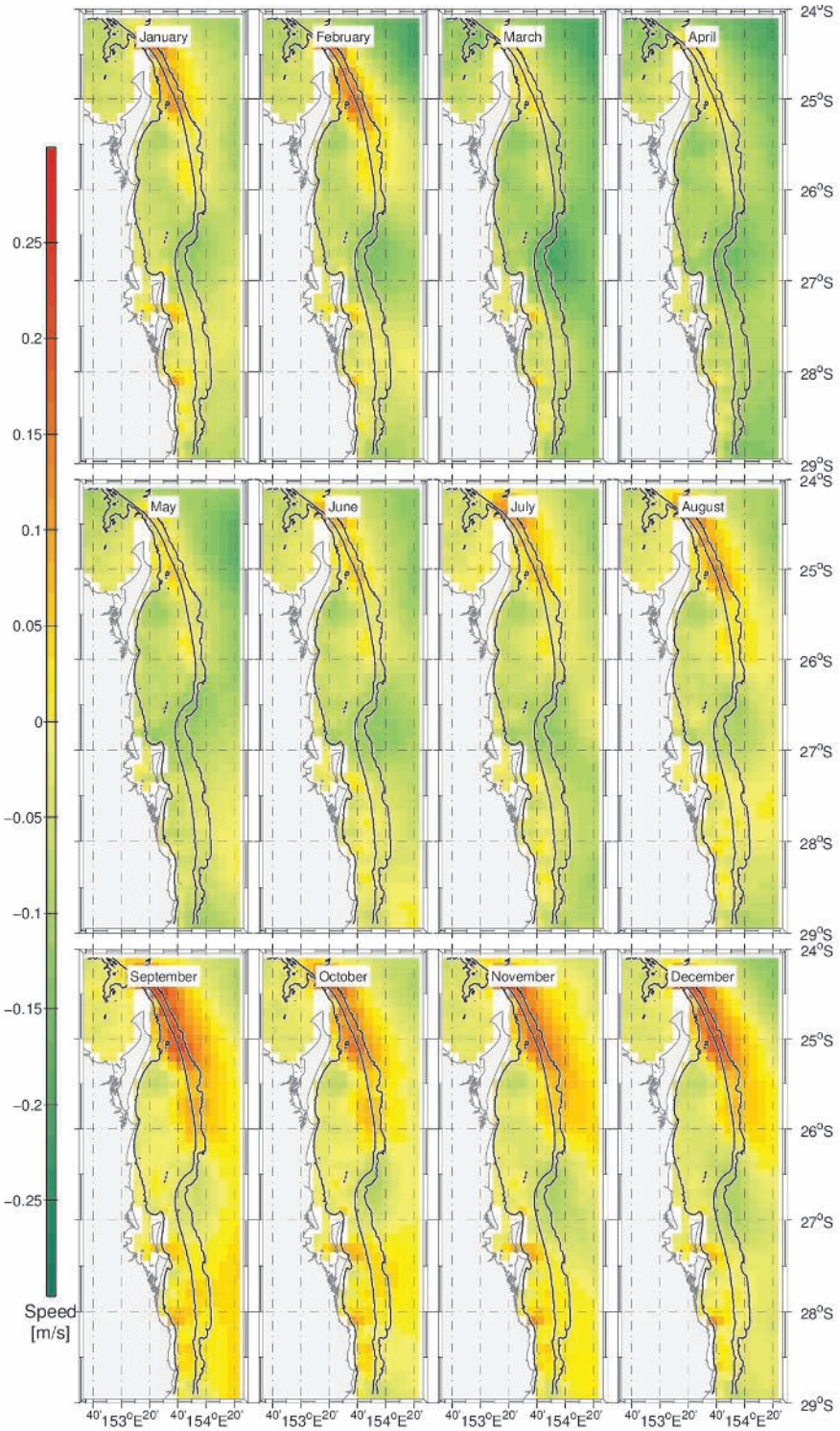

Figure A.1: Monthly averages of u-velocity component in the nearest vertical coordinate to the surface from BRAN3.5.

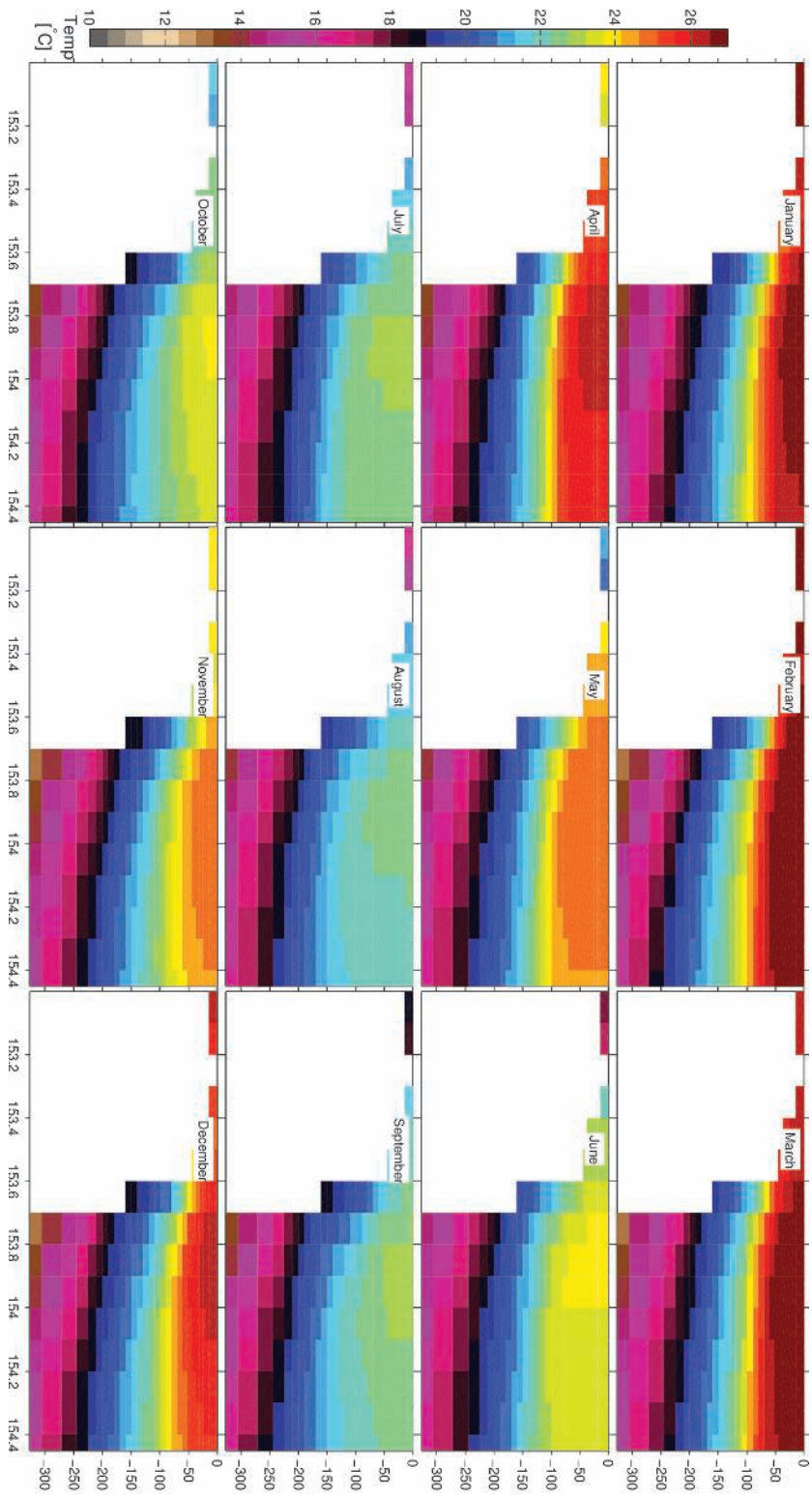

Figure A.2: Monthly averages of a cross section at 25°S of the vertical temperature based on BRAN3.5

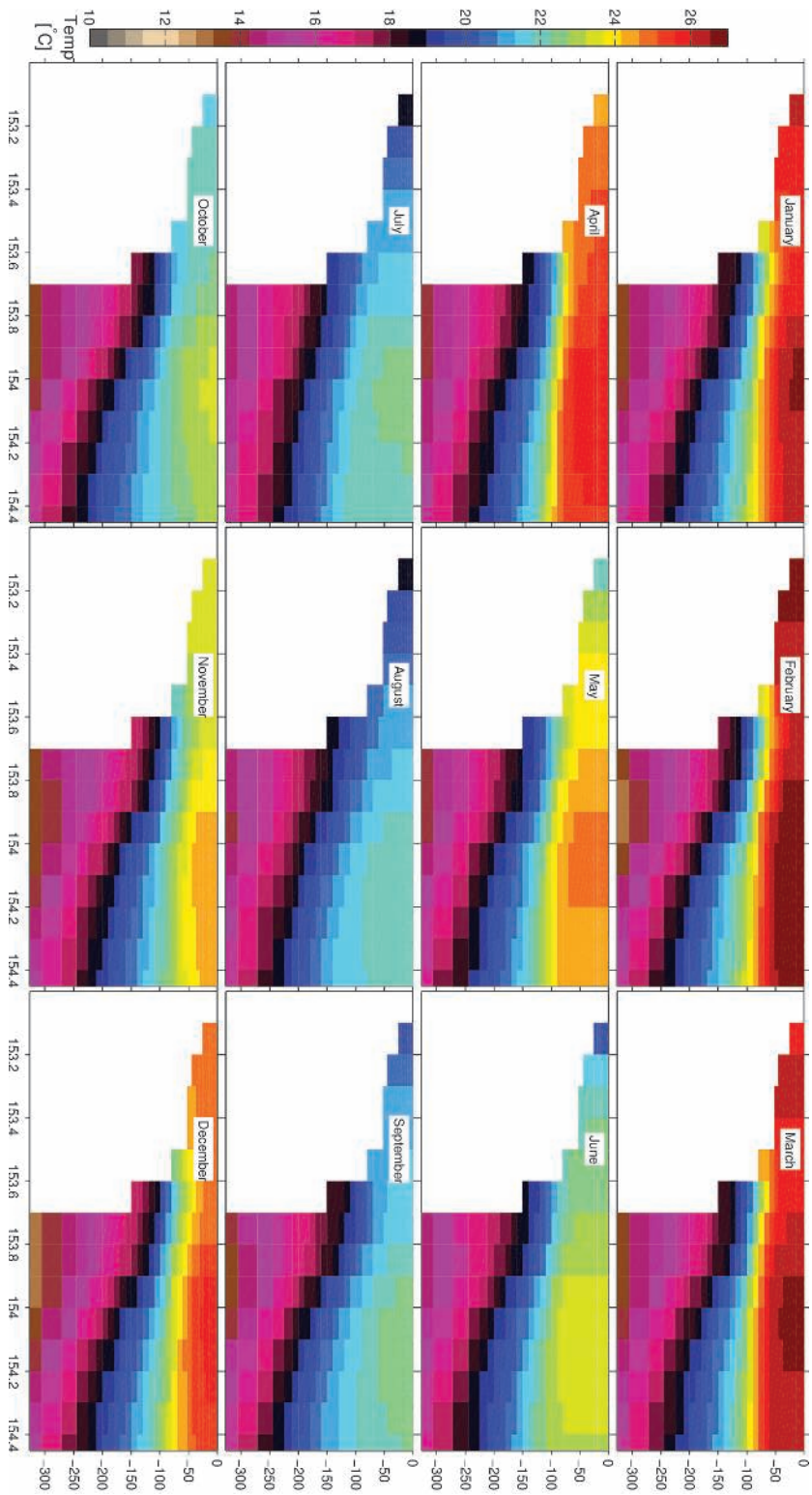

Figure A.3: Monthly averages of a cross section at 26.5°S of the vertical temperature based on BRAN3.5

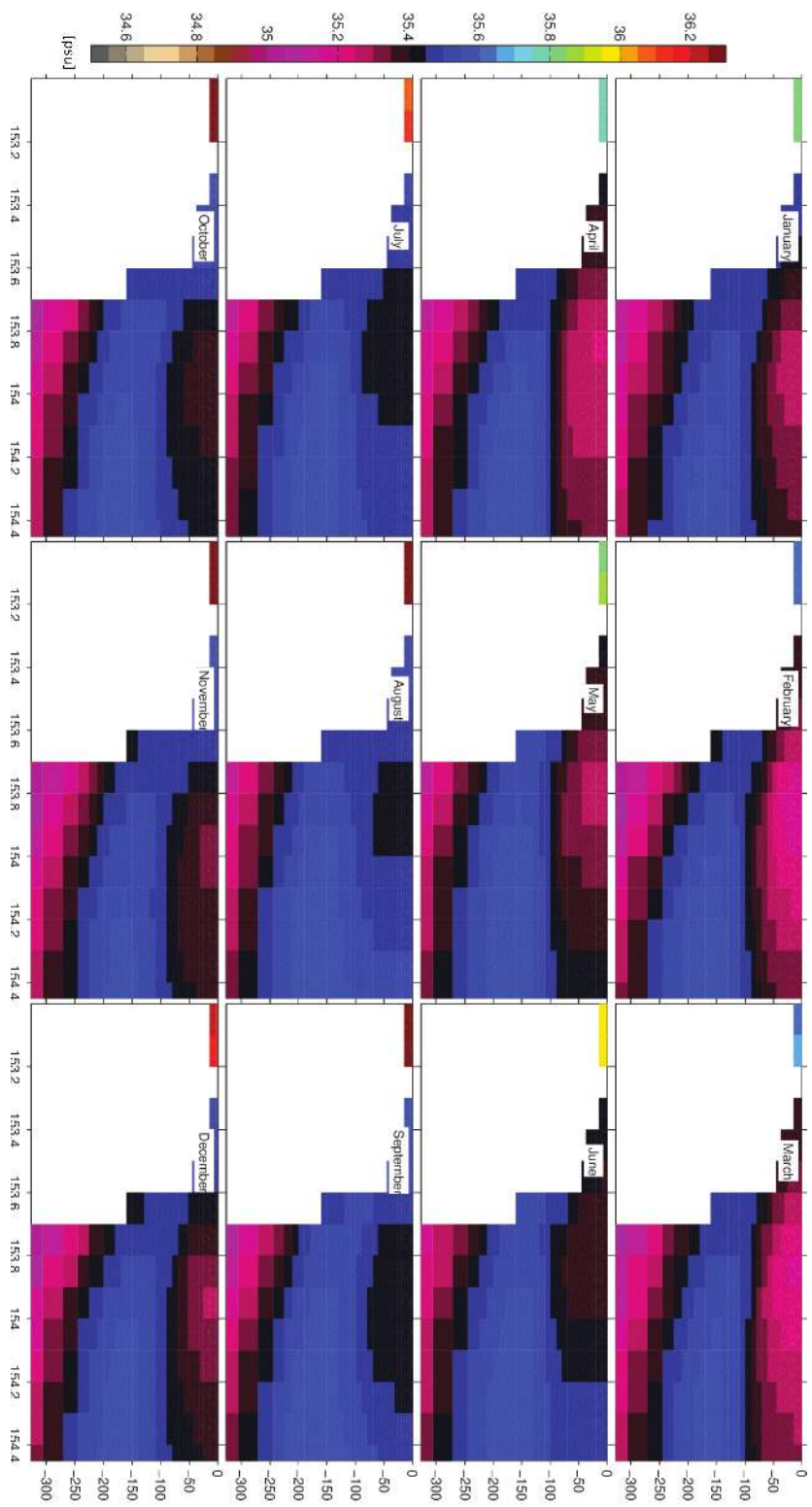

Figure A.4: Monthly averages of a cross section at 25°S of the vertical salinity based on BRAN3.5

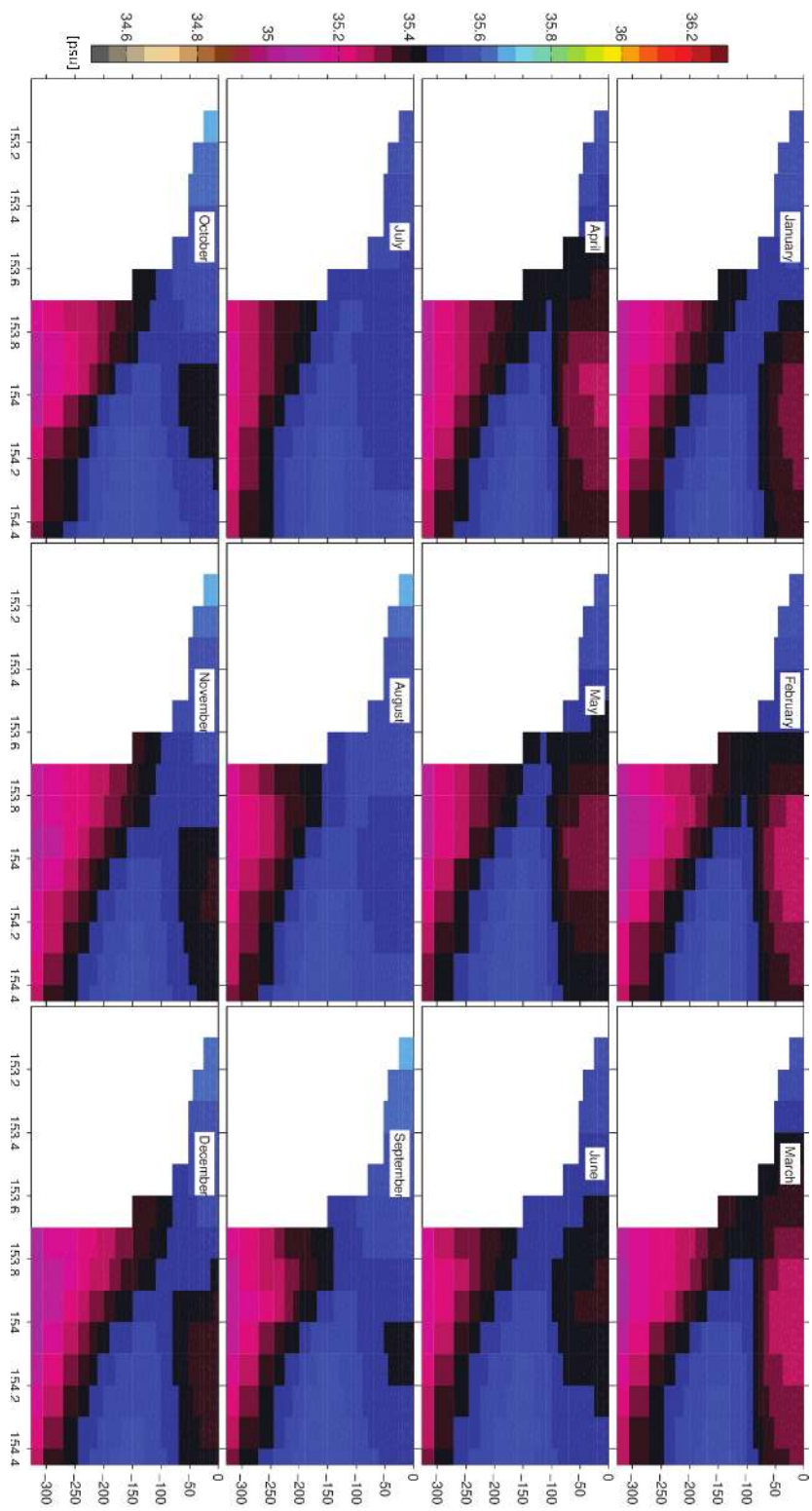

Figure A.5: Monthly averages of a cross section at 26.5°S of the vertical salinity based on BRAN3.5

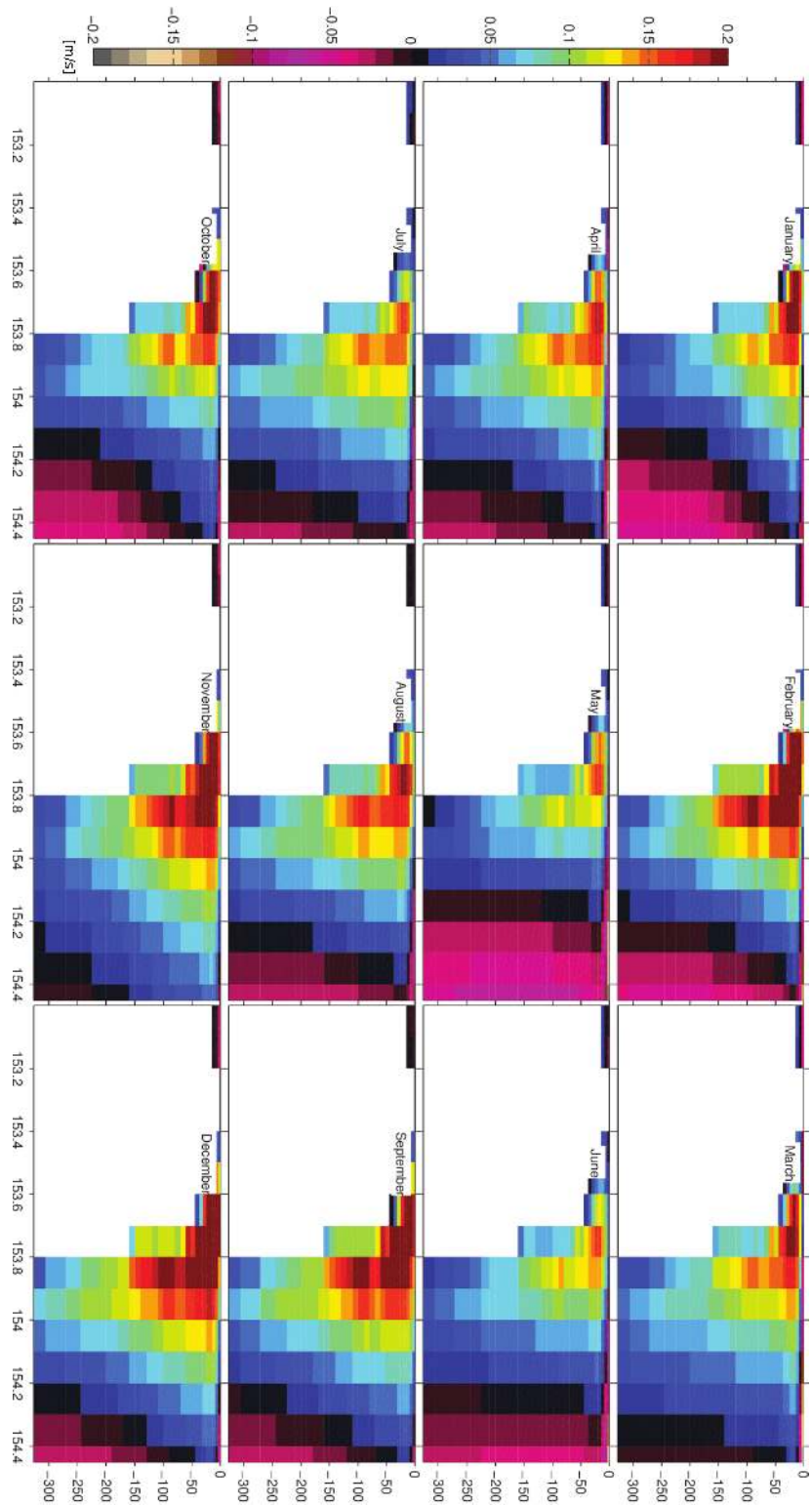

Figure A.6: Monthly averages of a cross section at 25°S of the u-velocity component based on BRAN3.5

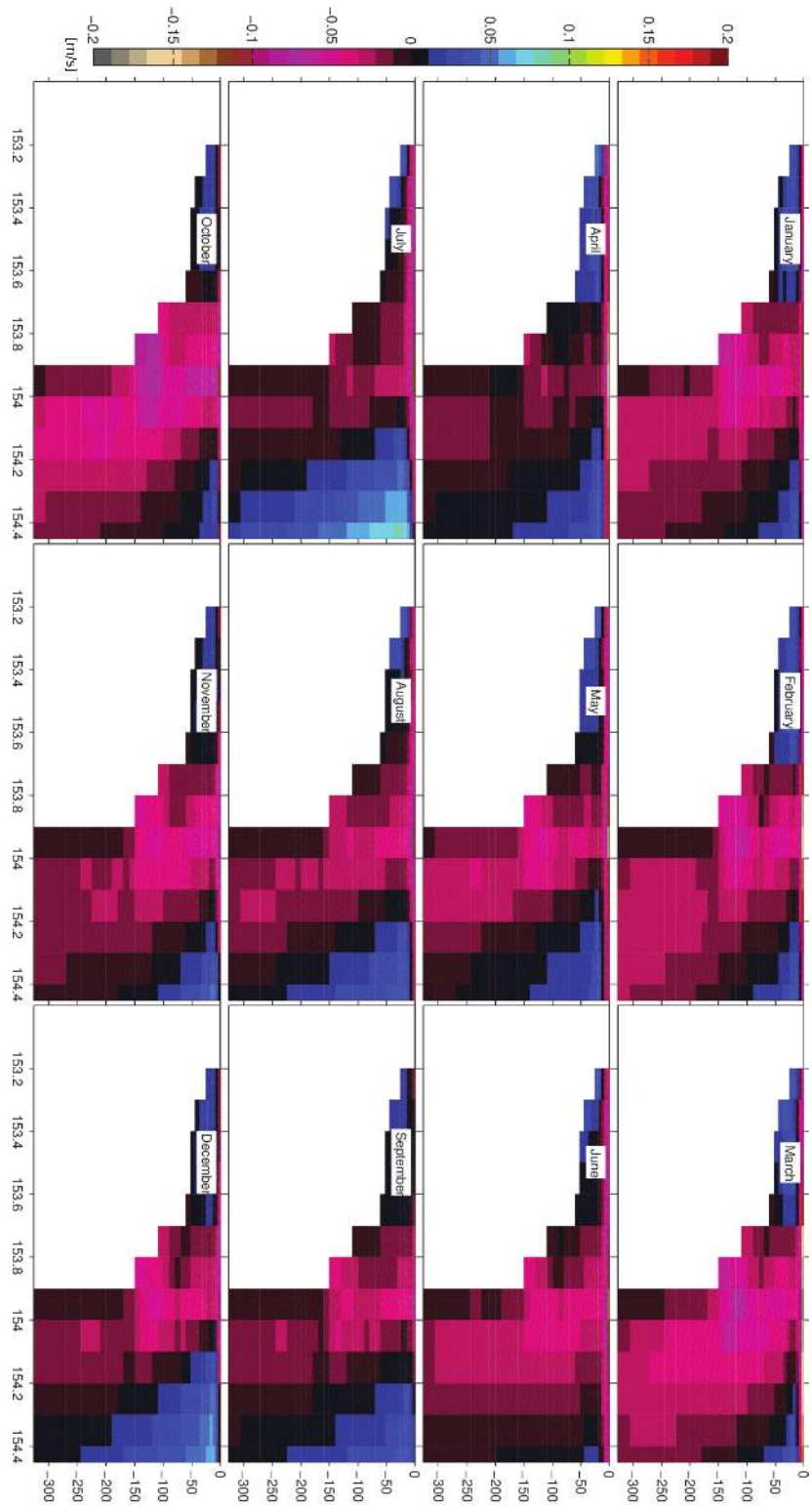

Figure A.7: Monthly averages of a cross section at 26.5°S of the u-velocity component based on BRAN3.5

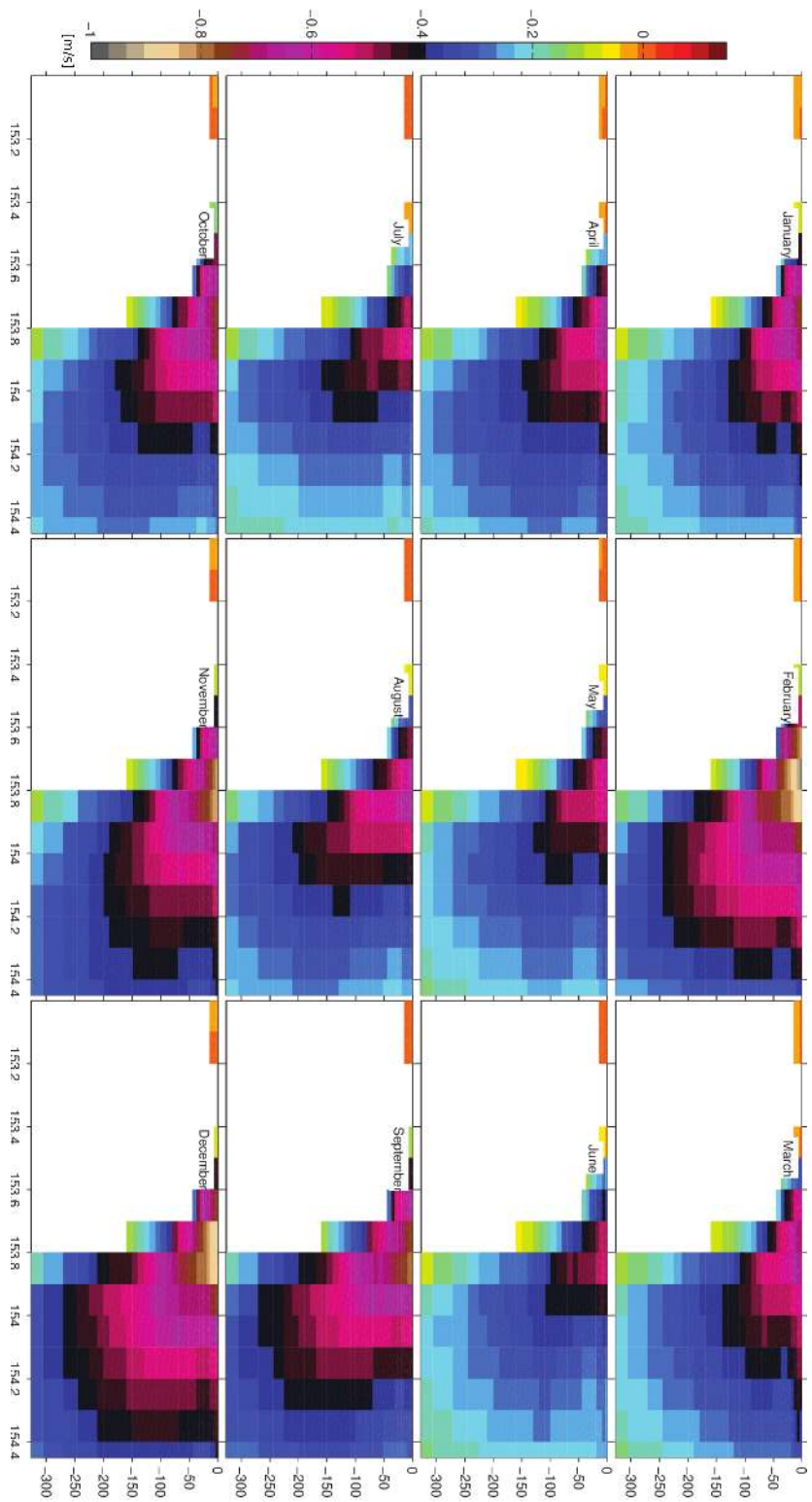

Figure A.8: Monthly averages of a cross section at 25°S of the v-velocity component based on BRAN3.5.

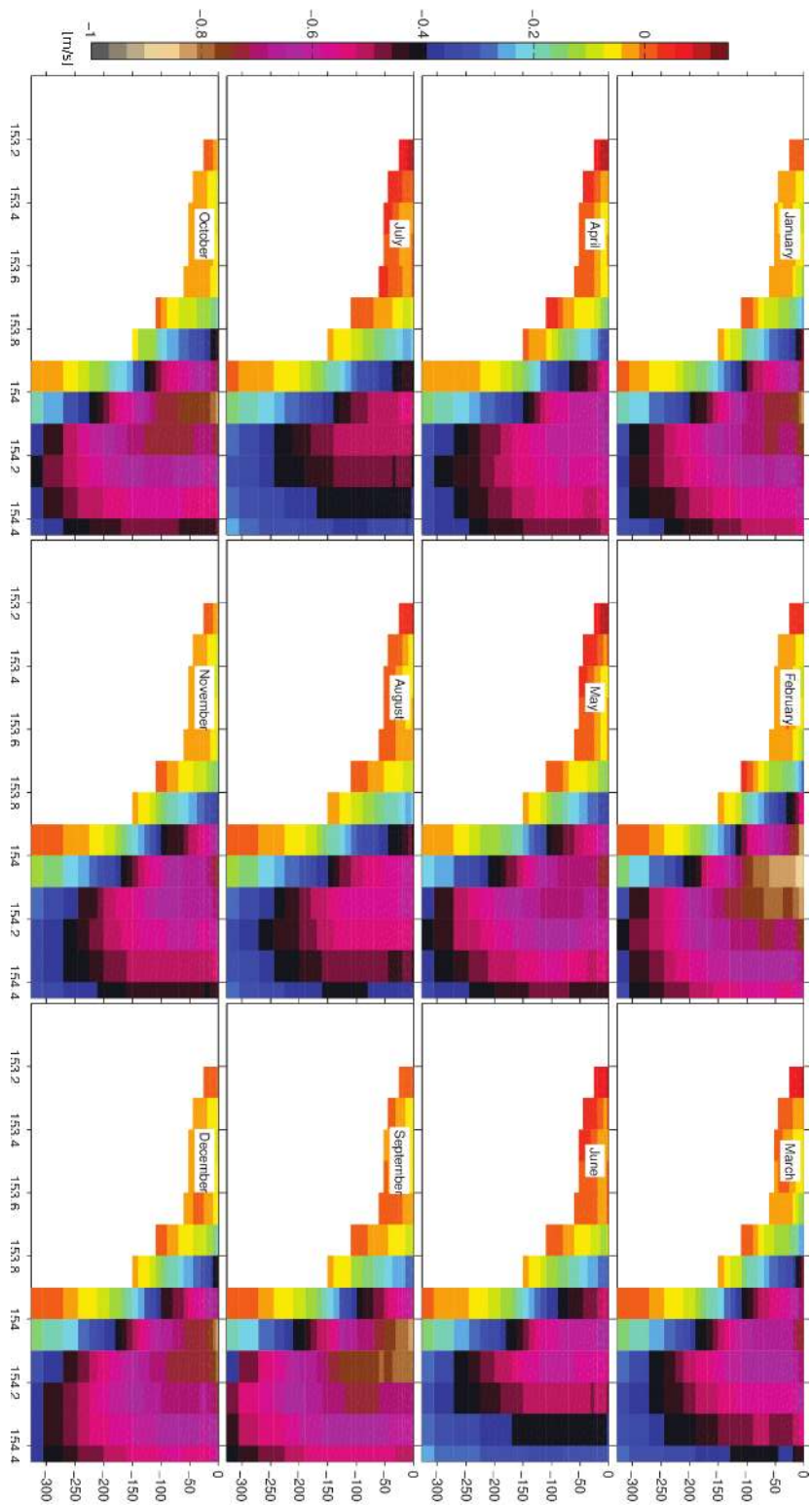

Figure A.9: Monthly averages of a cross section at 26.5°S of the v-velocity component based on BRAN3.5.

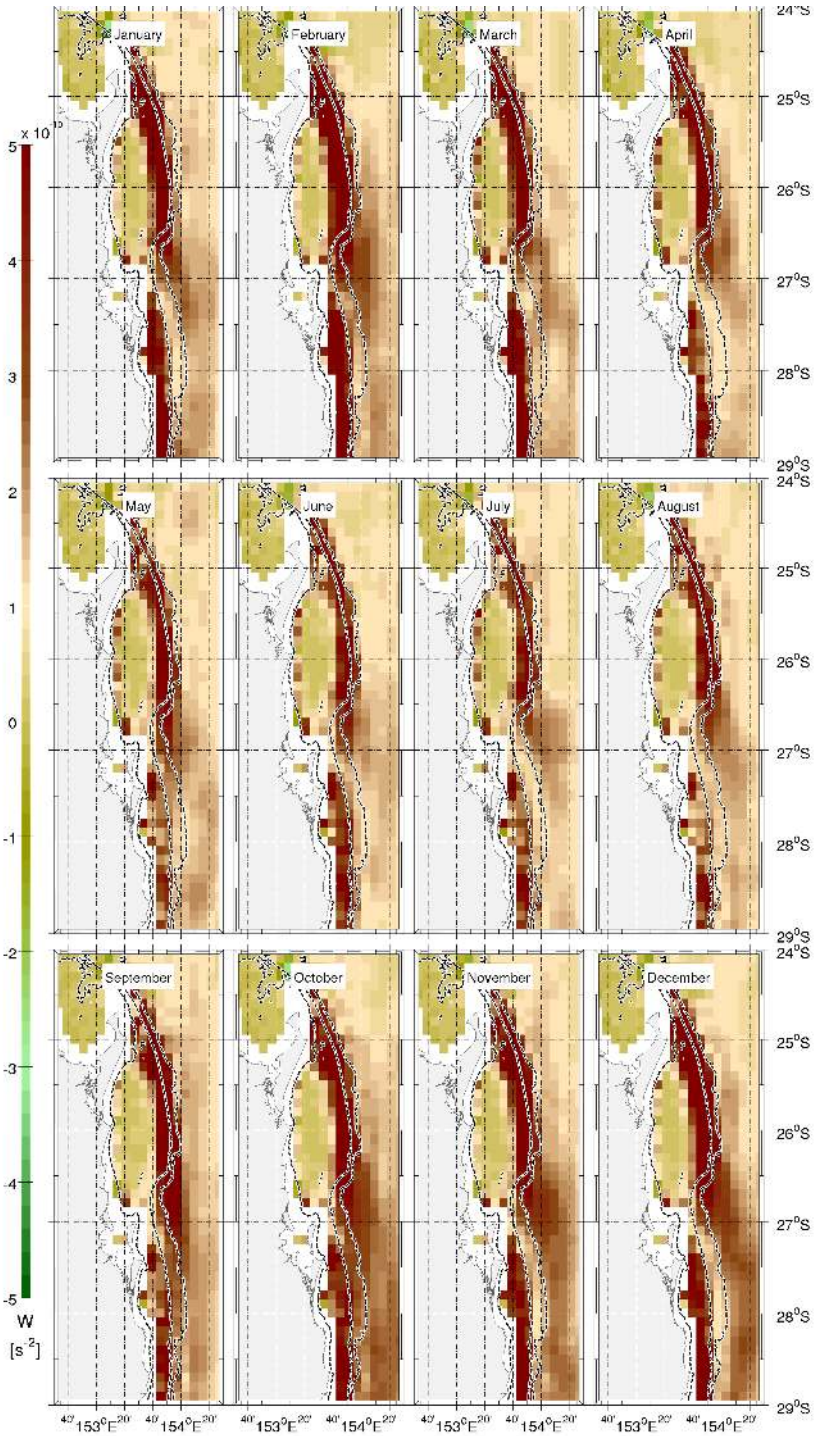

Figure A.10: Monthly averages of Okubo-Weiss parameter based on BRAN3.5 results. Negative values are place where the vorticity is dominant, whilst the positive values illustrate areas where the deformation dominates over vorticity.

Appendix B

Animations

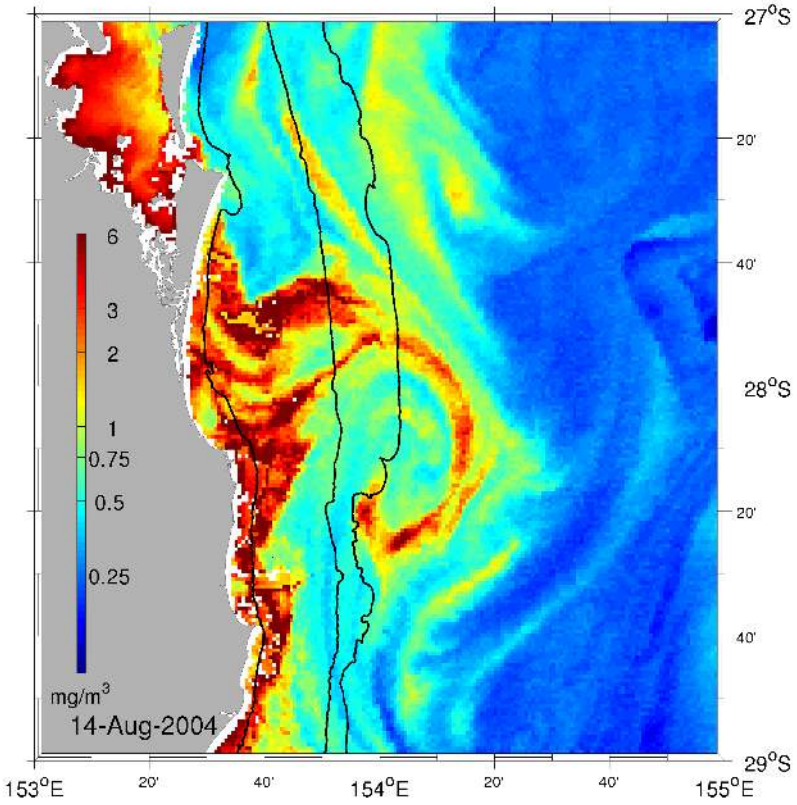

Animation B.1: Chla and SST off Sandy Cape from Oct. 2002 to Sept. 2014. Full animation is available at https://www.youtube.com/watch?v=WTAKEHMWRIk

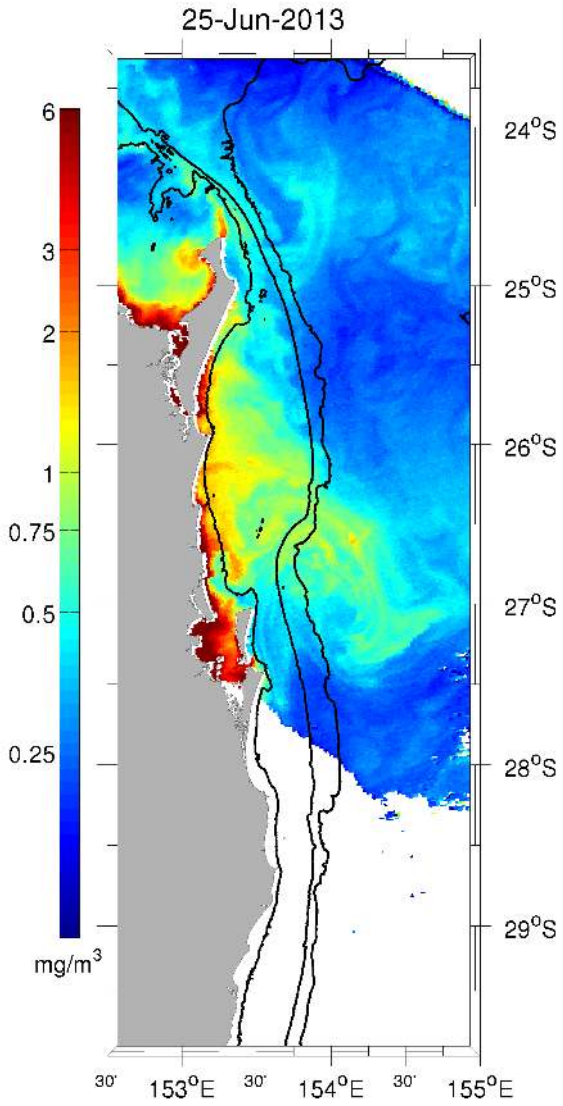

Animation B.2: Chla and SST off Fraser Island from Oct. 2002 to Sept. 2014. Full animation is available at https://www.youtube.com/watch?v=iutbBJnYWFg

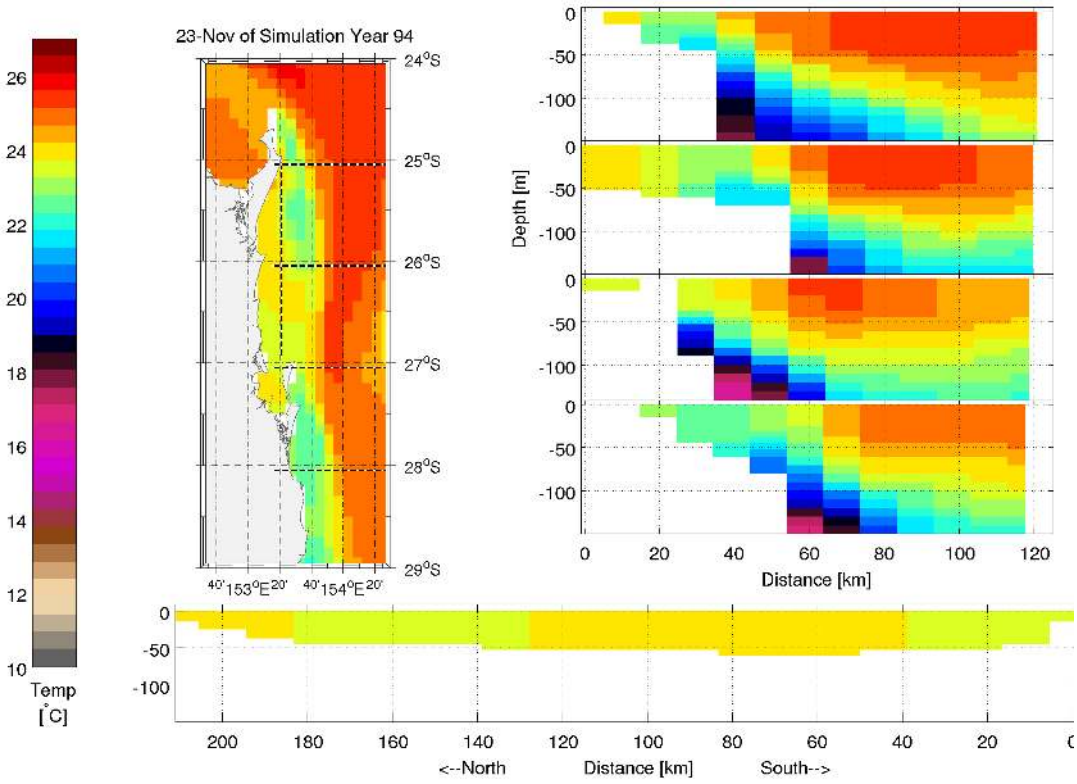

Animation B.3: Temperature represented by BRAN3.5 from 1993 to 2012. The full animation is available at https://www.youtube.com/watch?v=rlqKNaKmNZQ. The temperature scale is illustrated by the color bar at the left of the animation. The surface temperature is in the middle of the animation including the coastline, as well as indicating the location of the cross sections. The four longitudinal cross section are illustrated at the right, following the respective order from top to bottom that is indicated in the main central graph by the four horizontal dash lines. The location of the bottom latitudinal cross section is illustrated by the only vertical dashed line.

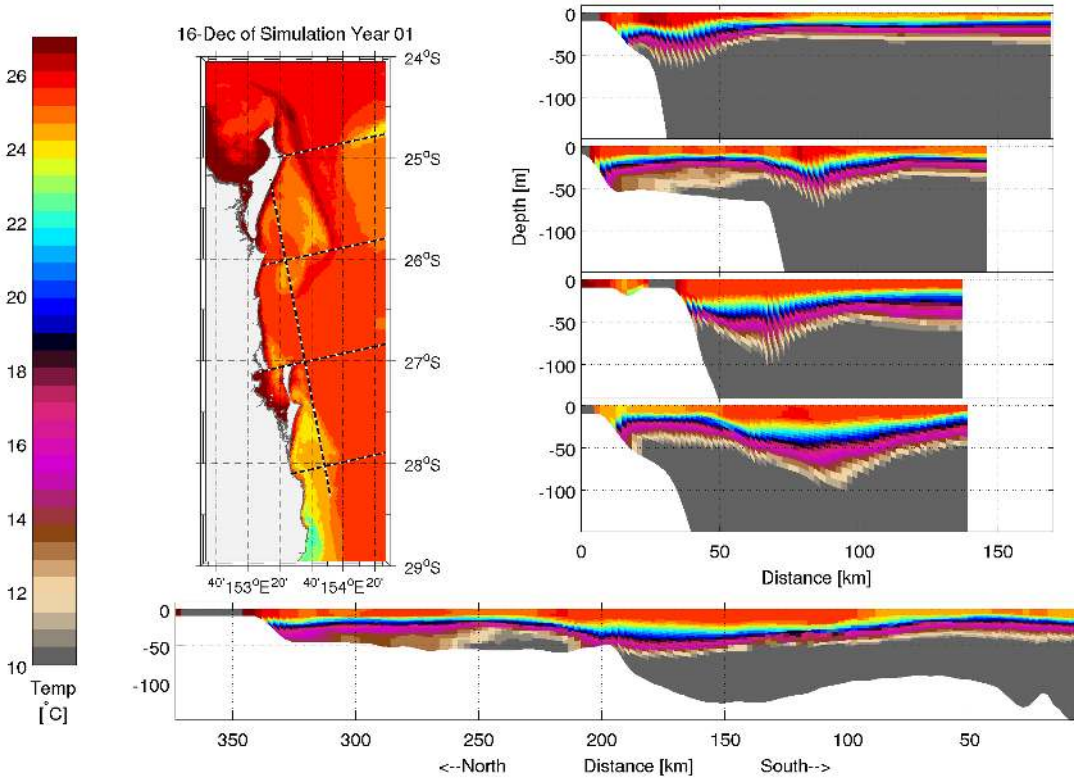

Animation B.4: Temperature represented by ROMSY2010 for 5 simulated years. The full animation is available at https://www.youtube.com/watch?v=xK3m0jPf9bs. The temperature scale is illustrated by the color bar at the left of the animation. The surface temperature is in the middle of the animation including the coastline, as well as indicating the location of the cross sections. The four longitudinal cross section are illustrated at the right, following the respective order from top to bottom that is indicated in the main central graph by the four parallel dark dash lines. The location of the bottom latitudinal cross section is illustrated by the only dark dashed line from Fraser Island to Gold Coast.